UNIVERSITÀ DEGLI STUDI DI MILANO

FACOLTÀ di MEDICINA E CHIRURGIA
Scuola di dottorato in Scienze Biomediche, Cliniche e Sperimentali
Dipartimento di Medicina Traslazionale

CORSO di DOTTORATO DI RICERCA in
PATOLOGIA E NEUROPATOLOGIA SPERIMENTALI
XXIII ciclo
Settori scientifico-disciplinari MED/03 MED/04 MED/05

DIFFERENTIAL INVOLVEMENT OF S AND L ISOFORMS OF THE CENTROSOMAL MARK4 KINASE IN GLIOMA INITIATION AND PROGRESSION

TESI di DOTTORATO DI RICERCA di
CHIARA NOVIELLI
Matricola R07780

Tutor: Dott.ssa IVANA MAGNANI
Docente guida: Prof.ssa LIDIA LARIZZA
Coordinatore: Prof. ALBERTO MANTOVANI

Anno Accademico 2009/2010

Abstract

MARK4 (MAP/Microtubule Affinity-Regulating Kinase 4) belongs to a family of serine-threonine kinases that are able to phosphorylate the Microtubule Associated Proteins, causing their detachment from the microtubules and thus increasing microtubule dynamics. *MARK4* gene is ubiquitously expressed and encodes at least two alternatively spliced isoforms, L and S, which differ in the C-terminal region and are differentially regulated in human tissues, especially in the Central Nervous System (CNS). MARK4S predominance in normal brain has been related to a putative role in neuronal differentiation; MARK4L has been found up-regulated in hepatocarcinoma cells and highly expressed in gliomas, suggesting an involvement of the kinase in cycling cells. Gliomas are the most common tumors of the CNS and are characterized by elevated cellular heterogeneity, which has been imputed to the presence of different cells (mature cells / progenitors / stem cells) from which each glioma originates.

To further investigate MARK4 up-regulation in glial tumors, we analyzed a panel of 35 glioma tissue samples and 21 glioma cell lines (both low and high malignancy grade) and 6 glioblastoma-derived cancer stem cell populations (GBM CSC; glioblastoma is a IV grade glioma). Human neural progenitors, total human normal brain and mouse neural stem cells (NSC, isolated from the sub-ventricular zone) were also included in the study. A quantitative approach (Real-time PCR; q-PCR) was applied for mRNA analyses whereas MARK4 protein levels and localization were tested by Immunoblotting (IB), Immunohistochemistry (IHC) and Immunofluorescence (IF).

We first carried out mutational analysis of the main *MARK4* domains, but it didn't reveal any genomic alteration, as did not the previously performed array-CGH analysis.

Integrated approaches of q-PCR, IB and IHC studies show that, although MARK4S and L have a heterogeneous expression within and across different glioma subtypes (consistent with the intrinsic cell heterogeneity of these brain tumors), MARK4L is the prevalent isoform in near all the glioma samples. Conversely, MARK4S mRNA levels display a significant decrease inversely correlating with malignancy grade and are also hardly detectable in both neural and GBM-derived cancer stem cell populations. Therefore, a higher MARK4L prevalence in parallel to low levels of MARK4S characterizes highly undifferentiated cells, such as NSC, and highly malignant cells, such as GBM CSC and glioblastomas, favouring the hypothesis that the ratio between the two MARK4 isoforms is strictly regulated along neural differentiation and may be subverted in gliomagenesis. These findings, together with the observation that in normal brain only the L isoform localizes in the embryonic ventricular zone (VZ) and

adult sub-ventricular zone (SVZ), where stem cells reside, suggest that some GBM of our panel originated from the SVZ. In contrast, the concomitant expression of both MARK4 isoforms in the main substrates of glioma transformation, mature glial cells and progenitors, could explain the origin of the Oligodendrogliomas, Astrocytomas and of some GBM here studied. Furthermore, both MARK4 isoforms are expressed in neurons, extending published data of MARK4S as a neuron-specific marker in mouse CNS.

By Immunofluorescence we found that the two MARK4 isoforms localize at centrosomes and midbody of normal and glioma cell lines, showing that MARK4 association with these cell compartments is neither isoform- nor tumor-specific. It has been reported that both normal and cancer stem cells can display centrosome amplification, genetic instability and loss of asymmetry with switch to a prevalent symmetric division, which may converge in malignant transformation and unrestrained growth of stem cells. Interestingly, we previously found MARK4 protein in association with glioma aberrant centrosomes, a hint for a possible role of the kinase in the abnormal mitotic processes of human glioma. Symmetric division, besides promoting the expansion of stem cell numbers, may also be permissive for secondary events leading to aneuploidies, since the machinery that controls asymmetric division also regulates the orientation of mitotic spindles and of centrosomes.

Finally, an intriguing finding, delineating MARK4L as a tumor marker through its nucleolar association, comes from the evidence that L isoform, in contrast to MARK4S, is detectable in nucleoli and exclusively in cancer cells. Furthermore, the differential expression of MARK4 isoforms in undifferentiated and glial malignant cells expands the concept of MARK4 splice variants dysregulation in mediating tumor initiation and progression.

Background

1.1 THE FAMILY OF MARK KINASES

MAP/Microtubule affinity-regulating kinases (MARKs) constitute a family of serine-threonine kinases originally discovered for their ability to phosphorylate Microtubule Associated Proteins (MAPs, including tau, MAP2, MAP4 and doublecortin), causing their detachment from microtubules and thus increasing microtubule dynamics [Drewes 1997]. Microtubules indeed consist of assembled α and β tubulin dimers and are stabilized by MAP association; phosphorylated MAPs detach from microtubules which therefore lose stability and disassemble. In mammals the MARK family consists of four members, namely MARK1, MARK2 (EMK1), MARK3 (C-TAK1) and MARK4 (MARKL-1), encoded on chromosomes 1, 11, 14 and 19 in the human genome [Espinosa 1998] and presenting 28 pseudogenes.

MARKs belong to the AMPK (AMP-activated protein kinases) subfamily of the Ca^{2+}-calmodulin dependent protein kinases (CAMPK), on the basis of their elevated homology with the other proteins of these families. The AMPK group includes 12 kinases, namely BRSK1 and BRSK2, NUAK1 and NUAK2, SIK1, SIK2 and SIK3, MELK, MARK1, MARK2, MARK3 and MARK4 [Bright 2009].

MARK kinases also have homologues in lower eukaryotes, such as Par-1 (partition-defective) in *Caenorhabditis elegans* and KIN1, KIN2 in yeast.

1.1.1 Protein structure

All MARK proteins have a very conserved structure, similar to that of other AMPK kinases, consisting of six sequence segments [Marx 2010] (figure 1.1):

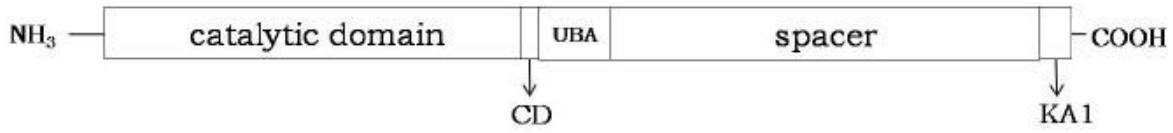

Figure 1.1: schematic representation of MARK protein structure. Boxes are not drawn to scale.

- the N-terminal header, whose role is still unknown;
- the catalytic domain, containing the activation loop (also called T-loop), the catalytic loop and the P-loop (phosphate-binding loop);
- a linker, that is a highly and negatively charged motif that resembles the Common Docking (CD) site in MAP kinases and may bind interactors or co-factors;
- the UBA domain, that is probably autoregolatory;

- a spacer, the most variable region among the MARK members; it is probably important for regulating MARK activity, since it holds phosphorylation sites that are targeted by aPKC;
- the C-terminal tail, consisting of the Kinase-Associated (KA1) domain with a probably autoinhibitory function.

The three major domains are here described in details.

The catalytic domain: MARK kinases are activated by phosphorylation in the T-loop (that contains a conserved sequence, LDTFCGSPP, where the threonine and serine residues are phosphorylation targets) and exert their activity by subsequently linking a phosphate group to substrate proteins.

The catalytic domain forms, with the CD domain, the linker and the UBA domain, a bi-lobal structure creating a cleft for substrate and ATP. This structure is very flexible, allowing conformational changes depending on the activation/inactivation state. In the inactive state, the T-loop is disordered and folded into the cleft, blocking the access of substrate peptide and ATP. Both the phosphorylation sites (threonine and serine) are nevertheless accessible for kinases: once they have been phosphorylated (activation), the T-loop is reoriented and folds out of the cleft, which becomes open enabling ATP and substrate access [Timm 2008].

The UBA domain is a small, globular domain which has sequence homology with UBiquitin-Associated proteins but, differently from them, it is unusually folded and probably doesn't bind ubiquitin, interacting instead with the MARK catalytic domain by binding close to its N-terminal lobe and locking it in an open (inactive) conformation. Based on this feature, two different functions were proposed for MARK UBA domain, an autoinhibitory role (1) or a positive regulatory one (2):

(1) by locking the kinase in an open conformation, the UBA domain prevents substrate and ATP binding [Panneerselvam 2006];

(2) on the other hand, this open conformation increases the accessibility of the activation loop for activating or deactivating kinases [Murphy 2007].

The UBA domain may thus serve several functions – inhibitory, activating, stabilizing – depending on the phosphorylation state of the kinase domain or on cofactor interactions (for example, ubiquitin could bind the UBA domain competing with the kinase domain) [Marx 2010].

The C-terminal tail (KA1 domain) is a 100 aminoacid-long motif and is characterized, on its N-terminal region, by a hydrophobic and concave surface, surrounded by positively charged residues. This region may interact with negatively

charged regions of (1) cytoskeletal proteins, (2) MARK catalytic domain, or (3) MARK CD domain [Tochio 2006]. The tail domain could therefore be another autoinhibitory domain, as reported for yeast KIN1 and KIN2 and for Snf1-pKD (an AMPK protein from *Schizosaccharomyces pombe*). In particular, Snf1 C-terminal region is an autoinhibitory domain (AID) that binds both the N-terminal and C-terminal lobes of the kinase domain, reducing its mobility [Chen L. 2009]. In yeast, the C-terminal tail physically interacts with the N-terminal kinase domain (presumably when it is in an open conformation) with an autoinhibitory effect [Elbert 2005].

The KA1 (Kinase Associated) domain was also reported to be involved in protein localization [Tochio 2006].

1.1.2 MARK regulation: activation mechanisms

MARK kinases, containing several domains, appear to be regulated by multiple mechanisms. In general, MARK activation increases microtubule dynamics, while its inhibition stabilizes microtubules.

MARK activation by phosphorylation: all MARK kinases are activated by Liver Kinase B1[1] (**LKB1**) and MARK Kinase (**MARKK**) by phosphorylation on the threonine residue in the T-loop (MARK1 T215; MARK2 T208; MARK3 T211; MARK4 T214). Moreover, the Calcium/calmodulin-dependent protein kinase I (**CaMKI**) phosphorylates MARK2 at a different site in its kinase domain [Matenia 2009].

1.1.3 MARK regulation: inhibition mechanisms

MARK inhibition by phosphorylation: the Glycogen Synthase Kinase 3β (**GSK3β**) phosphorylates a serine residue, near the threonine activation site in the T-loop, in all the MARKs (MARK1 S219; MARK2 S212; MARK3 S215; MARK4 S218), negatively regulating protein activity. This inhibition occurs even if the threonine site is phosphorylated, since the phosphorylated serine is no longer able to stabilize, by interactions with other aminoacids, the activating loop [Timm 2008].

Mammalian **aPKC** (atypical Protein Kinase C) phosphorylates MARK2 in the spacer region at T595 and MARK3 at the equivalent site, downregulating kinase activity, enhancing MARK binding to the 14-3-3[2] protein and promoting a change in localization [Hurov 2004].

[1] LKB1 is a tumor suppressor gene; loss-of-function mutations of LKB1 lead to Peutz-Jeghers Syndrome, characterized by the onset of many tumors.

[2] 14-3-3 proteins are phospho-serine/phospho-threonine binding proteins that interact with many partners and regulate different biological processes.

The human **PIM1** kinase phosphorylates MARK3 inhibiting its activity [Matenia 2009].

MARK inhibition by interaction: as previously indicated, **14-3-3** proteins (Par-5) bind MARK kinases in their catalytic domain [Benton 2003] or in the spacer region (after MARK phosphorylation by aPKC) altering MARKs localization and reducing their activity, probably by stabilizing the inhibitory interaction between the KA1 domain and the catalytic domain.

MARK2 is also inhibited by interaction with **PAK5** (p21-activated kinase) at the catalytic domain [Matenia 2005].

As previously mentioned, also **ubiquitin** and MARK **UBA and KA1 domains** can interact with MARK kinase domain.

A novel proposed mechanism for MARK autoinhibition is **dimerization**: dimer formation is common in many kinases and MARK proteins were observed to persistently crystallize as dimers, covalently linked by a disulfide bridge between T-loops. In this particular conformation, the molecules are in an open state and the activation loop is folded into the cleft and locks it, inhibiting MARK activity. Despite experimental data, there is no direct *in vivo* evidence of this interaction [Marx 2010].

1.1.4 MARK localization and functions

MARK1, MARK2 and MARK3 show a uniform cytoplasmic localization, associating to the intracellular network and, as concerns MARK2, possibly linking to membrane components [Drewes 1997]. MARK4 localization is discussed further on.

Since MARK kinases regulate the affinity between MAP proteins and microtubules, they are implicated in many cellular processes involving the microtubule network, such as cytoskeleton dynamics [Schneider 2004], centrosome formation, chromosome segregation in mitosis and cytokinesis [Fukasawa 2002]. Some cellular processes involving MARK activity are here described; particularly attention is focused on cellular processes occurring in neurons and in pathologies, such as tumors and Alzheimer's disease. MARK4 functions are reported further on in detail.

Microtubule-dependent transport. It has been reported that MARK proteins, especially MARK2, control microtubule-dependent transport, for example in axons, since they phosphorylate MAPs which often interfere with motor proteins (that are responsible for protein, vesicle and organelle transport) [Mandelkow 2004]. In addition, MARK co-localization with clathrin-coated vesicles (CCV) was recently demonstrated, confirming a function of MARK4 in the regulation of microtubule-dependent transport of CCV during endocytosis [Schmitt-Ulms 2009].

Cell polarity. Par-1 homologues of MARK were discovered for their role in establishing polarity in *C. elegans* and *Drosophila* cells: they accumulate asymmetrically in the embryo and induce asymmetric division and polarized axis formation, which are necessary for correct embryonic development [Tomankak 2000]. Also KIN1 and KIN2 homologues in *Schizosaccharomyces pombe* establish cell polarity, inducing a bipolar growth that leads to the acquisition of the classical rod-shape of yeasts [Drewes 2003].

In mammals, MARK proteins are similarly asymmetrically localized in epithelial cells and are required, with aPKC and Par-5 (14-3-3) proteins, in polarization processes in epithelial and neuronal cells [Bohm 1997; Matenia 2009]. In particular, **MARK2** is involved in the reorganization of the microtubule network during epithelial differentiation of liver and kidney cells [Cohen 2004]. MARK/Par-1 also interacts with *Helicobacter pylori* CagA protein: a peptide of CagA mimics MARK substrate and occupies the catalytic loop of the kinase, inhibiting MARK activity [Nesic 2009]. Described effects in gastric carcinomas are the disorganization of the gastric epithelial structure [Saadat 2007] and spindle misorientation with mitotic delay [Umeda 2009]. It has also been reported that MARK2 plays a role in the maintenance of neuronal

polarity: strong MARK2 expression inhibits axon formation and dendrite development, whereas reduced MARK2 levels induce multiple axons in hippocampal neurons. This MARK2 activity is negatively regulated by aPKC phosphorylation that leads to MAPs detachment, microtubule assembly and axon elongation [Chen 2006; Terabayashi 2007].

Neuron migration. One of MARK substrates is doublecortin, which is highly enriched in leading processes of migrating neurons: phosphorylation by MARK proteins, regulating doublecortin affinity for microtubules, affects the motility of neurons [Schaar 2004]. Indeed, after MARK2 knockdown, neurons of the developing mouse cortex fail to migrate beyond the intermediate zone [Sapir 2008].

MARK3 and 14-3-3 proteins - cycle control, cell signalling and subcellular localization. MARK3 phosphorylation of Cdc25 phosphatase induces 14-3-3 binding to Cdc25 and doesn't allow Cdc25 to activate the Cdc2/cyclinB complex, which is required for mitotic entry [Peng 1998]. In addition, Pim-1 phosphorylation and inhibition of MARK3 promote cell cycle progression at the G2/M phase [Bachmann 2004].

Phosphorylation of KSR1 (Kinase Suppressor of Raf-1) by MARK3 induces its binding to 14-3-3 proteins and regulates the Ras-MAPK pathway [Muller 2001].

Finally, MARK3 phosphorylates class IIa histone deacetylases (HDAC) on one of their 14-3-3 binding sites, preventing 14-3-3 binding and thus altering HDAC subcellular localization (14-3-3 usually mediates HDAC nuclear exclusion; after MARK3 phosphorylation HDAC are instead retained in the nucleus) [Dequiedt 2006]. Also PKP2 (Plakophilin 2) is phosphorylated by MARK3, creating a 14-3-3 binding site that induces PKP2 localization in the nucleus [Muller 2003].

MARK2 - other physiological functions: experiments in mice demonstrated, by knocking-down MARK2, that this kinase is involved in many physiological functions, such as fertility, homeostasis of the immune system, memory, growth and metabolism [Bessone 1999; Hurov 2001; Hurov 2007; Segu 2008].

Tau and Alzheimer. Tau is a microtubule-associated protein, particularly expressed in the Central Nervous System. It can be phosphorylated by MARK and, subsequently, by CDK5 and GSK3 kinases, that alter tau localization and induce tau proteolytic cleavage [Drewes 2004]. It is thought that as an effect of this proteolytic cleavage, hyperphosphorylated tau accumulates in neuron somatodendritic compartments and abnormally aggregates in paired helical filaments that form insoluble neurofibrillary tangles [Chin 2000; Gamblin 2003]. All these phenomena, also including loss of

synapses and neurons, are characteristic of Alzheimer's disease and MARK role in this pathology has been evaluated by many studies, demonstrating, as an example, MARK co-localization with neurofibrillary tangles [Chin 2000].

Recently, other studies have revalued microtubule alterations in Alzheimer's disease, hypothesizing that tau phosphorylation is not the initial event of the pathology [Chatterjee 2009] but a consequence of β-amyloid aggregation. In particular, abnormal β-amyloid causes transport defects (due to increase and bundling of microtubules) and improper distribution of tau into the somatodendritic compartments (in contrast to axonal sorting in normal neurons) [Zempel 2010]. Very interestingly, MARK2 activation in this early step of Alzheimer's disease could rescue transport mechanisms and synapses [Thies 2007]. Instead, if pathogenesis goes on, hyperphosphorylated tau, elevated kinase activities (including MARK) and breakdown of microtubules are commonly found in the missorted dendritic regions [Zempel 2010].

MARK1 and pathologies. *MARK1* gene was recently identified as a susceptibility gene for autism, since several SNPs within the gene were significantly associated with autism and MARK1 was found overexpressed in the prefrontal cortex on post-mortem brain tissues from autistic patients. Authors suggested that MARK1 may be involved in cognition and be responsible for subtle changes in dendritic functioning [Maussion 2008]; an earlier study had also hypothesized that MARK1 might be implicated in the regulation of synaptic plasticity [Jeon 2005].

Many studies have hinted that MARK1 could have a role in neoplastic transformation: *MARK1* gene is localized in a fragile site (FRA1H) and its expression levels presented significant modifications in tumor-derived cell lines compared to normal controls [Pelliccia 2007]. *MARK1* was found to be methylated, and thus silenced, in primary gastric cancers [Yamashita 2006], whereas it was up-regulated in lung carcinoma compared to normal bronchial epithelium [Sun 2004].

1.2 MARK4 (MAP/MICROTUBULE AFFINITY-REGULATING KINASE 4)

1.2.1 Gene, alternative transcripts and protein structure

MARK4 is the less characterized and studied member among MARK proteins.

The gene codifying for MARK4 was discovered by Kato and colleagues in 2001, among few genes whose expression resulted significantly increased in hepatocarcinoma cells with elevated β-catenin levels accumulated in their nucleus, and named *MARKL1* (*MARK-Like 1*) on the basis of its homology to *MARK3* [Kato 2001].

MARK4 gene is located on chromosome 19q13.2 and consists of 18 exons. At least two MARK4 isoforms are known (figure 1.2):

- MARK4S (Short) mRNA, the native isoform, consists of 18 exons and is 3609 base pairs (bp) long; it encodes a 688 aa[3]-long protein whose predicted molecular weight (MW) is 75.3 kilo Daltons (kDa);
- MARK4L (Long) mRNA (3529 bp) is originated by the skipping of exon 16 and the consequent shift of the reading frame, leading to the production of a 752 aa-long protein with a predicted MW of 82.5 kDa.

MARK4 sequence has near 55% homology with the other MARKs, with the higher homology with MARK3. MARK4 isoforms have the characteristic protein structure and domains of the other MARKs, consisting of the N-terminal catalytic domain, a linker (common docking domain), the UBA domain, a spacer and the C-terminal tail. The kinase domain shows 90% homology compared to the other MARK members and contains the T-loop with the phosphorylation sites (T214 and S218), while the spacer region (the most variable segment among family members) is wide. As a consequence of the alternative splicing, the two isoforms differ in the C-terminal tail, since MARK4L includes the Kinase-Associated 1 (KA1) domain as the other MARK proteins, whereas MARK4S contains a domain with no homology to any known structure [Espinosa 1998], suggesting different functions for the two isoforms. Actually, MARK4 shows much less sequence homology in the tail domain compared to the other MARKs, nevertheless MARK4 tail seems to fold in a conformation similar to those of MARK1, 2 and 3, and thus the suggested autoinhibitory and interactor role of the C-terminal region applies also to MARK4 [Marx 2010].

[3] Aminoacids.

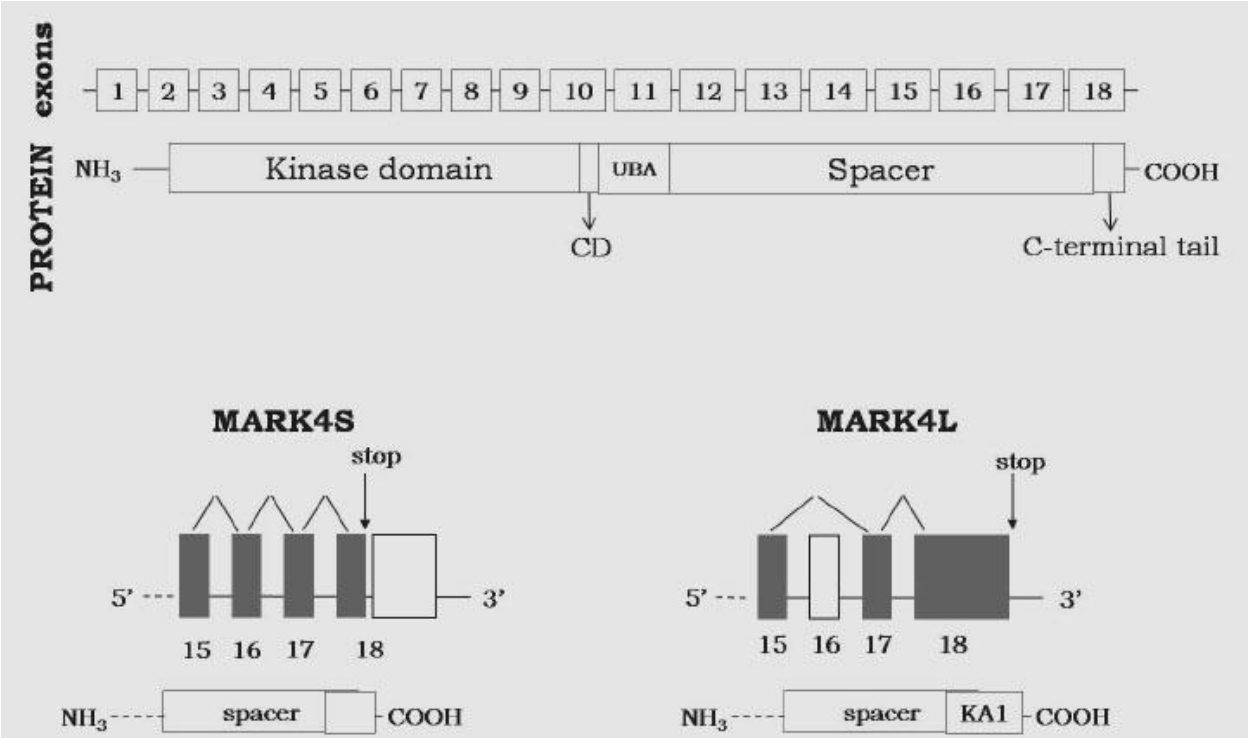

Figure 1.2: [top] schematic representation of MARK4 exons and respective protein domains; **[bottom]** alternative splicing of exon 16 gives origin to MARK4 isoforms. When exon 16 is included in the mRNA, the stop codon is inside exon 18 and the encoded protein, MARK4S, lacks the KA1 domain at the C-terminal tail (left); if exon 16 is skipped, a shift of the reading frame also occurs, changing the stop codon and generating a longer MARK4L protein, which has the classical KA1 domain (right). Boxes are not drawn to scale.

1.2.2 MARK4 regulation

Since the protein structure is conserved among MARK family, regulation of MARK4 is similar to that of the other MARK members.

MARK4 is activated by LKB1 that phosphorylates Threonine 214 in the T-loop [Lizcano 2004; Brajenovic 2004]. A recent study demonstrated that MARK4 is polyubiquitinated and interacts with the deubiquitinating enzyme USP9X. Non-USP9X-binding mutants of MARK4 are hyperubiquitinated and not phosphorylated at their T214, therefore polyubiquitination may inhibit LKB1 activation of MARK4. The proposed model implicates that in the steady state MARK4 UBA domain is bound by ubiquitin and cannot interact with the catalytic domain, making the T-loop less accessible to LKB1 (see also - in chapter 1.1.1 - the positive regulation of UBA domain proposed by Murphy). Alternatively, ubiquitin may cover and hide theT214 site or induce conformational modifications favouring the activity of phosphatases [Al-hakim 2008].

It has also been demonstrated that MARK4 interacts with aPKC [Brajenovic 2004] and could therefore be phosphorylated and inactivated by this kinase, as reported for MARK2 and MARK3 [Hurov 2004].

1.2.3 MARK4 interactors

By Tandem Affinity Purification and Immunoprecipitation experiments, near twenty proteins have been identified as putative MARK4 interactors [Brajenovic 2004]. Among them, PKCλ and Cdc42 are implicated in cell polarity control and TGFβIAF (Transforming Growth Factor β-Inducing Anti-apoptotic Factor) is thought to be a hortologue of Miranda, a protein involved in the asymmetric division of neuroblasts in *Drosophila*. MARK4 interacts with the 14-3-3η isoform [Brajenovic 2004; Angrand 2006]: 14-3-3 proteins, as previously reported, control many cellular processes by binding phosphorylated proteins and could directly regulate MARK4 or act as bridges among different pathways. Other MARK4 interactors are ARHGEF2, a cytoskeleton binding protein, and Phosphatase 2A, which is associated to microtubules and regulates Tau [Brajenovic 2004].

MARK4 protein was also found to co-localize and co-precipitate in complex with α, β, and γ tubulin, myosin and actin [Trinczek 2004; Brajenovic 2004].

As previously indicated, MARK4 interacts with LKB1 and aPKC kinases and also with the deubiquitinating enzyme USP9X.

1.2.4 Gene expression and protein localization

Few *MARK4* expression studies are reported in literature; they were performed with non-quantitative methods, such as Northern Blot [Kato 2001; Trinczek 2004; Schneider 2004] and semi-quantitative competitive PCR [Moroni 2006], on different organisms (human, rat and mouse tissues) not always discerning between the two MARK4 isoforms. As a result from all these data (that sometimes were discordant), *MARK4* gene appeared to be ubiquitously expressed, with particularly elevated levels in brain and testis. In general, MARK4L seemed to be highly expressed in testis, brain and also in kidney, liver and lung [Trinczek 2004; Schneider 2004; Moroni 2006], whereas MARK4S levels were elevated in testis, heart and brain [Kato 2001; Moroni 2006]. In details, Northern Blot analysis on rat tissues pointed out that MARK4L and S expression levels are equal in testis, whereas the L isoform is prevalent in brain and lung [Schneider 2004]. On the contrary, semi-quantitative PCR on mouse samples highlighted high MARK4L levels along with reduced S expression in testis and high MARK4S levels in brain [Moroni 2006].

In brain, MARK4 protein (presumably the L isoform) was observed on the tips of neurite-like processes [Trinczek 2004]; Immunohistochemistry on rat cerebral cortex and hippocampus showed MARK4L and S expression in neurons of the grey matter, whereas the white matter was unlabeled [Moroni 2006].

Exogenous GFP-conjugated MARK4 protein was reported to localize in normal and aberrant interphase centrosomes in CHO[4] and neuroblastoma cell lines. It was hypothesized that inactive MARK4 is located near the nucleus, possibly associated to the endoplasmic reticulum, and once activated it co-localizes with microtubules in the centrosome, exerting its function [Trinczek 2004]. Very recently, endogenous MARK4L localization was assessed by Immunofluorescence (IF), with a specific MARK4L antibody, in glioma cell lines. MARK4 protein localizes in normal and aberrant interphase centrosomes and maintains this association also in mitosis, co-localizing with γ-tubulin in all the cell cycle phases. This centrosome association was not abolished by nocodazole-induced depolymerization of microtubules, suggesting that MARK4L is a core component of centrosomes. Moreover, two novel MARK4 localization sites were highlighted, by showing MARK4L additional association with the nucleolus and the midbody. All these IF results were confirmed by Immunoblotting in centrosome, nucleolus and midbody fractions [Magnani 2009].

[4] Chinese Hamster Ovary.

The **CENTROSOME** is a little organelle, not bound by any membrane, positioned centrally in the cell near the nucleus [Fukasawa 2002]. It is the primary MicroTubule Organizing Center (MTOC), as it can nucleate and organize microtubules. It consists of two distinct domains:

- the centriolar domain, including the centrioles, which are cylindrical organelles important for centrosome organization and replication. Each centriole consists of 9 triple microtubules;
- the pericentriolar domain, consisting of many fibers and proteins that surround the centriole. In this domain microtubules are nucleated, by associating α and β-tubulin dimers from a γ-tubulin ring [Doxsey 2001].

The centrosome plays a key role in organizing the interphase cytoskeleton (regulating cell polarity, adhesion and motility) and the mitotic spindle [Kramer 2002]. It also contributes to cell cycle progression and cytokinesis [Martinez-Garay 2006] and is involved in cell cycle transitions, in the cellular response to stress and signal transduction [Doxsey 2005]. The centrosomes duplicate only once in the cell cycle, during G1/S transition and in S phase, and forms a strictly bipolar spindle during mitosis.

Centrosomes that were aberrant in their size, shape, number or composition (also presenting improper phosphorylation or expression of centrosomal proteins) were observed in many tumors [Yamamoto 2004; Katsetos 2006]. A surplus of centrosomes causes the formation of aberrant multipolar mitotic spindles, which can be responsible for errors in chromosome segregation and, subsequently, for the chromosomal instability (CIN) often found in tumors.

CYTOKINESIS is the process occurring at the very end of mitosis, when the cell splits into two daughter cells.

During mitosis the mother cell develops the mitotic spindle, consisting of two asters (star-shaped microtubular structures) located at the cell poles, from which bundles of microtubules start and overlap at the equator (midzone). The spindle allows the accurate and equal segregation of chromosomes into the two daughter cells.

During cytokinesis, the mitotic spindle locates the cleavage furrow, which will divide the cell, exactly inside the midzone in a point which is equidistant from the two asters. In this furrow, a contractile ring of actin and myosin grows up and shrinks, causing the "stricture" of the cell, until the two opposing surfaces of the membrane come in contact and merge, closing and delimiting the two daughter cells [Bringmann 2005].

Initially the two daughter cells are connected by a narrow intercellular bridge, whose core is the **MIDBODY**, which consists of microtubules and of a dense matrix [Mullins 1982]. The diameter of the intercellular bridge then decreases until it vanishes, making effectively separated the two daughter cells. The midbody is finally discarded and undergoes degradation [Mullins 1977]. The midbody is thought to have an important role in maintaining a bipolar spindle and in correctly separating the cytoplasm between the two daughter cells.

The nucleolus is a subnuclear organelle not surrounded by membranes and whose main function is ribosome biogenesis. It originates at the end of mitosis (during mitosis the nucleolus doesn't exist) from the Nucleolus Organizing Regions (Nors), which are clusters of genes (rDNA) codifying for ribosomal RNA (rRNA) located on the acrocentric chromosomes. The nucleolus consists of three main components, each with a different role in the formation of ribosomes, here defined starting from the inside of the nucleolus to outside:

- the fibrillar center, which is a NOR (rDNA);
- the dense fibrillar component, consisting of pre-rRNA;
- the granular component, whose granular appearance is conferred by the presence of ribosomal subunits.

The transcription of the rDNA leads to the formation of pre-rRNAs, which then undergo rearrangements and are assembled with ribosomal proteins to form the pre-ribosomes. The pre-ribosomal particles then move into the cytoplasm, passing through the nuclear pores [Carmo-Fonseca 2000; Schwarzacher 1983].

Besides this traditional ribosome biogenesis activity, the nucleolus is characterized by multiple functions, including the response to cellular stress, the regulation of cell cycle [Visintin 2000] and cell growth [Zhang 2010] and of post-translational modifications (phosphorylation and sumoylation) of proteins.

1.2.5 MARK4 in the Central Nervous System and in tumors

MARK4 gene was first discovered in hepatocarcinoma cells, since after inactivation of the Wnt/β-catenin pathway many cells accumulated β-catenin in the nucleus and showed elevated expression levels of certain genes, including the novel *MARK4* gene. Kato and colleagues hypothesized that it could be a downstream component of the Wnt-signalling pathway involved in hepatocellular carcinogenesis [Kato 2001].

MARK4 gene was also found rapidly and transiently up-regulated after an ischemic event in brain, mainly in the hippocampus. Many genes were overexpressed in the injured brain compared to the healthy counterpart, including LKB1 which phosphorylates MARK4. Experimental overexpression of MARK4S in hepatocytes led to a reduction in cell vitality, thus it was hypothesized that MARK4S up-regulation in the early stages of an ischemic event might increase the probability of neuron death [Schneider 2004].

By analyzing frequent rearrangements involving chromosome 19q13 in gliomas, which are glial cancers and the most frequent tumors in the Central Nervous System, an amplified region in 19q13.2 was discovered. This was very interesting, since the amplified region was centromerical to the LOH[5] area in gliomas [Hartmann 2002] but never deleted in these tumors, so it could harbour a gene probably important for cancer cells. DNA sequence of the amplified region corresponded specifically to the *MARK4* gene [Beghini 2003].

MARK4 gene was found duplicated in one glioblastoma (IV grade glioma) cell line (MI-4) [Beghini 2003] and this duplication was confirmed by array-CGH[6] analyses [Roversi 2006]. By a semi-quantitative PCR approach, MARK4L was also seen up-regulated in 8 tissue samples and 26 cell lines (10 I and II grade, 11 III grade and 5 IV grade gliomas) with a direct correlation between malignancy grade and MARK4L levels. MARK4S was found highly expressed in normal brain (with low L levels) and hardly detectable in tissue samples and human neural progenitors (data about glioma cell lines are not available). It was therefore suggested that MARK4L might be a mitogen protein, necessary for proliferation and thus highly enriched in proliferating or undifferentiated cells [Beghini 2003].

MARK4L and S isoforms were analyzed by competitive PCR (a semi-quantitative method) in human and mouse normal brain, neural progenitors, NT2[7] cells and cells differentiated in neurons. S was the main expressed isoform in mouse and human brain but appeared undetectable in neural progenitors and in un-differentiated NT2

[5] Loss Of Heterozygosity.
[6] Comparative Genomic Hybridization.
[7] NTera2 (NT2) is a cell line derived from a human embryonic teratocarcinoma.

cells. MARK4S expression levels were shown to increase during neuronal differentiation of NT2 cells and progenitors, whereas MARK4L expression was maintained at the same levels in differentiated neurons. The S isoform was therefore suggested to be a neuron-specific marker in the CNS and to mark neuronal commitment. Nevertheless, both MARK4L and S proteins were found expressed in neurons by means of Immunohistochemistry, suggesting that both forms play a general role in neurons [Moroni 2006].

Finally, many hints were given about *MARK4* association with Alzheimer's disease (AD), since this kinase phosphorylates tau protein which is involved in this pathology, and also because *MARK4* gene is located nearby a locus of susceptibility (*ApoE*) for AD [Trinczek 2004]. Several studies have also suggested that chromosome 19 could harbour another mutated gene linked with the disease [Podusio 2001]. Recently, the rs597668 locus, fairly close to the ApoE gene, was identified as significantly associated with AD. This locus is near *EXOC3L2*/*BLOC1S3*/*MARK4* genes but does not improve Alzheimer risk prediction [Seshadri 2010].

1.2.6 MARK4 hypothetical functions

As the other MARK members, MARK4 phosphorylates MAP proteins, increasing microtubule dynamics and cell shape alterations [Brajenovic 2004] suggesting its involvement in regulating microtubule dynamics and in the processes implying microtubules. MARK4L may probably take part in cell cycle progression and in coordinating cytokinesis, since it interacts with microtubules and, in glial tumors, it was found associated with centrosomes and midbody, as several kinases involved in cell cycle regulation [Magnani 2009]. Being up-regulated in some tumors, MARK4 could indeed have a role in cell proliferation [Kato 2001; Beghini 2003].

MARK4 direct interactors, or proteins bound by 14-3-3 proteins after MARK4 phosphorylation, were thought to be involved in cytoskeleton remodeling [Brajenovic 2004].

MARK4L association with the nucleolus in glial tumors is very interesting and should be further studied, since MARK4L could have a functional impact on the nucleolus (as many kinases do) as well as it could be spatially regulated by alternate translocation in and out the nucleolus [Magnani 2009].

MARK4S isoform was suggested to be a neuron-specific marker in the CNS and to mark neuronal commitment; both MARK4L and S proteins were thought to play a general role in neurons [Moroni 2006].

1.2.7 *MARK4* mutations

Mutations in protein kinase genes are often implicated in cancer initiation and development, since most kinases are involved in cell proliferation. Most of the activating alterations occur inside the catalytic domain, including the ATP-binding site.

However, few *MARK4* alterations are reported in literature data and only a splice-site mutation (exon 13 +1 G>A; spacer region) was identified in one glioblastoma sample (among 91 GBM samples analyzed) [The Cancer Genome Atlas Research Network 2008]. In a huge study involving 518 protein kinase genes in 210 diverse human cancers, five *MARK4* mutations were also found [Greenman 2007]:

- two missense mutations in exon 12 (spacer region) occurred in two colorectal adenocarcinomas (R377Q and R418C);
- two silent mutations were found in exon 5 (Y137Y) and in exon 9 (I286I) (kinase domain) in multiple tumor samples;
- one intronic mutation occurred (exon 8 +5 C>T; kinase domain) in a lung cancer specimen.

No *MARK4* mutations, but only few SNPs[8], were found in patients affected by Peutz-Jeghers Syndrome, which is characterized by LKB1 mutations [de Leng 2007].

[8] Single Nucleotide Polymorphism.

1.3 GLIOMA

Glioma is the most common type of primary brain tumor in adults, accounting for more than 70% of all the tumors in the Central Nervous System (CNS) [Ohgaki 2009].

Gliomas have a high incidence in children between 0-8 years and in adults between 50-70 years and there is a slight male predominance [Gladson 2010].

1.3.1 Classification

The human brain is composed of two main cell types: neurons (2-10% of the cells in the CNS) and glia (90-98%). There are three different glial sub-populations: astrocytes, oligodendrocytes and microglia. Astrocytes ("star-shaped") are the most abundant glial cells and have a role in neuron nourishing and protection, regulation of synapse formation and activation of the immune response. Oligodendrocytes release neuronal growth factors and cover neuronal axons with their cytoplasmatic processes to form the myelin. Microglial cells, finally, are mainly located near blood capillaries and have phagocytic and protective activities.

Histologically, gliomas can resemble astrocytes, oligodendrocytes or ependymal cells, thus they are classified on the basis of their morphologic appearance.

Accordingly to the World Health Organization (WHO) classification, drafted in 1993 and updated in 2008 [Rousseau 2008], gliomas are histologically sub-divided in:

- ASTROCYTIC TUMORS:
  - Pilocytic astrocytoma
  - Diffuse astrocytoma (fibrillary, protoplasmic and gemistocytic astrocytomas)
  - Anaplastic astrocytoma
  - Pilomyxoid astrocytoma
  - Glioblastoma
  - Giant cell glioblastoma
  - Gliosarcoma
  - Pleomorphic xantoastrocytoma
  - Subependymal giant cell astrocytoma;
- OLIGODENDROGLIAL TUMORS:
  - Oligodendroglioma
  - Anaplastic oligodendroglioma;
- MIXED GLIOMAS:
  - Oligoastrocytoma
  - Anaplastic oligoastrocytoma;

- EPENDYMOMAS;
- OTHER NEURONAL, NEURO-GLIAL AND NEUROEPITHELIAL TUMORS.

Besides this histological classification, gliomas are separated in four different malignancy grades, on the basis of the presence/absence of nuclear atypia, mitosis, microvascular proliferation and necrosis:

- WHO grade I: lesions with low proliferative potential and with a good prognosis (treatment with surgical resection is usually sufficient for the complete recovery).
- WHO grade II: generally infiltrating lesions with low mitotic activity and possible recurrences. Some of these tumors can progress to higher malignancy grade lesions.
- WHO grade III: lesions with histological evidence of malignancy, generally characterized by high mitotic activity, pronounced anaplasia and infiltrative capacity.
- WHO grade IV: lesions with high mitotic activity, prone to necrosis and generally associated with a rapid pre- and post-operation evolution of the disease.

The WHO classification, however, is not sufficient for a correct diagnosis and especially for the prediction of survival and response to therapy, since gliomas show considerable heterogeneity and variability among tumors of the same type and grade and also within individual tumors. Therefore, biopsies are often not fully representative of the whole tumor mass, because of the intrinsic heterogeneity that makes it difficult to obtain complete samples. In addition, genetic alterations have been reported to differ in tumors of the same histotype, thus classification on the basis of genetic phenotype could lead to a more accurate prognosis prediction.

1.3.2 Clinics

The main ***symptoms*** of gliomas are characteristic of brain tumors and depend on the anatomical site of the tumor in the brain:

- partial or generalized seizures (epilepsy);
- nausea, vomiting, drowsiness, headache, visual abnormalities, changes in speech, hearing or balance. All these symptoms are caused by increased intracranial pressure, especially in rapidly growing lesions;
- focal and progressive neurological deficits. The type of deficit (motor or sensory) is generally indicative of the tumor site;

- cognitive dysfunctions, in most cases symptomatic of meningeal involvement or diffuse tumor infiltration.

Diagnosis. Magnetic resonance imaging (MRI) or computed tomography (although less sensitive) are used to confirm a suspect of brain tumor. Surgical biopsy with histological examination is then necessary to diagnose tumor type and grade.

Therapy. Glial tumors are treated by surgery, radiation and chemotherapy. Since the tumor is located in the brain and often infiltrates extensively into surrounding normal tissue, complete resection is difficult. Nevertheless, when surgery is not completely curative, at least it relieves symptoms by decompressing the brain. Surgery is usually combined with adjuvant post-operation radiotherapy and chemotherapy (represented by temozolomide, nitrosurea or by the combination of procarbazine, lomustine and vincristine – PCV) to increase survival; however disease recurrence is very common [Park 2009].

Advances in understanding the molecular mechanisms of gliomagenesis are leading to the development of new therapies, mainly targeted to inhibit signal transduction pathways, which are often constitutively altered in glial tumors and can drive uncontrolled tumoral proliferation [Sathornsumetee 2007]. In particular, monoclonal antibodies and kinase inhibitors are studied in order to target protein kinases; these inhibitors, however, have shown little efficacy, probably because of their low specificity and reduced ability to cross the blood brain barrier [Chi 2007]. Recent advances include immunotherapy and anti-angiogenic drugs; anti-VEGF drugs are of particular interest, since the Vascular Endothelial Growth Factor is responsible for the high vascularization commonly found in gliomas [Jain 2007] and is involved in a pathway frequently altered in these tumors.

Survival. The median survival is 5-8 years for patients with grade II tumors, 3 years for patients with grade III anaplastic astrocytomas and 12-18 months for patients with glioblastomas (older patients, > 60 years old, typically have a shorter survival) [Gladson 2010].

1.3.3 Etiology I – risk factors

Specific risk factors have not been identified; occupational exposure to organic solvents or pesticides appears to be a predisposing factor [Gladson 2010], as well as exposure to ionizing radiations [Fisher 2007]. There are evidences of a possible association between immunological factors and gliomas: atopic people seem to have a lower risk of developing gliomas [Linos 2007] and patients with high IgE levels have a longer survival [Wrensch 2006]. Cytomegalovirus (CMV) infection has also been

suggested to play a role in the etiology and progression of some gliomas, on the basis of CMV RNA detection in glioblastoma tumors [Mitchell 2008].

1.3.4 Etiology II – genetic alterations

Familiar forms. Most brain tumors are sporadic, nevertheless few familiar syndromes are known to be associated with an increased incidence of brain neoplasia. In these syndromes gliomas occur in combination with other clinical signs, in particular tumors in other locations. Examples are the Li-Fraumeni syndrome, involving *p53* gene on chromosome 17p13, the neurofibromatosis I (*NF1* on chromosome 17q11) and the Cowden syndrome (*PTEN* 10q22-q23).

Sporadic forms. The sporadic forms of glioma show different cytogenetic abnormalities, such as deletions and duplications of entire chromosomal segments, Loss Of Heterozigosity (LOH) and gene amplification, genetic alterations in oncogenes and tumor suppressor genes. These anomalies cause deregulation of specific pathways involved in cell cycle control, proliferation and cell differentiation. The oncogenes and tumor suppressor genes found altered in gliomas are not specific of this class of tumors, but their combination and their particular accumulation inside glial cell are typical of gliomas and correlate with neoplastic transformation and tumor progression [Zhu 2002]:

- **Oligodendroglioma** (WHO **grade II**) and **Anaplastic oligodendroglioma** (WHO **grade III**) frequently exhibit specific loss of heterozygosity on chromosomes 1p (1p36.22-p36.31) and 19q13.3 [Smith 2000], which predicts a favorable response to therapy and a longer survival [Collins 2004]. It is not yet known which genes present in these loci are tumor suppressor genes or, *vice versa*, may be involved in tumor initiation and/or growth promotion so that their loss may lead to a favorable prognosis [Gladson 2010]. The tumor suppressor *PTEN* gene (10q22-q23) is often downregulated, as a consequence of promoter methylation or 10q chromosome loss. *PDGFRa (Platelet-Derived Growth Factor Receptor a)* amplification (4q12) is frequently present and leads to uncontrolled cell proliferation. Growth factor receptor signaling plays indeed an important role in promoting both a highly proliferative phenotype and an invasive phenotype, in cooperation with cell-adhesion receptors and proteases. Anaplastic oligodendrogliomas (grade III) show genetic and epigenetic aberrations of *INK4A-ARF* and *INK4B* which are involved in regulating the G1/S transition in the cell-cycle.

- **Astrocytomas** (WHO **grade II**) frequently exhibit amplification of the *PDGFRa* and/or *PDGFRβ* genes and of the genes encoding their ligands (PDGF-A, -B, -C and –D). The increased expression of both ligands and receptors suggests that an autocrine or paracrine loop exists which amplifies signaling [Shapiro 2002]. Loss of *p53* is a common genetic event in astrocytomas, perhaps one of the first events of the neoplastic transformation [Reifenberger 1996]: the tumor suppressor p53 activity is lost for LOH of chromosome 17p or for missense mutations in the gene locus.
- **Anaplastic astrocytomas** (WHO **grade III**) originate from II grade astrocytomas and thus present the same mutations, such as loss of *p53*. In addition, they show other genetic alterations, mostly involving genes which control cell-cycle progression, resulting in deregulated cell proliferation. In particular, loss of the *Rb* gene (13q13) is frequently found, as well as *CDK4* amplification, *p16/CDKN2A* deletion or promoter hypermethylation and *MDM2* (an endogenous p53 inhibitor) amplification (12q).
- **Glioblastomas** (WHO **grade IV**) are the most aggressive glial tumors; they can arise *de novo* (**primary GBM**, showing mainly an astrocytic component) or originate from pre-existing low-malignancy grade lesions (figure 1.3). A small subgroup of grade IV GBM contains areas of oligodendrocytes and is thus indentified as oligodendroglioma-derived and named **GBMO**; in contrast, most of grade IV GBM originate from grade II/III astrocytomas and are referred to as **secondary glioblastomas**. Between astrocytic tumors, primary and secondary GBM develop through distinct genetic pathways, show different RNA and protein expression profile and epigenetic aberrations and may differ in their response to therapy, despite the fact that they are histologically largely indistinguishable [Ohgaki 2009].
- In **primary glioblastomas**, amplification and/or mutation of the *EGFR* gene (*Epidermal Growth Factor Receptor*; chromosome 7) are very common and can promote glioma cell proliferation and invasion. *EGFR* alterations are mutually exclusive with *MDM2* overexpression (an endogenous p53 inhibitor; interestingly, no *p53* mutations or deletion are present). LOH of chromosome 10q causes deletion of *PTEN* gene; other potential tumor suppressor genes mapping in this locus are *DMBT1* (*Deleted in Malignant Brain Tumors 1*) and the Myc antagonist *Mxi1* [Gladson 2010], but they have not been definitively associated with glioblastoma development. Mutations and/or deletions in *NF1* (*NeuroFibromin 1*, a tumor suppressor gene associated to neurofibromatosis

type 1 and negative regulator of Ras signaling) are also present in sporadic glioblastomas [Huse 2010].

- Hypermethylation of the promoter of the *MGMT* gene (06-*Methyl-Guanine-MeThyltransferase*) occurs in both primary and secondary GBM and indicates a better response to temozolomide therapy, since *MGMT* repairs DNA damage that is induced by alkylating agents, such as temozolomide [Ney 2009].
- Recently, genome-wide association screens have identified single nucleotide polymorphisms (SNPs) in *RTEL1* (*Regulator of Telomere Elongation Helicase*) and *TERT* (*Telomerase reverse Transcriptase*) genes with increased glioma incidence [Shete 2009; Wrensch 2009]. Missense mutations in *IDH1* and *IDH2* (*Isocitrate DeHydrogenase*) were found in a significant number of astrocytomas and oligodendrogliomas, but are largely absent in primary glioblastomas, suggesting that primary and secondary GBM may originate from different progenitor cells [Ohgaki 2009]; multivariate analysis also suggests that they are favorable prognostic markers [Huse 2010].
- It has recently been shown that microRNA (miRNA) play a role in gliomagenesis, since they may repress control genes or, when down-regulated, do not target oncogenes anymore [Huse 2010].

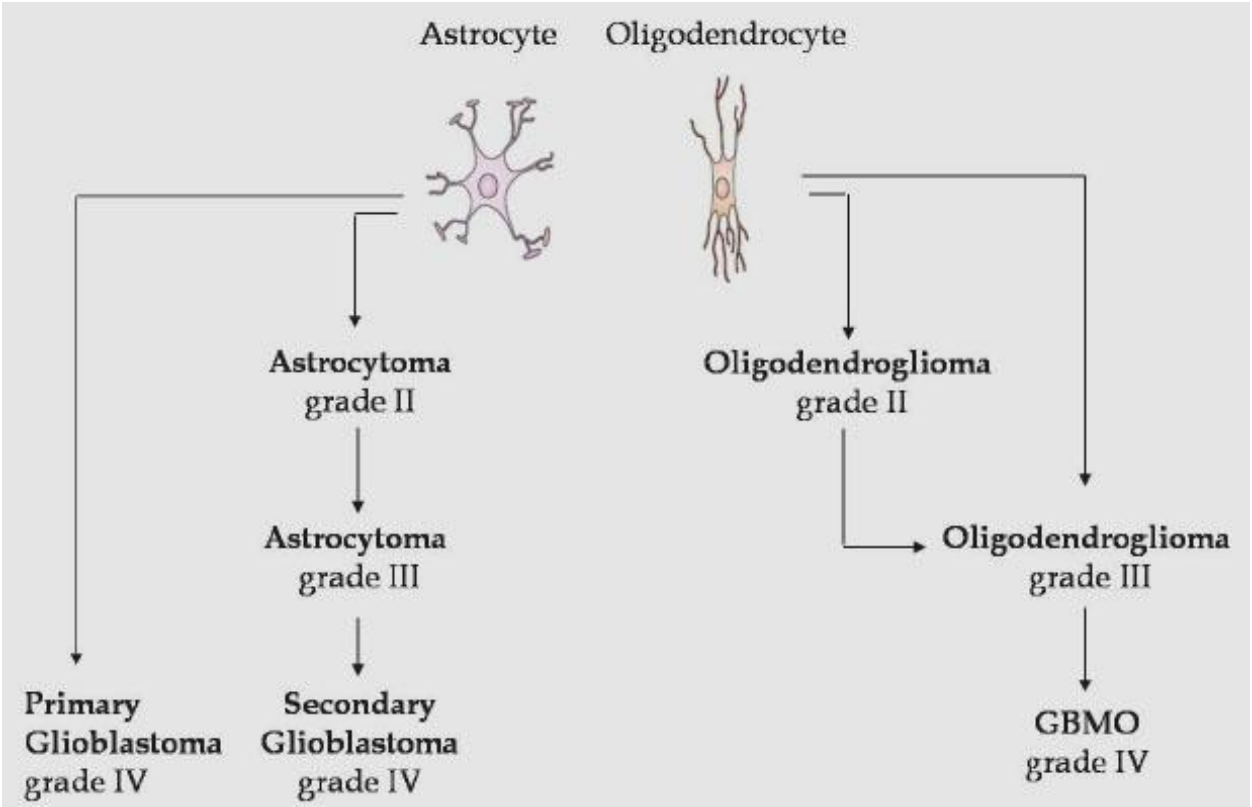

Figure 1.3: schematic representation of different grade gliomas.

1.4 HYPOTHESES ON THE ORIGIN OF GLIOMAS

All the formulated hypotheses on the origin of gliomas agree in asserting that glioma arises from a tumor initiating stem-like cell (named brain tumor stem cell, BTSC), whereas from which normal cell the BTSC derives is still widely debated.

1.4.1 Brain Tumor Stem Cells

The presence of Cancer Stem Cells in glioma was hypothesized to explain the cellular heterogeneity and resistance to therapy which especially characterize malignant glioblastomas [Reya 2001]. Several cancer stem cells may be present inside the tumor, differing in their genetic and epigenetic features and "escaping" therapy since they can split infinitely.

Cancer stem cells were isolated from glioblastoma biopsies for the first time in 2002 [Ignatova 2002] and were identified as stem-like cells, growing in neurospheres and being able to differentiate in neuronal and astroglial cells. The term "Brain Tumor Stem Cell" refers to cells which can long-term proliferate and self-renew, are multipotent (can differentiate into the three neural cell lineages) and are capable of giving rise to tumors *in vivo* [Vescovi 2006].

Self-renewal and multipotent differentiation are features of **stem cells**:

- self-renewal: stem cells can split infinitively;
- multipotent differentiation: stem cells can give origin to mature cells belonging to different lineages, through differentiation.

These features of stem cells are allowed and influenced by the stem niche, which is mainly composed of mature tissue cells, physically associated with blood vessels and lodges the stem cell. In the niche, specific growth factors (also coming from bloodstream) and adhesion molecules regulate stem cell polarization towards the niche basal membrane, determining the way the stem cell splits [Spradling 2001]. Stem cells can indeed divide in two ways (figure 1.4):

- by symmetric division the stem cell gives origin to two identical daughter cells which maintain stem features;
- asymmetric division generates two completely different daughter cells: one is a stem cell and will maintain the stem cell pool in the tissue, the other will differentiate into a specific cell type.

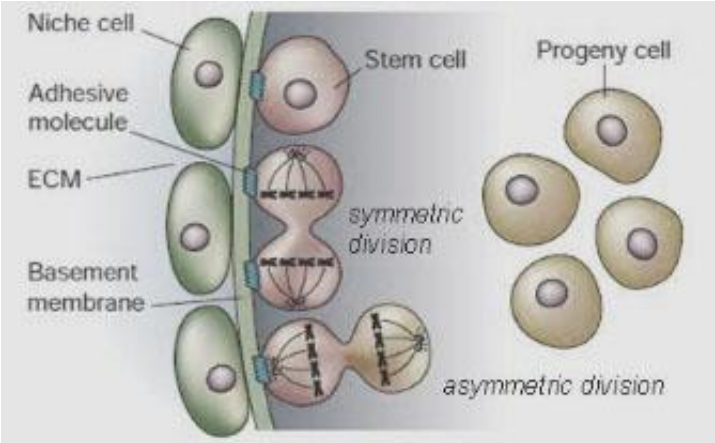

Figure 1.4: schematic representation of the symmetric and asymmetric division of the stem cell (red); differentiating progeny cells are yellow-coloured [modified from Spradling 2001].

Typically, cancer stem cells account for less than 5% of the cells within the tumor mass [Gladson 2010] and are thought to reside in the perivascular area of the tumor, referred to as the **vascular niche**. Here the capillary network seems to provide both the signals and the nourishment required for CSC support, offering a specialized microenvironment which allows the maintenance of their features [Huse 2010]. Changes in this local microenvironment (niche; increased expression of growth factors; interactions with immune cells) are indeed thought to play a role in glioma formation [Germano 2010; Park 2009]. This may suggest that therapeutic targeting of the tumor-associated vasculature, with anti-angiogenic drugs, may at least indirectly interfere with glioma CSC growth [Park 2009].

Many studies have been made so far to facilitate the identification and isolation of glioma-initiating cells from GBMs by using intracellular and/or surface markers, such as CD133, BMI1, nestin, Sox2, Notch. Reliance on markers alone is however insufficient, because, unlike normal stem cells, the genetic dysregulation that occurs in cancer may lead to ectopic protein expression [Park 2009]. Thus current identification methodology is considered limited.

As an example, the only CD133 marker is not suitable for identifying cancer stem cells, since also CD133 negative cells fulfilling stem cell criteria were found among GBM-derived CSC; this evidence suggested the presence of distinct CSC subgroups with distinct molecular, phenotypic and prognostic profiles [Günther 2008; Lottaz 2010]. CSC isolated from primary glioblastomas were indeed divided in two groups:

- type I CSC were CD133 positive, displayed neurosphere-like growth and formed highly invasive tumors *in vivo*; they were multipotent and characterized by the expression of neurodevelopmental genes or proneural genes resembling fetal neural stem cell lines;

- type II CSC were CD133 negative, grew semi-adherently and had a lower proliferation index, with less – but not absent – *iv vivo* tumorigenicity and invasion; they had a more restricted differentiation capacity and shared expression signatures enriched for extracellular matrix-related genes (or "mesenchimal" signature) similar to adult neural stem cells.

On the other hand, few studies demonstrated that CSC proliferative and tumorigenic capacities are not associated with CD133 expression, whereas they may derive from specific altered pathways, such as *PTEN* loss or mutation and *EGFR* expression [Chen 2010; Mazzoleni 2010].

The overall data suggest that both a **hierarchical** and a **stochastic mechanism** may be involved in tumor formation. According to the hierarchical model, only an identifiable CSC population, among the numerous CSC subpopulations present in the tumor mass, drives and repopulates the tumor. In contrast, the stochastic mechanism implies that different types of cancer stem cells, characterized by different tumorigenic ability, lead to tumor formation. This latter model could explain the cellular heterogeneity often found in glioblastomas.

1.4.2 Cell of origin

Different hypotheses have been formulated, suggesting that the Brain Tumor Stem Cell may derive from oncogenic transformation of:

- mature glial cells which de-differentiate;
- neural progenitor cells;
- neural stem cells.

Neural stem cells (NSC) have self-renewal ability and an indefinite life-time making them likely to accumulate mutations in respect to mature cells. On the other hand, stem cells are in most circumstances quiescent, thus they may not experience an adequate number of divisions to acquire genomic errors [Park 2009]. Nevertheless, many pathways constitutively activated in gliomas are also important for maintaining the undifferentiated state and the survival of neural stem cells (Notch, EGFR, SHH[9], PTEN, BMI1) [Purow 2005; Vescovi 2006; Stiles 2008].

[9] Sonic HedgeHog.

Neural stem cells have been identified in two regions of the adult nervous system, the Sub-Ventricular Zone (SVZ) of the forebrain and the dentate gyrus of the hippocampus. In these two regions the genesis of new neurons, which can be integrated in pre-existing neuronal circuits to maintain brain functionality and plasticity, has been consistently documented.

The ***sub-ventricular zone*** is the adult brain region with the highest neurogenic rate; it creates a niche inside the CNS parenchyma, since it is proximal to the cerebrospinal fluid and present large intercellular spaces with reduced cell-cell contacts.

In this region three main undifferentiated and highly proliferative cell types are found, named type A, B and C cells (figure 1.5). Type B cells express markers of both mature astrocytes (GFAP[10]) and immature and radial glial cells (vimentin and nestin) and are thought to represent relatively quiescent stem cells that proliferate at low rate and generate fast-proliferating, transit-amplifying progenitor cells (C cells). Type C cells are multipotent and in turn originate neuronal precursors (type A cells or neuroblasts), which leave the SVZ and migrate in several brain areas where they terminally differentiate [Galli 2003]. Some C cells express oligodendrocytic markers (Oligo2, NG2) and originate oligodendrocytes [Stiles 2008].

While *in vivo* endogenous NSC seem able to produce almost exclusively neurons, *in vitro* they are able to generate mainly astrocytes but also oligodendrocytes and neurons. This evidence highlights the importance of epigenetic signals in the neurogenic niches, where glial cells and neurons exert mutual influences [Gritti 2007].

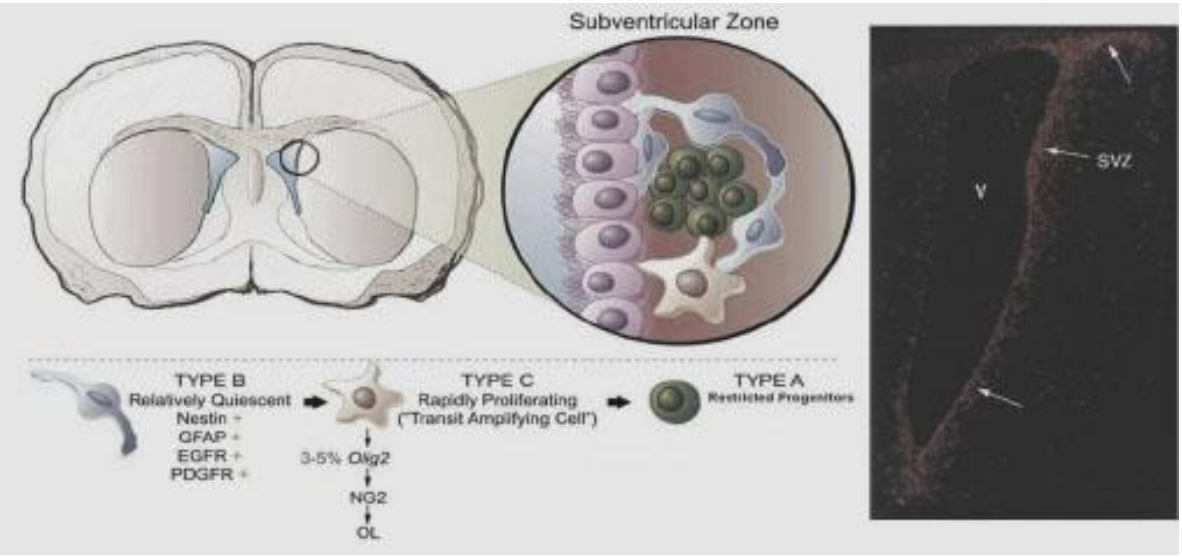

Figure 1.5 [left]: stem cells (B cells; blue), neural progenitors (C cells; amber) and neuroblasts (A cells; green) in the sub-ventricular zone [Stiles 2008]. **[Right]:** adult rodent brain ventricle (V) and sub-ventricular zone (SVZ). Arrows point to some of the proliferating cells in the SVZ that were labeled after intraperitoneal injection of the thymidine analogue, 5-bromodeoxyuridine [modified from Galli 2003].

[10] Glial Fibrillary Acidic Protein.

Neural progenitors are more proliferative than stem cells and differentiated cells, thus they are more likely to get oncogenic mutations and to fix them during replication. Many of the pathways found abnormally activated in gliomas are also sustained in neural progenitor cells, since they are necessary for progenitor proliferation and migration. Progenitors can migrate as well as tumor cells, even if glioma cells can proliferate and migrate at the same time, whereas progenitor cells have limited migration capacities and enter mitosis only after they have reached their destination [Canoll 2008].

In contrast, they need to recover the self-renewal capacity. Neural progenitors are characterized by a high plasticity, and were observed to change their differentiation state as a result of specific stimuli [Vescovi 2006]. Oligodendroglial progenitors were demonstrated to regain stem features after *in vitro* treatments which reactivated *Sox2*, a neural stem cell marker [Kondo 2000].

De-differentiated mature glial cells. Glioma cells express both undifferentiated and differentiated markers, and the tendency of gliomas to become more aggressive is associated to a progressive increase of markers of de-differentiation and decrease of markers of differentiation [Germano 2010]. Many studies demonstrated that activation of oncogenes or signal transduction pathways in cortical neurons reproduces brain tumors in animal models [Bachoo 2002]. Despite these evidences, there is no knowledge of the de-differentiation phases that these mature cells should undergo to originate multipotent malignant cells.

A recent study classified primary glioblastomas in four groups on the basis of their closeness and spatial relationship with the sub-ventricular zone and the cortex. Group I GBMs, contacting the SVZ and infiltrating the cortex, were characterized by multifocality and tumor recurrences noncontiguous with the initial lesion (so they had a more invasive and migratory phenotype), whereas group IV GBMs, neither contacting SVZ nor involving cortex, were never multifocal and their recurrences were always bordering the primary lesion. Authors therefore suggested that group I GBMs may originate from transformed neural stem cells: an invasive and migratory tumor phenotype is indeed more common to stem cell-derived cancer, since it is possible that gliomas arising from stem cells maintain expression of matrix metalloproteinases which are present in neural stem cells but not in the whole adult brain. The SVZ zone, or niche, may also be permissive for tumor growth and migration. Group IV GBMs may instead arise from white matter glial progenitors, which have very limited migration potential [Lim 2007].

Neural progenitor or stem cells may be at the origin of mixed glial tumors (oligoastrocytomas), since a transformed pluripotential cell may express some elements of both astrocytes and oligodendrocytes [Quingley 2007].

Different studies demonstrated that driving PDGFB expression in nestin-positive progenitor cells, committed oligodendroglial precursors or mature GFAP-positive astrocytes generates gliomas [Huse 2010]. Stimulation of PDGFR signaling by infusion of the ligand was sufficient to induce tumor-like proliferation of neural stem cells, whereas the combined activation of two oncogenes was needed to drive tumor formation of progenitor cells and combination of oncogene activation *plus* disruption of a tumor suppressor gene prompted tumorigenesis of differentiated astrocytes [Park 2009]. These findings suggest that several different cell types probably harbor tumorigenic potential and that their ability to initiate neoplasia may depend on specific oncogenic mechanism (alteration type, involved pathway) and/or on the molecular subclass of the tumor in question [Huse 2010].

In conclusion, summarizing all these hypotheses, we can say that gliomas are maintained by a population of malignant cells that exhibit stem-like properties, irrespective of the cell of origin which may be a stem cell, a progenitor cell or a differentiated cell that has reacquired the stem-like properties [Park 2009].

Materials and methods

2.1 TISSUE SAMPLES

2.1.1 Human glioma tissue samples

A total of 35 human glioma tissue samples were provided by Professor Lorenzo Bello (Department of neurological sciences, Università degli Studi di Milano, Milano) and are parts of glial tumors excised from patients who had received no previous chemotherapy or radiation treatment, in accordance with a protocol approved by the Internal Review Board of the University of Milan's Neurosurgery department. Features of the glioma samples are reported in table 2.1.

The specimens were stored at -80°C immediately after surgery.

2.1.2 Human normal brain (HNB)

Human samples for Immunohistochemistry (Professor Carolina Frassoni; Clinical epileptology and experimental neurophysiology unit, Istituto neurologico Carlo Besta, Milano) were obtained from:

- autopsies of three stillborn infants, died after premature delivery at the 23rd-27th gestational week; the death was due to non-neurological disorders and no brain malformation was detected at macroscopic and microscopic examination; following the Italian law, the autopsies were performed 24 hours after death;
- two drug-resistant patients operated on for intractable epilepsy; the surgery was performed for strictly therapeutic reasons after the patients had given their informed consent; at the neuropathological investigation, the samples did not show any cytological alteration.

As control for Real-time PCR and Immunoblotting, we used a sample of brain obtained from a male patient operated on for intractable epilepsy; the sample was stored at -80°C immediately after surgery. RNA from total human normal brain (*MVP Total RNA, Human Brain*) was also purchased by Stratagene (La Jolla, CA, USA); the donor was a 60-year-old male man.

SEX/AGE at surgery	TISSUE SAMPLE	HISTOLOGICAL DIAGNOSIS	WHO GRADE	ANATOMIC LOCATION	SVZ	PROGNOSIS	mMGMT	Del 1p	Del 19q
F / 52	**4**	Oligodendroglioma (O)	II	*not available*	N.A.	*not available*	+	+	+
M / 54	**6**	O	II	left temporal-insular lobe	-	alive - no relapses	-	-	-
M / 49	**42**	O	II	right frontal lobe	-	alive - relapse	N.E.	+	+
M / 59	**71**	O	II	right temporal-insular lobe	-	alive - no relapses	+	-	-
M / 29	**98**	O	II	right parietal lobe	-	alive - CHT	+	+	+
M / 38	**106**	O	II	right frontal-insular lobe	-	alive - relapse	+	+	+
F / 41	**107**	O	II	left frontal lobe	-	alive - relapse	+	+	+
M / 50	**118**	O	II	right frontal-insular lobe	+	alive - no relapses	+	+	+
M / 36	**112**	O	II	right parietal lobe	+	alive - no relapses	+	+	+
F / 39	**186**	O	II	right temporal-insular lobe	-	alive - no relapses	+	+	+
M / 68	**190**	O	II	left frontal lobe	+	alive - no relapses	+	+	+
M / 45	**193**	O	II	right frontal lobe	+	alive - no relapses	+	+	+
M / 31	**196**	O	II	right parietal lobe	-	alive - no relapses	-	-	-
F / 44	**200**	O	II	left temporal-insular lobe	-	alive - no relapses	+	+	+
M / 40	**217**	O	II	left temporal lobe	-	alive - no relapses	+	+	+
M / 46	**219**	O	II	right frontal lobe	-	alive - no relapses	+	+	+
M / 32	**1**	Protoplasmatic astrocytoma with anaplastic areas	II (III)	left parietal lobe	-	alive - no relapses	+	-	-
N.A.	**41**	Astrocytoma	II	*not available*	N.A.	*not available*	N.E.	N.E.	N.E.
M/34	**64**	Protoplasmatic astrocytoma	II	left frontal lobe	N.A.	alive - relapse	N.E.	-	-
N.A.	**94**	Astrocytoma	II	*not available*	N.A.	*not available*	N.E.	N.E.	N.E.
F / 52	**108**	Anaplastic astrocytoma	III	left temporal lobe	-	dead - 32 months	+	-	-
F / 35	**164**	Fibrillary astrocytoma	II	left temporal lobe	-	alive - no relapses	+	-	-
M/34	**216**	Protoplasmatic astrocytoma	II	left temporal lobe	N.A.	alive - relapse	+	-	-
F / 72	**21**	Giant Cell Glioblastoma (GC-GBM)	IV	frontal lobe	+	dead - 5 months	N.E.	N.E.	N.E.
F / 65	**81**	Glioblastoma (GBM)	IV	frontal lobe	+	dead - 11 months	+	+	+
M / 68	**96**	GBM	IV	frontal lobe	-	dead - 18 months	+	N.E.	N.E.
F / 66	**100**	GBM	IV	frontal lobe	-	dead - 12 months	+	+	+
M / 63	**113**	GBM	IV	*not available*	N.A.	dead - 15 months	+	-	-
M / 70	**117**	GBM	IV	*not available*	N.A.	dead - 16 months	+	-	-
M / 44	**121**	GBM	IV	left temporal lobe	+	dead - 3 months	+	-	-
M / 51	**132**	GBM	IV	left temporal lobe	+	dead - 26 months	-	-	+
F / 56	**144**	GBM	IV	*not available*	N.A.	dead - 5 months	-	-	-
M / 50	**194**	GBM	IV	right temporal lobe	+	alive - no relapses	-	+	-
M / 64	**207**	GBM	IV	*not available*	N.A.	alive - relapse	-	-	+
M / 58	**218**	GBM	IV	right temporal lobe	+	dead - 14 months	-	+	+

Table 2.1: clinic and pathological features of gliomas, divided in Oligodendrogliomas (O; n=16), Astrocytomas (A; n=7) and Glioblastomas (GBM; n=12). SVZ+ = the tumor is close to the Sub-ventricular Zone. mMGMT = methylation of *MGMT* gene. Del = deletion. N.A. = not available; N.E. = not evaluated.

2.1.3 Rodent normal brain

Rodent normal brains for Immunohistochemistry (Professor Carolina Frassoni) were obtained from three adult mice (C57B6/CD1), two adult rats (CD1) and one rat embryo at embryonic day (E) 15 from Charles River Laboratories International (Inc., Calco, Italy). Animals were brought up and sacrificed in accordance with the European Community Council Directive (86/609/EEC) and every effort was made to limit the number of animals used.

2.2 CELL CULTURES

2.2.1 Human primary glioma cell lines

A total of 21 human primary glioma cell lines were obtained from post-surgery specimens and characterized as described elsewhere [Magnani 2004; Perego 1994; Beghini 2003; Roversi 2006]. Features of cell lines are reported in table 2.2.

Cells were grown in RPMI[11] supplemented with 5% fetal bovine serum (FBS), 100 U/ml penicillin (Pen) and 100 U/ml streptavidin (Strep) at 37°C in a 5% CO_2 atmosphere. After reaching 80% confluence, cells were detached using trypsin-EDTA[12] and split.

Cells were tested by Immunofluorescence with DAPI[13] to verify the absence of mycoplasma contamination.

2.2.2 Human neural progenitor cells

ReNcellCX

The established human neural progenitor cell line *ReNcellCX* (Millipore, Billerica, MA, USA) derive from progenitors isolated from the cortex of a human fetal brain and immortalized by *c-myc* oncogene. Cells were grown as a monolayer on laminin diluted with DMEM[14]/F12 medium to 20µg/ml, and maintained by serial passages (within ten) in a defined serum-free medium supplemented with 20 ng/ml Epidermal Growth Factor (EGF) and 20ng/ml Fibroblast Growth Factor-2 (FGF-2) at 37°C in 5% CO_2 (Laminin was from Sigma, Saint Louis, MI, USA; DMEM/F12 medium and the serum-free *ReNcell NSC Maintenance Medium* were from Millipore/Chemicon; EGF was from Sigma and FGF-2 from Invitrogen, Camarillo, CA, USA).

Cells were detached using Accutase (Millipore/Chemicon) after reaching 80% confluence.

NHNP

Normal Human Neural Progenitor Cells (NHNP) (Lonza, Walkersville, MD, USA), grown as neurospheres, were kept in *Neural progenitor maintenance bulletkit* according to the manufacturer's protocol, at 37°C in a 5% CO_2 atmosphere.

[11] Developed by Moore at the Royal Park Memorial Institute.
[12] Ethylenediaminetetraacetic acid.
[13] 4',6-Di Amidino-2-Phenyl Indole.
[14] Dulbecco's Modified Eagle's Medium.

SEX/ AGE at surgery	CELL LINE	HISTOLO-GICAL DIAGNOSIS	WHO GRA-DE	KARYOTYPE
M / 4	**G91**	Pilocytic astrocytoma	I	46, XY / 92, XXYY
M / 31	**G157**	Oligo astrocytoma	II	*not evaluated*
M / 30	**G6**	Anaplastic astrocytoma (AA)	III	*not evaluated*
F / 6	**T29**	AA	III	*not evaluated*
N. A.	**G47**	AA	III	*not evaluated*
N. A.	**G110**	AA	III	*not evaluated*
F / 10	**G114**	AA	III	46, XX
N. A.	**G141**	AA	III	*not evaluated*
N. A.	**G151**	AA	III	*not evaluated*
F / 36	**MI4**	Glioblastoma (GBM)	IV	**Clone A**: 47, XX, der(1)t(1;19)(p10;p10), +7,-10, -19,+2mar **Clone B**: 45, X, -X, der(1)t(1;19)(p10;p10), del 5(p11), +7, add(9)(p11), -10, -14, -19, +1 mar **Clone C**: 48, idem, -21, +2 mar
M / 63	**G32**	GBM	IV	64, XXY, +1, +7, +7, +8, +8, +10, +13, +14, +14, +18, +19, +21, +22, +3mar
F / 73	**MI38**	GBM	IV	46, XX / 48, XXXX
N. A.	**T45**	GBM	IV	*not evaluated*
N. A.	**T51**	GBM	IV	*not evaluated*
F / 36	**MI60**	GBM	IV	45-46, XX, add(1)(q12), +7, -10, -13, -19, der(19)t(19;19)(pter;q12), del(19)(q12), -21, [+18, -22]
M / 45	**MI63**	GBM	IV	**Clone A**: 63, XXYY, +1, +1, +2, +3, +6, +8, +8, +9, +9, +20, +22, +4mar **Clone B**: 44, XY, -14, -15 **Clone C**: 40, XY, -10, -12, -14, -14, -17, -22
F / 66	**MI70**	GBM	IV	**Clone A**: 45, XX, +3, +7, -10, -14, t(18;21)(p11;p11), -21, +1 mar **Clone B**: 90, XXXX, +3, +3, +7, +7, del9(p12)x2, add(9)(q34)x2, -10, -10, -14, -14, t(18;21)(p11;p11)x2, -21 ,-21, +1mar
N. A.	**G150**	GBM	IV	*not evaluated*
M / 48	**GBM**	GBM	IV	**Clone A**: 72-74, XXYYYY, +Y, +Y, +Y, +1, -2, del(2)(p21), -5, -6, add (7)(p22), add(7)(p11)del(q34), +del(7)(p11)del(q34), add(9)(p11), add(9)(p11), -10, del(10)(p11), -12, -13, add(14)(p11), +20, +1-3 mar **Clone B:** 65-66, XYY, -X, +Y, der(1)t(1;Y)(q24;q12), -2, del(2)(p21), -4, -5, -10, -12, -13, +15, -16, -16, -17, +20, -22, +3-4mar
F / 62	**G1**	Giant cell glioblastoma (GC-GBM)	IV	68, XX, del(1)(q31.1), +3, -5, +7,+9,-10, -11, -13, -14, -17, -18, +19, +21, -22, -X, +2mar
M / 51	**MI7**	GC-GBM	IV	**Clone A**: 45, X, -Y **Clone B**: 46, X, -Y, +7 **Clone C**: 46, XY

Table 2.2: clinic and pathological features of gliomas from which the cell lines under study derive. In this study cell lines were divided in NOT-GBM (grade I, II; III) and GBM (grade IV). Data about karyotypes come from Roversi *et al.*, 2006. N.A. = not available.

2.2.3 Human primary normal cell line: fibroblasts and myoblasts

Adult fibroblasts were grown at 37°C in a 5% CO_2 atmosphere in RPMI supplemented with 10% FBS and 100 U/ml Pen-Strept.

Myoblasts were grown at 37°C in 5% CO_2 in DMEM + 20% FBS + 100 U/ml Pen-Strept + 2mM L-glutamine + 10 µg/ml insulin + 25 ng/ml FGF-2 + 10 ng/ml EGF.

2.2.4 Human glioblastoma-derived cancer stem cell lines and mouse neural stem cell lines

Human glioblastoma-derived cancer stem cell lines (GBM CSC) and a mouse neural stem cell line (NSC), both undifferentiated and differentiated, were grown, harvested and gently provided by Dr. Rossella Galli and Stefania Mazzoleni (Neural stem cell biology unit, Division of regenerative medicine, stem cell and gene therapy, Istituto scientifico san Raffaele, Milano).

GBM CSC were isolated from post-surgery specimens of primary glioblastomas, while the neural stem cell culture was established from the sub-ventricular zone of post-natal day 7 C57 mice (wild-type mice).

Characterization of GBM CSCs and NSCs stem cell lines is reported in literature [Mazzoleni *et al.* 2010; Galli *et al.* 2004; Foroni *et al.* 2007]. Briefly, tissue was dissected, enzymatically digested (in the case of GBM CSCs) and dissociated into a single cell suspension. Viable cells were plated at clonal density in DMEM/F12 medium containing 20 ng/ml of both EGF and FGF2: these serum-free, stringent and low-density conditions select away differentiated/differentiating cells, while enriching for the stem cell component (Reynolds and Rietze, Nature Methods, 2006). The resulting neurospheres were analyzed and validated for being *bona fide* stem cells, by assessing their ability for long-term proliferation, self-renewal (by subcloning experiments), multipotency (that is the ability to differentiate into the three neural cell lineages) and, for GBM CSC, tumorigenicity (by assessing their capacity to give rise to tumors *in vivo*).

L0627, L0104 and L1210 GBM CSC and Neural Stem cells were terminally differentiated in the three major neural cell types (in descending order: astrocytes, oligodendrocytes and neurons) by culturing them in mitogen-free medium supplemented with 2% FBS. Immunofluorescence for neural antigens was performed to assess differentiation.

2.3 NUCLEIC ACID AND PROTEIN EXTRACTION

Tissue samples: specimens were homogenized and divided in two equivalent parts, one was processed for nucleic acid extraction and the other for protein extraction.

Cell lines: after reaching 80% confluence, cells were harvested and washed in PBS[15]. Three pellets were destined to DNA, RNA and protein extraction, respectively.

I used three separated and specific extraction methods, when possible, to gain the best extraction results for DNA, RNA and proteins.

2.3.1 Nucleic acid extraction

RNA extraction (from cells and tissue samples) and DNA extraction (from tissue samples) were performed using the *TRIreagent* (*Total RNA Isolation reagent*, Sigma), a solution of phenol and guanidine thiocianate that dissolves cell components leaving the nucleic acids intact.

Tissue specimens were homogenized in an appropriate volume of *TRIreagent* (according to their weight) with a ULTRA-TURRAX T25 (Janke & Kunkel, IKA-Labortechnik, Staufen, Germany) homogenizer; cell pellets were instead resuspended in *TRIreagent* by repetitive pipetting. After 10 min[16] incubation, the homogenates were supplemented with chloroform, vigorously shaken and centrifuged at 14,000 rpm for 15 min at 4°C. Following centrifugation the mixture separates into three phases: RNA is in the upper-aqueous phase, DNA is in the interphase, while the lower-organic phase contains the proteins; RNA and DNA were then extracted as indicated in the manufacturer's protocol.

DNase I (RNase-free, New England Bio-Labs, Inc., Ipswich, MA, USA) was added to RNA to remove residual DNA.

DNA extraction (from cell lines)

Cell pellets were resuspended in 100 µl of PBS and DNA extracted using the *QIAmp DNA mini kit* (Qiagen S.P.A., Milano, Italy), according to the manufacturer's protocol.

RNA and DNA quantity and quality were determined by measuring absorbance at 230, 260 and 280 nm with the *ND-1000 Spectrophotometer* (NanoDrop products, Waltham, MA, USA, by Thermo Fisher Scientific, Inc.).

[15] Phosphate Buffered Saline.
[16] Minute/s.

2.3.2 Protein extraction

Cells were counted and incubated in 100 µl ***lysis buffer***/2,000,000 cells; tissue samples were homogenized using a ULTRA-TURRAX T25 homogenizer (Janke & Kunkel) in 400 µl lysis buffer/50 mg. The suspensions were placed on ice for 30 min with occasional inversion to ensure complete lysis. Lysates were then spun at 16,000 g for 25 min (at 4°C to prevent protein degradation) and the supernatant (whole cell lysate) was stored at -20°C.

Protein concentration was determined using the *BCA Protein Assay Kit* (Pierce, Rockford, IL, USA), according to the manufacturer's protocol, and the *ND-1000 Spectrophotometer*.

> ***Lysis buffer:*** 150 mM NaCl, 50 mM Tris pH 7.5, 1% NP-40, 0.25% deoxycholic acid, protease inhibitor cocktail (*Complete EDTA-free,* from Roche Diagnostic, Manheim, Germany)

MARK4 recombinant proteins

Recombinant proteins (RP) corresponding to the whole C-terminal of MARK4S and MARK4L were produced by GenScript Corporation (Piscataway, NJ, USA) and Primm (Milano, Italy), respectively. MARK4S RP is 66 aa[17] long and its theoretical molecular weight (MW) is 7 kDa[18]; conversely, MARK4L RP has a theoretical MW equal to 15.8 kDa and is 143 aa long.

Whole cell lysates of MARK4L-overexpressing HEK293T cells

Overexpression experiments were performed by Davide Rovina. Briefly, full-length MARK4L cDNA, amplified from the *ReNcellCX* cell line, was digested and cloned into the mammalian expression vector pcDNA4/HisMax (Invitrogen). This vector includes a cleavable *Xpress*™ tag for the detection of the recombinant protein with an anti-Xpress™ antibody. HEK[19]293T cells were transfected, by calcium-phosphate precipitation, with this plasmid DNA and proteins extracted.

[17] Aminoacids.
[18] Kilo Dalton.
[19] Human Embryonic Kidney.

2.4 MUTATION ANALYSIS

Partial analysis of *MARK4* genome and transcript sequence was achieved by PCR[20] and direct sequencing of most of the glioma samples under study.

2.4.1 Polymerase Chain Reaction (PCR)

To amplify *MARK4* genomic sequence (NM_031417; UCSC database) we identified primers using the *OLIGO Primer analysis* software (version 4.0; Molecular Biology Insights, Inc., Cascade, CO, USA). We looked for primer couples possibly showing a similar melting temperature and a balanced AT/GC quantity, avoided repeated sequences (e.g. LINE) and regions including SNPs, and excluded primers prone to inner secondary structures (hairpin) and/or duplex formation. Identified primers were checked with a Blast alignment (http://blast.ncbi.nlm.nih.gov/Blast.cgi) to ensure their specificity for *MARK4* sequence.

We analyzed *MARK4* exons 2-12 (corresponding to the kinase and UBA domain) and exon 13 (in keeping with literature data) with intronic primers, in order to look for mutations both in the coding sequence and in the flanking regulatory regions (involved in the splicing process). We examined all the intronic and exonic sequences among exons 15, 16 and 17, where the alternative splicing between MARK4S and L takes place (exon 16 is skipped in MARK4L). We additionally chose exonic primers to analyze possible splicing defects in *MARK4* cDNA[21] (ENST00000262891 for MARK4L, ENST00000300843 for MARK4S; Ensembl database), especially between exons 3-4, 5-6 and 11-12, where the intronic sequence was less than 100 bp[22] long and could potentially be affected by retention. In this case primers were chosen, when possible, on the boundary between flanking exons.

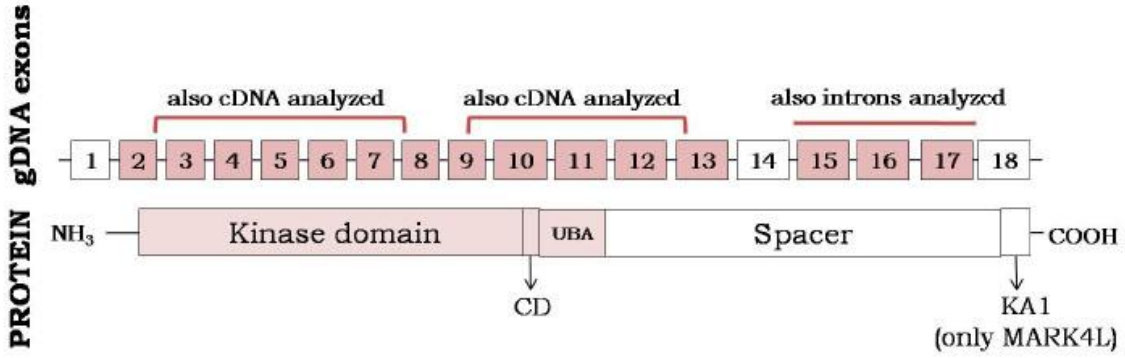

Figure 2.1: schematic representation of *MARK4* exons and respective protein domains. Colored boxes indicate the analyzed exons. [Boxes are not drawn to scale.]

[20] Polymerase Chain Reaction (PCR) technique enables to produce a huge number of copies from a specific DNA sequence, *in vitro*.
[21] Complementary DNA.
[22] Base pair.

We determined PCR conditions based on those suggested by the *Optimase Protocol Writer* software (that can be consulted at www.mutationdiscovery.com). Reactions were performed using *GoTaq polymerase* and reagents from Promega (Madison, WI, USA), and the *2720 Thermal Cycler, GeneAmp PCR system 9700* (Applied Biosystems, Foster City, CA, USA) or *My cycler* (Bio-Rad, Hercules, CA, USA) thermal cyclers were used.

PCR products were loaded on a 2% agarose gel and stained by ethidium bromide to verify that amplification occurred correctly.

PCR from genomic DNA (gDNA)

The reaction mix was prepared according to this protocol:

H_2O	to 25 µl
Buffer 5x	5.0 µl
$MgCl_2$	1.8 µl
dNTPs[23] (10 mM)	0.3 µl
DMSO[24] (for exons 2, 3-4)	0.75 µl
Forward (**F**) primer (11 pmol/µl)	0.3 µl
Reverse (**R**) primer (11 pmol/µl)	0.3 µl
Taq polymerase	0.3 µl
gDNA	50-80 ng/ µl

PCR conditions are displayed in figure 2.2:

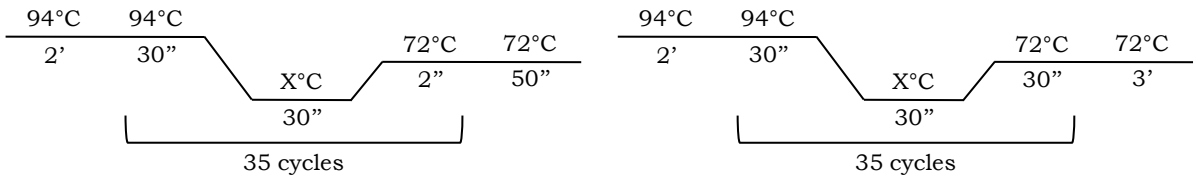

Figure 2.2: PCR conditions for exons 2-12 (on the left) and exons 13-17 (on the right).

Primer sequences, annealing temperatures and PCR fragment sizes are reported in table 2.3.

[23] De-oxinucleotide triphosphate.
[24] Dimethyl Sulfoxide.

PRIMER NAME	PRIMER SEQUENCE	FRAGMENT LENGTH	ANNEALING TEMPERATURE
Exon 2	**F** 5' ggaaggtgggattggatagc 3'	310 bp	60°C
	R 5' aacatacaccgaagacctgg 3'		
Exons 3-4	**F** 5' caccttgaccgtccctcc 3'	320 bp	61.7°C
	R 5' cctgcccctgctcccatt 3'		
Exons 5-6	**F** 5' cctttctccctaatgcccta 3'	342 bp	59°C
	R 5' accatgcccagctctcag 3'		
Exon 7	**F** 5' ggagccacaaataaccaacc 3'	283 bp	56.4°C
	R 5' ctggaggaatttgctggagg 3'		
Exon 8	**F** 5' gccttgagtcccactttcc 3'	430 bp	61.7°C
	R 5' gacttgaatcctgcccatc 3'		
Exon 9	**F** 5' agacccccctcctccagtaac 3'	362 bp	62.5°C
	R 5' ggcagagtttaggggagtca 3'		
Exon 10	**F** 5' agatgatgcggaggaggga 3'	360 bp	63°C
	R 5' tgggtgacaggatggctctc 3'		
Exons 11-12	**F** 5' gttaaagtttctgggagtctga 3'	491 bp	58.8°C
	R 5' acgtaactgtaagtctgggc 3'		
Exon 13	**F** 5' gtgcgttggtaatcttgagg 3'	455 bp	58.3°C
	R 5' gaatgagatgaaggcagggc 3'		
Exons 15-16	**F** 5' cctgcctcagtcccccaccc 3'	664 bp	69.5 ->62.5 °C
	R 5' tgcccgcacacacaggtcag 3'		
Intron 16a	**F** 5' cctgcatgtctgacctgtgt 3'	781 bp	57°C
	R 5' ctgttgccaagactgatgatc 3'		
Intron 16b	**F** 5' gagcccagaagttcaagacc 3'	641 bp	60°C
	R 5' acacacacactccctcgct 3'		
Exon 17	**F** 5' gggcaggcctcacgaaggag 3'	608 bp	63°C
	R 5' ggtgcttggggttgggtggg 3'		

Table 2.3: primer sequences, PCR fragment sizes and annealing temperatures for *MARK4* gDNA analysis. A Touchdown PCR protocol was chosen for exons 15-16.

PCR from cDNA

cDNA was obtained by Reverse Transcription PCR (see 2.5.1); the reaction mix was prepared and PCR performed according to this protocol:

H_2O	to 25 µl
Buffer 5x	5.0 µl
$MgCl_2$	1.5-2 µl
dNTPs (10 mM)	0.5 µl
Taq polymerase	0.3 µl
F primer (11 pmol/µl)	0.4 µl
R primer (11 pmol/µl)	0.4 µl
cDNA	20-40 ng

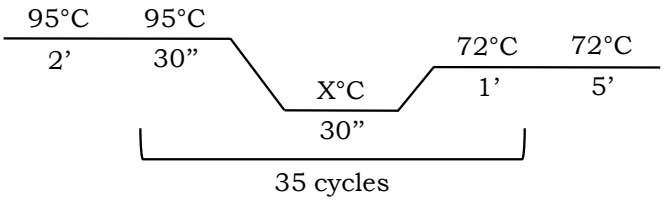

Primer sequences, annealing temperatures and PCR fragment sizes are reported in table 2.4:

PRIMER and ANNEALING TEMPERATURE	**PRIMER SEQUENCE**	**FRAGMENT LENGTH**
cDNA - exons 2-8 58°C	**F** 5' ggtcgggaggttgccatc 3'	316 bp (wild-type) 406 bp (intron 5-6 retention) 468 bp (intron 3-4 retention) 558 bp (retention of both the introns)
	R 5' ggttctcagccttcaggtcc 3'	
cDNA - exons 9-13 53.9°C	**F** 5' ctaaacgctgtactctcg 3'	395 bp (wild-type) 486 bp (intron 11-12 retention)
	R 5' gccacagaaatcgctatg 3'	
cDNA - exons 15-18 62°C	**F** 5' ctgacctccaaactgacccg 3'	283 bp (wild-type, MARK4L) 363 bp (wild-type, MARK4S)
	R 5' cgaagtgggacaggggctc 3'	

Table 2.4: annealing temperatures, primer sequences and PCR fragment sizes for *MARK4* exons 2-8, 9-13, and 15-18 (cDNA).

2.4.2 Sequencing[25] analysis

PCR products were sequenced using the *Big Dye Terminator v.3.1 Cycle Sequencing Kit* (Applied Biosystems), consisting of a 5x saline buffer and a premix with DNA polymerase, dNTPs and fluorescine-labelled ddNTPs[26] (terminators). For each exon two separate reactions were performed, one with the forward primer and one with the reverse one.

Reactions were carried out according to this protocol:

H_2O	5.2 µl
Buffer 5x	1.5 µl
Premix	1.0 µl
Primer (11 pmol/µl)	0.3 µl
PCR product	2.0 µl (opportunely diluted to have 5-20 ng of DNA)

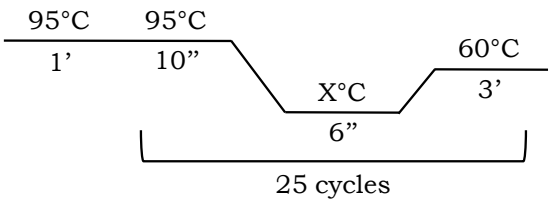

Annealing temperature was chosen among 50°C and 60°C in accordance with each primer melting temperature.

Reaction product was precipitated by adding 2.5 volumes of 95% ethanol for 15 min and by centrifuging at 13,000 rpm for 15 min. After a wash with cold 70% ethanol, sequence reaction was spun at 13,000 rpm for 10 min and air dried.

Samples were sequenced by Primm (Milano, Italy) and electropherograms aligned and analyzed with *ChromasPro* software (version 1.42; Technelysium Pty Ltd, Tewantin QLD, Australia). Sequences were compared with the wild-type *MARK4* genomic sequence (NM_031417; UCSC database) and cDNA sequence (ENST00000262891 for MARK4L, ENST00000300843 for MARK4S; Ensembl database).

[25] Based on Sanger method.
[26] Dide-oxinucleotide triphosphate.

2.5 GENE EXPRESSION ANALYSIS

To quantify *MARK4* S and L expression levels we carried out Real-time quantitative PCR on cDNAs from tissue samples and cell lines under study. cDNA was obtained through reverse transcription of extracted RNAs.

2.5.1 Reverse transcriptase PCR (RT-PCR)

Reverse transcriptase PCR (RT-PCR) allows transcribing the messenger RNA (mRNA) into its complementary DNA (cDNA) by using the *reverse transcriptase* enzyme.

500 ng of RNA extracted from cell lines and 250 ng of RNA from tissue samples were processed using the *High capacity cDNA reverse transcription kit* (Applied Biosystems), with random examers, according to the manufacturer's protocol.

All mRNAs were reverse-transcribed in two independent reactions; to verify that cDNAs were efficiently generated by RT, we performed a PCR amplifying the housekeeping gene *GAPDH*[27], using the previously reported PCR conditions and these specific *GAPDH* conditions:

forward primer sequence: 5'-ACAACAGCCTCAAGATCATCAG-3';
reverse primer sequence: 5'-GGTCCACCACTGACACGTTG-3';
annealing temperature: 62°C.

2.5.2 Real-time quantitative PCR

The Real-time PCR enables to measure the cDNA quantity of a target gene with high sensitivity, specificity and reproducibility. This technique is based on a traditional Polymerase Chain Reaction with the addition of a TaqMan probe that is complementary to an inner region of the PCR product (hence it is specific for the target gene) and emits a fluorescent signal every time the template is amplified[28]. Detected fluorescence is therefore directly proportional to the accumulation of PCR products.

Data are analyzed during the PCR exponential phase and revealed by the instrument at a particular cycle (named C_T = Threshold cycle), at which the amount of PCR products generated is directly proportional to the original quantity of the target gene cDNA. Data normalization is needed for relative quantification, and control genes, which are constitutively expressed endogenous genes, are generally used for this aim.

Assays, data analysis and statistics were set with Dr. Silvia Tabano and Laura Fontana.

[27] GlycerAldehyde 3 Phosphate DeHydrogenase. A housekeeping gene is a constitutively expressed gene.
[28] TaqMan probe is an oligonucleotide with a Reporter fluorophore on the 5' end and a Quencher dye on the 3' end. During PCR elongation the DNA polymerase breaks the probe so that the Reporter fluorophore is no longer switched off by the Quencher and the emitted fluorescence is recorded.

TaqMan assays and Real-time PCR

We performed Real-time PCR with the *TaqMan Fast Universal PCR Master Mix 2x No AmpErase UNG* (consisting of DNA polymerase, buffer and dNTPs) and *TaqMan Gene Expression Assays* (specific for each target or control gene), all from Applied Biosystems. Features of the TaqMan assays are reported in table 2.5:

ASSAY	**PRIMER SEQUENCE**	**PROBE SEQUENCE**
MARK4L	**F** 5' CCGAAGGGTCGCAGACGAA 3'	5' CCTGAGGTCACAAGTT 3'
	R 5' CCGTTTGATCCCAAGGTAGATG 3'	
MARK4S	**F** 5' GTTACCCTCGATCCCTCTAAACG 3'	5' CAGAACTCTAACCGCTGTGT 3'
	R 5' GTTCGTCTGCGACCTGATCTT 3'	
ACTIN β	*Inventoried assay reagent;* ID: Hs99999903_m1	
GAPDH	*Pre-developed assay reagent*; ID:4333764F	
HPRT[29]	*Inventoried assay reagent;* ID: Hs99999909_m1	
RPLPO[30]	*Pre-developed assay reagent*; ID:4333761F	
18s[31]	*Inventoried assay reagent;* ID: Hs99999901_s1	

Table 2.5: primer and probe sequences for MARK4S and L *Assays on demand*; ID for control gene assays.

MARK4 probes and primers were identified so as to have specific assays for each of the two isoforms and, when possible, we chose them on the boundary between exons, to avoid genomic DNA amplification.

MARK4S forward primer and probe bind exon 16, which is absent in MARK4L mRNA, and reverse primer is on the boundary between exons 16 and 17. MARK4L forward primer was placed between exon 15 and 17 (adjacent to each other in MARK4L mRNA), while the probe and reverse primer bind exon 18.

For each assay the following mix was prepared:

H_20	2.5 µl	20 µl of cDNA underwent a 1.5 fold
Master Mix (2x)	5.0 µl	dilution and 1.5 µl were added to the
Assay (20x)	0.5 µl	reaction mix.

[29] Hypoxanthine-guanine PhosphoRibosylTransferase.
[30] Ribosomal Phosphoprotein Large PO.
[31] Eukaryotic 18s rRNA.

Reactions were performed on the *StepOne Real-Time PCR System* (a particular thermal cycler that also detects and records fluorescent signals; Applied BioSystems), under these conditions:

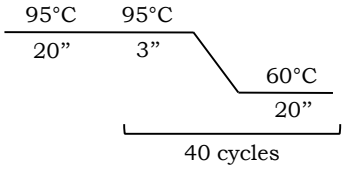

All samples were reverse transcribed in two independent reactions and loaded in triplicate in Real-time experiments.

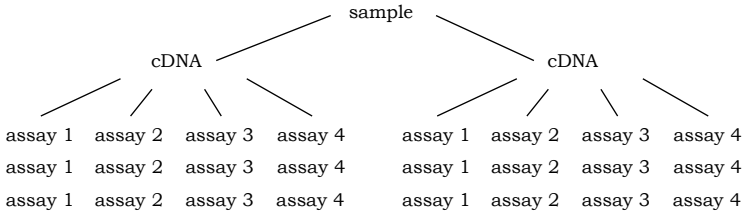

Relative quantification analysis

C_T data were recovered from the *StepOne Software* (v1.2; Applied Biosystems); the three values for each assay were averaged (arithmetic mean) and then analyzed using two different methods: the $2^{-\Delta\Delta C_T}$ method (also known as Livak method, [Livak 2001]) for cell lines (being more homogeneous, a single control gene was sufficient) and the geNorm method ($E^{-\Delta C_T}$) [Vandesompele 2002] for tissue samples and stem cell lines.

In both cases, MARK4S and L (target genes) expression levels were normalized by control genes and then referred to a sample chosen as reference (NHNP for cell lines and HNB for tissue specimens and stem cell lines), whose expression value was set as 1. Values with standard deviation exceeding 0.5% or standard error exceeding 0.3% were excluded and experiments repeated.

According to Livak method,

for each sample the **target gene expression level = $2^{-\Delta\Delta C_T}$**

where: $\Delta\Delta C_T$ = sample ΔC_T – reference ΔC_T;

sample ΔC_T = [target gene C_T – control gene C_T] in the sample;

reference ΔC_T = [target gene C_T – control gene C_T] in the reference;

(*sample and reference ΔC_T correspond to the mean value between the ΔC_Ts of the two independent RT reactions*)

In the geNorm method, instead, multiple control genes are used and the amplification efficiency (E, set as 2 in the $2^{-\Delta\Delta C_T}$ method) is calculated for each assay, taking into account the different efficiency of each assay.

Briefly,

1) for each assay, serial dilutions of a pool of cDNAs are processed by Real-time PCR and C_T values are put in a graph with the respective logarithmic dilution values. The **amplification efficiency E** corresponds to $\mathbf{10^{-1/S}}$, where S is the slope of the line interpolating all the C_Ts.
2) for each assay, the **relative quantity** (Q) is calculated: $\mathbf{Q = E^{-\Delta C_T}}$

   where ΔC_T = sample C_T – reference C_T
3) for each sample, **normalization factor** (NF) is set on the basis of the geometrical mean (GM) of the relative quantities (Qs) of control genes:

   NF = GM of control gene Qs for each sample / GM of all the GMs
4) for each sample, the **target gene relative quantity = Q / NF** is calculated.

Final target gene relative quantity corresponds to the mean value between those of the two independent RT reactions.

Real-time expression data were expressed as mean ± standard error.

For statistical analysis the Kruskal-Wallis test (H test) was used. This is a nonparametric (distribution free) analysis of variance.

In H test, null hypothesis (H_0) assumes that the samples are from identical populations. First, data of both samples need to be arranged in a single series in growing order and ranks are assigned to each of them. The following formula allows calculating the value of Kruskal-Wallis test (H):

$$H = \frac{12}{n\,(n+1)} \sum \frac{R_i^2}{n_i} - 3\,(n+1)$$

where n=total number of data in all samples; R_i=rank of each datum

The *StatistiXL 1.8* software for Microsoft Excel (www.statistixl.com) also calculates the probability that the differences between the two samples occur by chance. If this value is lower than 0.05 (H_0 was set as true with 95% probability), the null hypothesis must be rejected and you will say that the sample comes from a different population, or, in other word, that the differences found in the two data sets are statistically significant. The t-test (Student's test) was also used.

2.5.3 TaqMan assay validation

Before performing the relative quantification analysis on the samples under study, we evaluated amplification efficiency and stability of all the assays (MARK4S, MARK4L, *actin β*, *GAPDH*, *HPRT*, *RPLPO*).

Assay amplification efficiency

For each assay, we performed Real-time PCR on serial dilutions of a pool of glioma cDNAs. The obtained C_T values were put in a graph with the respective logarithmic dilution values and were interpolated by a line. Amplification efficiency (E) was calculated according to the $E=10^{-1/S}$ formula (S is the slope of the interpolating line) and was near 2 for all the assays (table 2.6). A 100% amplification efficiency has the E value equal to 2, since ideally PCR product quantity should double at every cycle, therefore all the tested assays proved to have a very good amplification efficiency.

Assay stability

Assay stability is the ability to amplify the target gene with the same efficiency in a broad range of sample dilutions.

To assess this parameter, we first calculated the relative quantity (Q) of each gene in the cDNA serial dilutions, according to the following formula: $Q=E^{-\Delta C_T}$ (ΔC_T =sample C_T – reference[32] C_T) and then used the *GeNorm* software (version 3.5; http://medgen.ugent.be/jvdesomp/genorm/) to sort the assays on the basis of their stability (table 2.6). We therefore decided to use *GAPDH* and *actin β* as control genes, since they were the most stable ones.

GAPDH was used for cell lines (being more homogeneous, a single control gene was sufficient) and *GAPDH* + *actin β* for tissue samples and stem cell lines. *rRNA 18S* was additionally used for the simultaneous normalization of mouse and human samples (GBM CSC and NSC).

[32] In this case the reference was the less diluted sample.

ASSAY	DILUTIONS	C_T	S	E	ΔCt	RELATIVE QUANTITY	STABILITY
GAPDH	1	16.52	-3.30	**2.01**	0.00	1.00	**more stable** ↑
	1:10	19.73			3.21	0.11	
	1.100	23.05			6.52	0.01	
	1:1000	26.41			9.89	0.00	
ACTB	1	16.78	-3.65	**1.88**	0.00	1.00	
	1:10	20.35			3.57	0.11	
	1.100	24.02			7.25	0.01	
	1:1000	27.71			10.93	0.00	
RPLP0	1	17.74	-3.28	**2.02**	0.00	1.00	
	1:10	20.85			3.10	0.11	
	1.100	24.18			6.44	0.01	
	1:1000	27.56			9.82	0.00	
HPRT	1	21.78	-3.31	**2.00**	0.00	1.00	
	1:10	24.95			3.18	0.11	
	1.100	28.20			6.43	0.01	**less stable** ↓
	1:1000	31.74			9.96	0.00	
MARK4L	1	23.75	-3.40	**1.97**	0.00	1.00	
	1:10	27.00			3.25	0.11	
	1.100	30.50			6.75	0.01	
	1:1000	33.92			10.17	0.00	
MARK4S	1	28.00	-3.54	**1.92**	0.00	1.00	
	1:10	31.26			3.25	0.11	
	1.100	35.00			6.99	0.01	
	1:1000	N.D.			/	/	

Table 2.6: assay amplification efficiency (E) and stability. For each assay, C_T values (3rd column), corresponding to serial dilutions of a pool of glioma cDNAs (2nd column), are displayed. S=slope of the interpolating line. N.D.=undetermined.

2.6 IMMUNOBLOTTING

The Immunoblotting technique allows to separate proteins, according exclusively to their molecular weight, and to identify the presence/absence of a specific protein, its size and its relative expression level.

Equal amounts of the extracted proteins (usually 20 µg) were supplemented with reducing SDS[33] loading buffer (*Blue loading buffer pack,* Cell Signaling Technology, Inc., Beverly, MA, USA) and denatured at 99°C for 3 min.

Proteins were separated by 4% (stacking; 100V) and 10% (resolving; 130V) SDS PolyAcrylamide Gel Electrophoresis (SDS-PAGE). Proteins were then transferred by electroblotting to a PVDF[34] membrane (Roche). *Mini-PROTEAN Tetra cell* and *Trans-blot semi-dry electrophoretic transfer cell* (both Bio-Rad) were respectively used for electrophoresis and electroblotting (10V, 30 min) as instructed by the manufacturer. The molecular weight standard were *Biotinylated protein ladder* (Cell Signaling Technology) and *ColorBurst electrophoresis marker* (Sigma).

Membranes were then washed twice (10 min each) in ***PBS-T*** and non-specific binding was blocked by incubating the membranes in 5% skimmed milk, PBS-T for 1.5 hours at Room Temperature (RT), in agitation.

PBS-T: PBS – 0.6% Tween20
PBS pH7.5: 100 mM NaCl, 80 mM HNa_2O_4P, 20 mM NaH_2PO_4.
Tween20 was from Sigma.

The membranes were incubated with primary antibodies (in PBS-T) at 4°C overnight in agitation, washed five times in PBS-T and then incubated with secondary antibodies (in PBS-T) at RT for 1.5 hours in agitation.

Primary antibodies *and dilutions**:***	
Rabbit anti-**MARK4L** (not commercial; GenScript Corporation)	1:5,000
Mouse anti-**GAPDH** (ab8245; Abcam, Cambridge, UK)	1:10,000
Rabbit anti-**MARK4S** (not commercial; GenScript Corporation)	1:6,500
Rabbit pre-immune serum (GenScript)	1:5,000

For quantification, the membranes were cut horizontally immediately after the blocking step and incubated with the appropriate antibodies.

[33] Sodium Dodecyl Sulphate.
[34] Polyvinylidene fluoride.

Secondary antibodies *and dilutions**:***	
Goat anti-rabbit IgG-HRP (sc-2004; Santa Cruz Biotechnology)	1:10,000
Goat anti-mouse IgG-HRP (sc-2005; Santa Cruz Biotechnology)	1:10,000
Anti-biotin, HRP-linked antibody (Cell Signaling)	1: 2,500

The secondary antibodies are conjugated to HRP (Horse Radish Peroxidase), the anti-biotin antibody allows detecting the biotinylated protein ladder.

After four washes in PBS-T and two washes in PBS, the bound antibodies were detected by covering the membranes with a peroxide/enhancer solution (*Protein detection system* from GeneSpin, Milano, Italy) for 5 min, exposing an *Amersham Hyperfilm ECL* plate (GE Healthcare, Waukesha, WI, USA) to the membrane, and developing the plate by *Dental X-Ray developer* and *Dental X-Ray fixer* (Kodak; Bagnolet Cedex, France).

2.6.1 Semi-quantitative analysis

To compare MARK4L protein expression in different samples we did a relative quantification analysis, using GAPDH as normalizer (to correct differences in lysate loading, protein transfer and antibody binding). We performed a double Immunoblotting experiment for every sample and used the same conditions for all the experiments. For quantification, a low exposure time was chosen, so that the signal intensity on the plate was directly proportional (in the linear range) to the emitted signal intensity.

TIF images were acquired from plates using a scanner and analyzed with the *Image J* software. *Image J* is a public domain JAVA image processing program (http://rsbweb.nih.gov/ij) and allows analyzing one-dimensional electrophoretic gel or membrane using a simple graphical method (http://rsbweb.nih.gov/ij/docs/menus/analyze.html). Briefly, each lane (including both MARK4L and GAPDH bands) was selected and lane profile plots were generated, displaying a two-dimensional graph reporting peaks corresponding to gel bands (on the X-axis) and their relative pixel intensities (on the Y-axis). After manually subtracting the background (required step to compare different plates), we measured the area of each peak of interest in square pixels. In each sample MARK4L area value was divided by the respective GAPDH value to normalize data.

MARK4L expression levels shown in this thesis are referred to a sample chosen as reference (NHNP for cell lines and HNB for tissue specimens), whose value was set as 1.

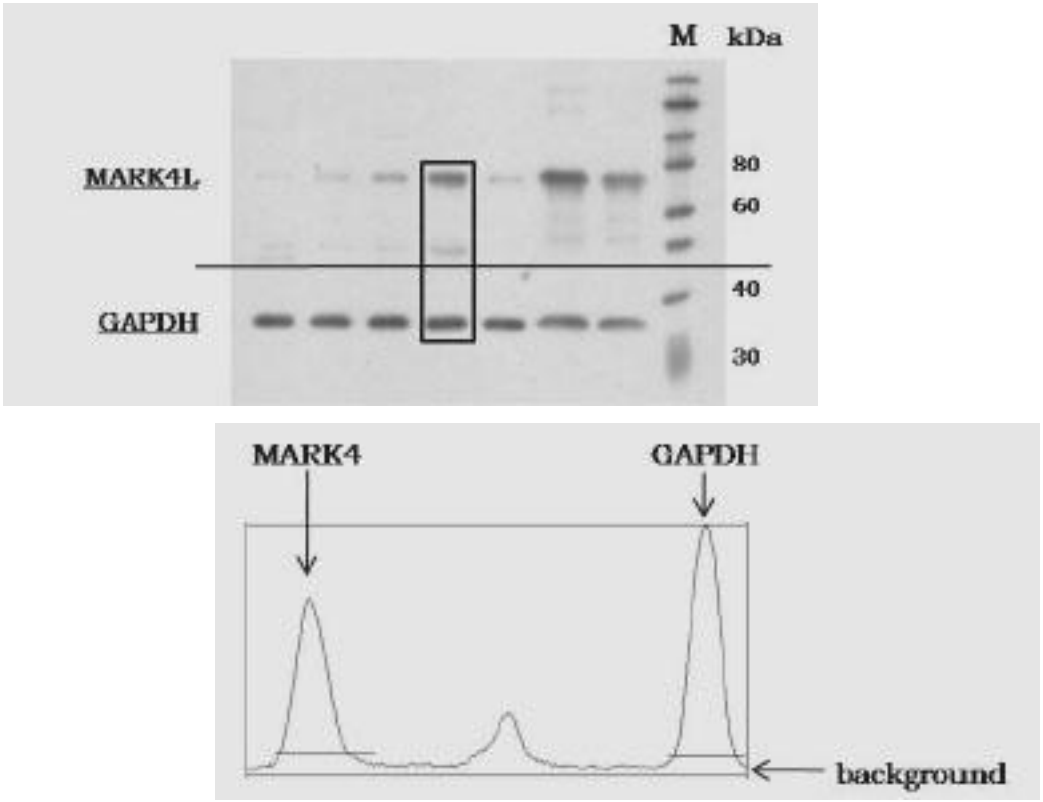

Figure 2.3[35]: [upper] one of the immunoblots analyzed with Image J software. The membrane was cut horizontally and incubated with anti-MARK4L (upper) and anti-GAPDH (lower) antibodies. The box indicates one of the lanes, selected to generate its profile plot in Image J **[lower]**. In the profile plot MARK4L and GAPDH peaks are indicated and background subtracted by manually defining the peak boundaries with a line. M=molecular weight standards.

[35] Only in this digital copy, low-resolution and degraded images are displayed.

2.7 IMMUNOFLUORESCENCE

ImmunoFluorescence (IF) enables to visualize the subcellular localization of a specific protein in cultured cells; IF experiments shown in this thesis were set by Dr. Ivana Magnani.

For IF analysis cells were seeded on glass chamber slides or round coverslips of Ø 1cm (for GBM-CSC and NSC) and processed at approximately 70% confluence.

For the better visualization of centrosomes, cells were washed in microtubule-stabilizing buffer[36] (0.1% Triton X-100, 80 mM PIPES[37], pH 6.9, 5 mM EGTA[38], 1 mM $MgCl_2$), fixed with methanol for 10 min at -20°C or with 2x paraformaldehyde (PFA) in PBS for 30 min on ice, and permeabilized in 0.1% Triton X-100 for 2 min.

Otherwise cells were washed in PBS, fixed with methanol for 10 min at -20°C or with 2x paraformaldehyde, and permeabilized in 0.1% Triton X-100 for 10 min.

Non-specific binding was blocked by incubating the fixed cells with 5% bovine serum albumin (BSA) in PBS for 10 min, before incubation with primary antibodies:

Primary antibodies *and dilutions**:***	
Rabbit anti-**MARK4L** (not commercial; GenScript)	1:100
Rabbit anti-**MARK4S** (M4947, Sigma)	1:200
Mouse anti-**γtubulin** (clone GTU-88; Sigma)	1:100/200
Mouse anti-**nucleolin** (C23 D-6, Santa Cruz Biotechnology)	1:100
Mouse anti-**nucleophosmin** (B23; clone FC82291, Sigma)	1:200

Antibodies were diluted in PBS with 0.1–0.5% Tween20, 2% BSA and 1% goat serum[39] (Sigma). MARK4L, MARK4S and γ-tubulin were incubated overnight at 4°C in a humidified chamber; nucleolin was incubated for 1 hour at RT.

After three washes in PBS, the secondary antibodies were incubated for 1 hour at RT in a dark humidified chamber:

Secondary antibodies *and dilutions**:***	
Goat anti-rabbit IgG-FITC[40] (Sigma)	1:200
Goat anti-mouse IgG-TRITC[41] (Sigma)	1:200

[36] Based on the protocol by T. Raemaekers (2003) with little variations.
[37] 1,4-piperazinediethanesulfonic acid.
[38] Ethylene Glycol Tetraacetic Acid.
[39] To reduce non-specific binding, the serum of the animal where the secondary antibodies are raised (goat) is added.
[40] Fluorescein IsoThioCyanate.
[41] TetramethylRhodamine IsoThioCyanate.

Antibodies were diluted in PBS with 0.1–0.5% Tween20, 2% BSA and 1% goat serum.

The slides were then washed three times in PBS, mounted with DAPI in antifade (Vector Labs, Burlingame, CA, USA) and examined using an Olympus IX51 inverted fluorescence microscope, equipped with an Olympus DP71 super high-resolution colour digital camera and U-MNIBA2 excitation 460/490 (FITC), U-MWIG3 excitation 530/550 (TRITC) and U-MNU2 (DAPI) filters.

Images were acquired and processed using the F-View II-Bund-cell F software (Olympus, Tokyo, Japan).

For ***RNA digestion,*** cells were permeated with 0.1% Triton X-100 for 5 min and subsequently RNA was digested with 800µ/ml RNase A (Sigma) + 5 µl of RNase Cocktail (Ambion) in 1xPBS for 30 min at RT.

2.8 IMMUNOHISTOCHEMISTRY

ImmunoHistoChemistry (IHC) allows to visualize, in tissue sections, the localization of a target protein (in specific cell types or tissue areas) and to *in situ* qualitatively assess its relative expression levels.

2.8.1 IHC on human, mouse and rat brain samples

Immunohistochemistry experiments on human, mouse and rat normal brain samples were set, performed and interpreted by Dr. Ramona Moroni and Professor Carolina Frassoni (Clinical epileptology and experimental neurophysiology unit, Istituto neurologico Carlo Besta, Milano).

Brain specimens were fixed in 4% PFA in 0.1M phosphate buffer (PB; pH 7.2), paraffin embedded and sectioned (10 µm) on a microtome.

After deep anaesthesia, the animals were perfused transcardially with 4% PFA in 0.1M PB. Their brains were dissected out, post-fixed in 4% PFA for 12 h, embedded in paraffin, and sectioned (10 µm).

The sections were dewaxed in xylene, rehydrated, and treated in a microwave oven (in Na-citrate 0.01M, pH 6.0). After three washes in PBS, the endogenous peroxidases were blocked with 1% H_2O_2. The sections were washed again in PBS, incubated in 1% BSA (Sigma) with 0.2% Triton X-100 for 1 hour, and then overnight in primary antibodies at 4°C in a humid chamber.

Primary antibodies *and dilutions**:***	
Rabbit anti-**MARK4L** (not commercial; GenScript)	1:500
Rabbit anti-**MARK4S** (not commercial; GenScript)	1:500
Rabbit anti-**MARK4S** (M4947, Sigma)	1:1000

Antibody staining was revealed using a biotinylated goat anti-rabbit IgG (Vector Labs) diluted 1:200 with 0.1% BSA in PBS.

The avidin-biotin-peroxidase protocol (ABC; Vector Labs) was followed, with DAB[42] (Sigma) being used as the chromogen.

[42] 3,3 DiAminoBenzidine.

2.8.2 IHC on glioma sections

Immunohistochemistry on glioma sections was set, performed and analyzed by Delfina Tosi and Professor Dario Bauer (Anatomical pathology, Department of Medicine, surgery and dentistry, Università degli studi di Milano, Milano).

IHC was performed on formalin-fixed paraffin embedded tissue sectioned at 3 mm onto positively charged slides (*Superfrost plus*, Menzel-Glaser, Germany). Paraffin sections were subjected to heat-induced epitope retrieval with citrate, pH 6.0. After inhibition of endogenous peroxidase, the slides were incubated with primary antibodies over night at 4°C. When using the anti-MARK4S antibody by Sigma, slides were first blocked with casein in saline phosphate for 45 min; anti-MARK4S antibody from GenScript was instead kept 1 hour at RT.

Primary antibodies *and dilutions**:***	
Rabbit anti-**MARK4L** (not commercial; GenScript)	1:1000
Rabbit anti-**MARK4S** (not commercial; GenScript)	1:600
Rabbit anti-**MARK4S** (M4947, Sigma)	1:1000

Slides were then incubated with a polymer penetration enhancer (*Novolink Polymer - anti mouse-rabbit IgG-poly-HRP*, Leica Mycrosystems and Menarini Diagnostics) containing 10% (v/v) animal serum and DAB chromogenic substrate (Dako or Vector Labs, Burlingame, CA, USA), counterstained with hematoxylin and coverslipped.

Labelling intensity and the proportion of immunopositive cells were assessed by light microscopy and independently evaluated by two investigators (D.B. and D.T.) with a minimum of 100 cells detected in each specimen. Staining intensity was graded visually on a scale ranging from 0 to 3 (0 = no staining; 1 = weak immunoreactivity; 2 = moderate staining; 3 = strong immunoreactivity). Labelling extent was scored following the percentage of immunopositive cells: 0 ≤ 5%; 1 = 6-35%; 2 = 36-66%; 3 ≥ 67%. Intensity and extent scores were multiplied to obtain the composite score, with the maximum value being 9 [Chauhan 2007].

Results

Aiming at enriching literature data on MARK4 involvement in neurons and in glial tumors in the Central Nervous System, this project further characterizes the role of both MARK4 isoforms (L and S) in gliomas and in brain, by means of different techniques.

As mutations in protein kinase genes are often implicated in the initiation and development of cancer, we first investigated whether genomic mutations could affect *MARK4* gene in glial tumors. We then analyzed MARK4L and S localization and expression pattern in a wide panel of gliomas, in glioblastoma-derived cancer stem cells, in normal brain and in neural stem cells, by Real-time quantitative PCR, Immunoblotting, Immunofluorescence and Immunohistochemistry.

3.1 MUTATION ANALYSIS

Results by array-CGH analysis on a representative collection of human glioma cell lines, which are included in the current work, showed that *MARK4* genomic region is not over-represented, with only one exception (MI4 cell line, which is duplicated), allowing to rule out increased gene dosage/amplification as underlying cause of MARK4 expression in glioma [Roversi 2006].

We then performed mutation analysis of the functionally relevant *MARK4* regions and of exons whose alterations are described in literature (exons 5, 8, 9, 12, 13), screening the kinase domain (exons 2-10), the ubiquitin-associated (UBA) domain (exons 10-12) and exon 13 (a schematic representation of the analyzed regions is reported in figure 3.1). By direct sequencing we looked for mutations both in the coding regions and in the flanking regulatory sequences. A subset of 12 glioma cell lines and 12 glioma tissue samples of different malignancy grade were tested.

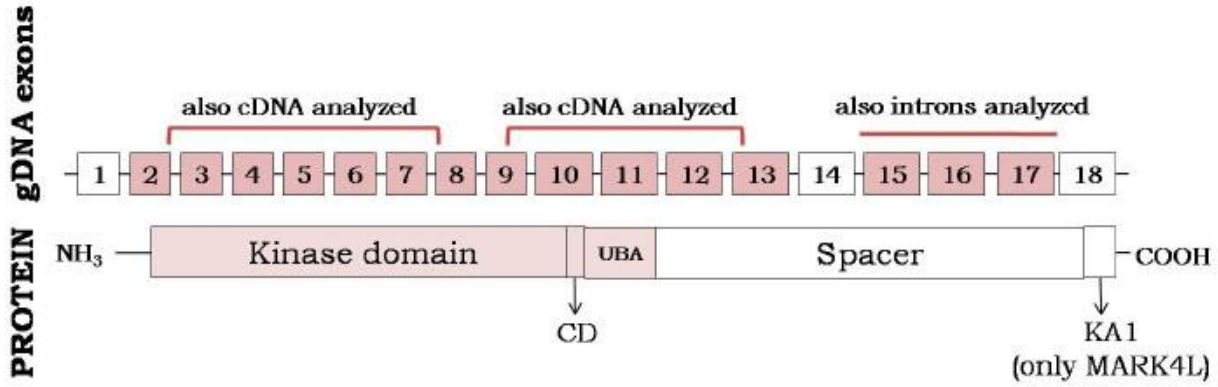

Figure 3.1: schematic representation of *MARK4* exons and respective protein domains. The colored boxes indicate the analyzed exons, covering 70% of *MARK4* coding sequence. [Boxes are not drawn to scale.]

We only found a synonymous substitution in a glioblastoma cell line (GBM) cell line which carries the c1101G>C variation in exon 11, occurring at the third base position of codon 367 and specifying the same amino acid (leucine). We couldn't find out whether this mutation occurred in culture or was present in the original tumor, or it was of somatic or germinal origin. Anyway, the variation does not affect the splicing process, as confirmed by cDNA analysis.

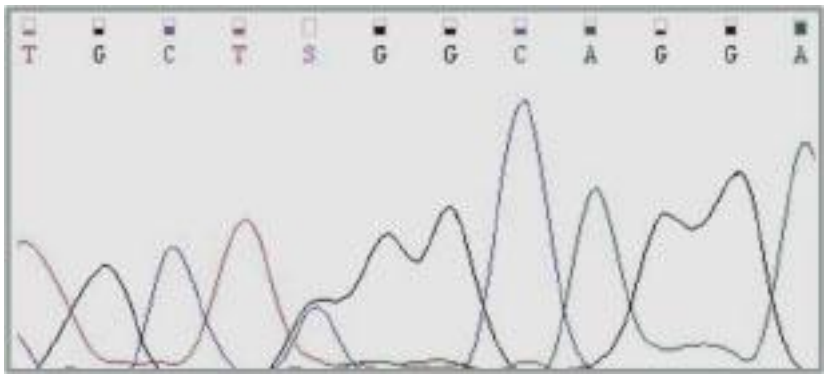

Figure 3.2[43]**:** GBM exon 11 electropherogram displaying the C>G variation.

MARK4 gene is characterized by the presence of short introns that could potentially be retained in the mature mRNA. Intron retention between exons 3-4 (152 bp), 5-6 (90 bp) and 11-12 (91 bp) was tested by performing PCR (and occasionally direct sequencing) on cDNA, but no splicing errors were detected.

Since *MARK4* undergoes alternative splicing (exon 16 is skipped in MARK4L), we examined all the genomic sequence between exons 15 and 17. We only found a yet unreported single nucleotide alteration, c1878-61G>A, in intron 16, which was present in 5/19 cell lines and in 3/12 tissue samples. This variation does not affect the splicing process, as confirmed by cDNA analysis.

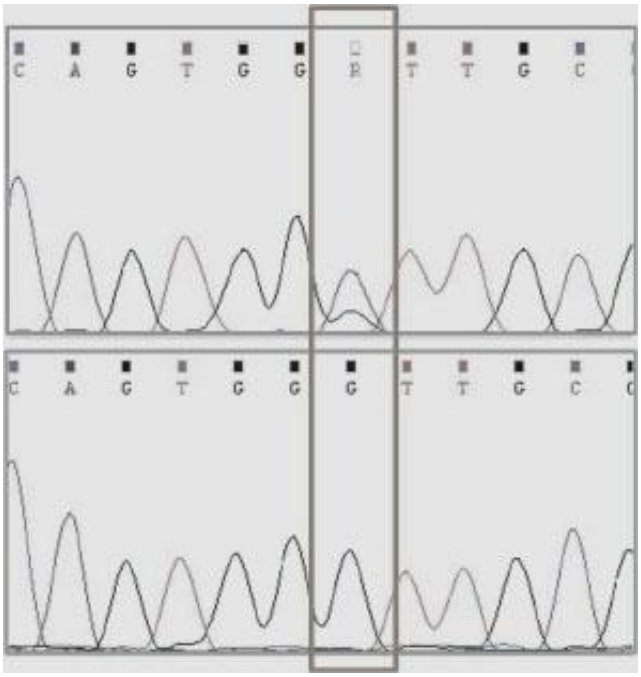

Figure 3.3: intron 16 electropherograms. Tissue sample 219, carrying the A>G alteration, is shown in the upper panel; wild-type sequence of tissue sample 112 is displayed in the lower panel.

[43] Only in this digital copy, low-resolution and degraded images are displayed.

3.2 MARK4 ANTIBODY VALIDATION

Anti-MARK4 antibodies used in our experiments were obtained by immunizing rabbits with different antigens from MARK4 C-terminal sequence, so as to have isoform-specific antibodies.

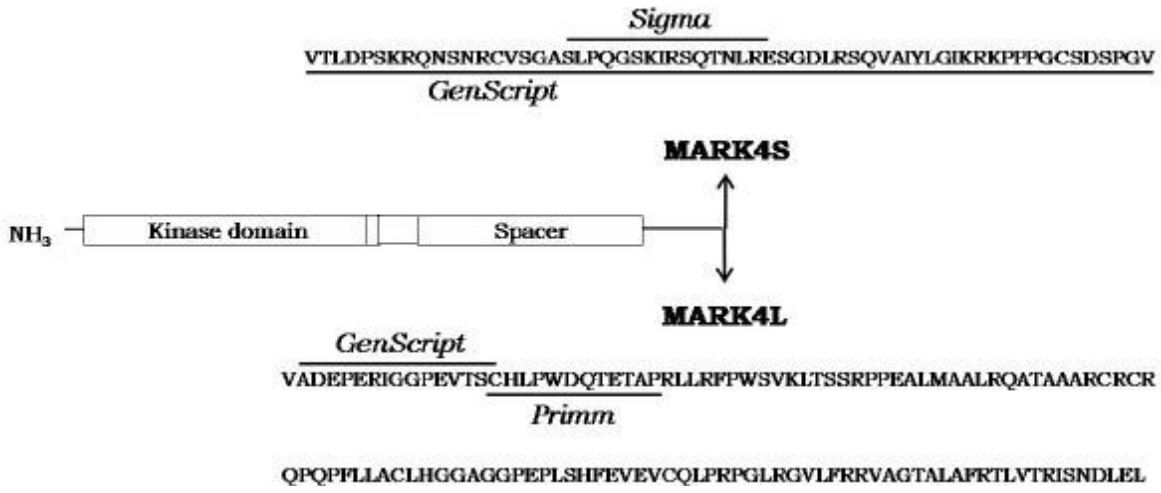

Figure 3.4: schematic representation of MARK4S and MARK4L proteins.
The two isoforms differ in the C-terminal region: protein sequences are reported and antigens used to raise antibodies are indicated by the bars.

For MARK4L (GenScript) and MARK4S (Sigma) antibodies short peptides (15 aa) were used as immunogens, while anti-MARK4S antibody from GenScript was raised against a recombinant protein corresponding to MARK4S whole C-terminal sequence. Anti-MARK4L antibody (Primm), raised against a short peptide which does not overlap GenScript peptide, was used in immunolabelling experiments in our previous report [Magnani 2009].

Human and mouse MARK4 protein sequence share an identity of about 97%.

3.2.1 MARK4L antibody validation

To validate the new and non-commercial anti-MARK4L antibody (GenScript), we assessed its specificity (that is, the ability to give a signal only in the presence of the target) by several immunoblotting assays.

To verify that the strongest band, visible around 80 kDa in the blot, was specific for MARK4L antigen and not due to non-specific interactions, we performed the peptide-competition assay. Briefly, we carried out SDS-PAGE on six identical samples, transferred the proteins and, after the blocking step, cleaved the membrane in six strips, corresponding to the six samples. Each strip was then incubated respectively with (1) anti-MARK4L antibody and (2-5) anti-MARK4L antibody pre-adsorbed against

progressively higher peptide quantities. The peptide was the 15-aa-long antigen used to raise the anti-MARK4L antibody and thus competed for the antibody binding with MARK4L proteins present in the lysate. MARK4L specific band (around 80 kDa) was more intense in the membrane incubated only with the antibody and became fainter at higher peptide quantities (data not shown). Equal protein loading and transferring was checked by blotting the same membrane with anti-GAPDH antibody.

Non-specific bands were also detected by incubating the membrane with the pre-immune rabbit serum (drawn from the animal before immunization), highlighting a secondary antibody non-specific band close to the one corresponding to MARK4L.

To verify that the antibody recognized MARK4L, we produced a fusion protein consisting of MARK4L protein and a N-terminal *Xpress*™ tag and assessed that both anti-MARK4L and anti-Xpress™ antibodies stained this fusion protein (figure 3.5). We also checked that the antibody was isoform-specific and did not cross-react with MARK4S: actually this antibody binds the recombinant protein corresponding to MARK4L whole C-terminal region but does not recognize MARK4S recombinant protein (figure 3.6).

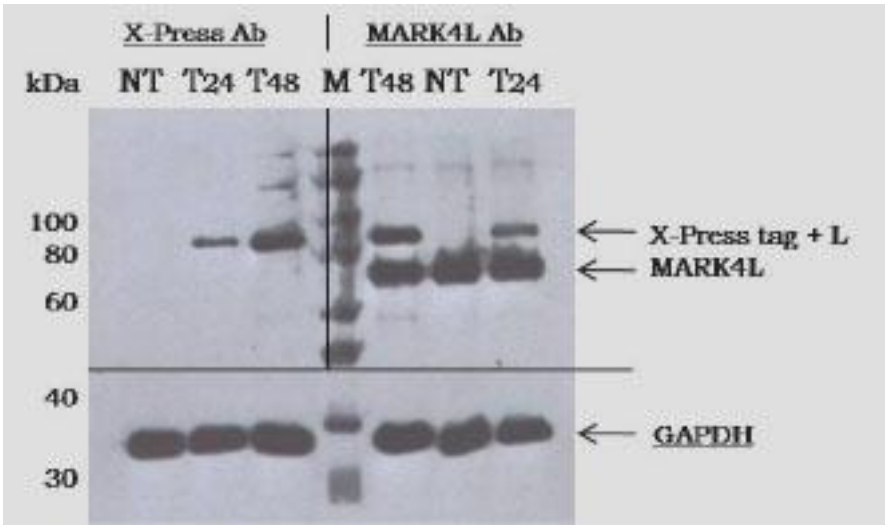

Figure 3.5: HEK293T cells transfected with a plasmid DNA producing the fusion protein MARK4L + Xpress tag (T24 and T48) and non-transfected HEK293T cells (NT). The membrane was incubated with anti-Xpress antibody (on the left) and anti-MARK4L antibody (on the right). The fusion protein was present only in transfected cells (T24 and T48) and was recognized by both the anti-Xpress antibody (left) and the anti-MARK4L antibody (right, upper band) which also stained endogenous MARK4L protein (right, lower band). The fusion protein had a higher molecular weight due to Xpress tag and histidine tail. M=molecular weight standards.

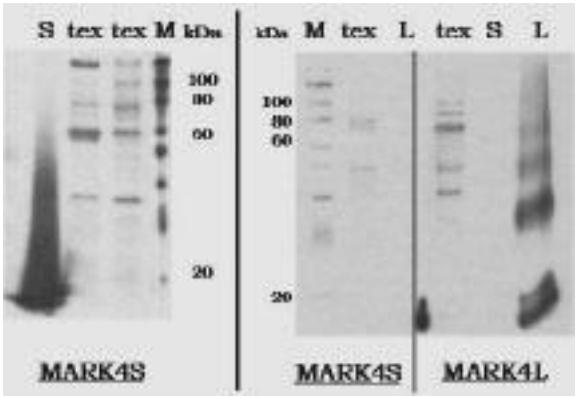

Figure 3.6: immunoblots of MARK4S (S) and MARK4L (L) recombinant proteins. Anti-MARK4S antibody recognizes the S recombinant protein (left) but not the L protein (middle); anti-MARK4L antibody does not cross react with the S recombinant protein, while it binds the L protein (right). M=molecular weight ladders. Tex=tissue sample.

The specificity of MARK4L antibody (Primm) was instead assessed by Mass Spectrometry (figure 3.7) [Magnani 2009].

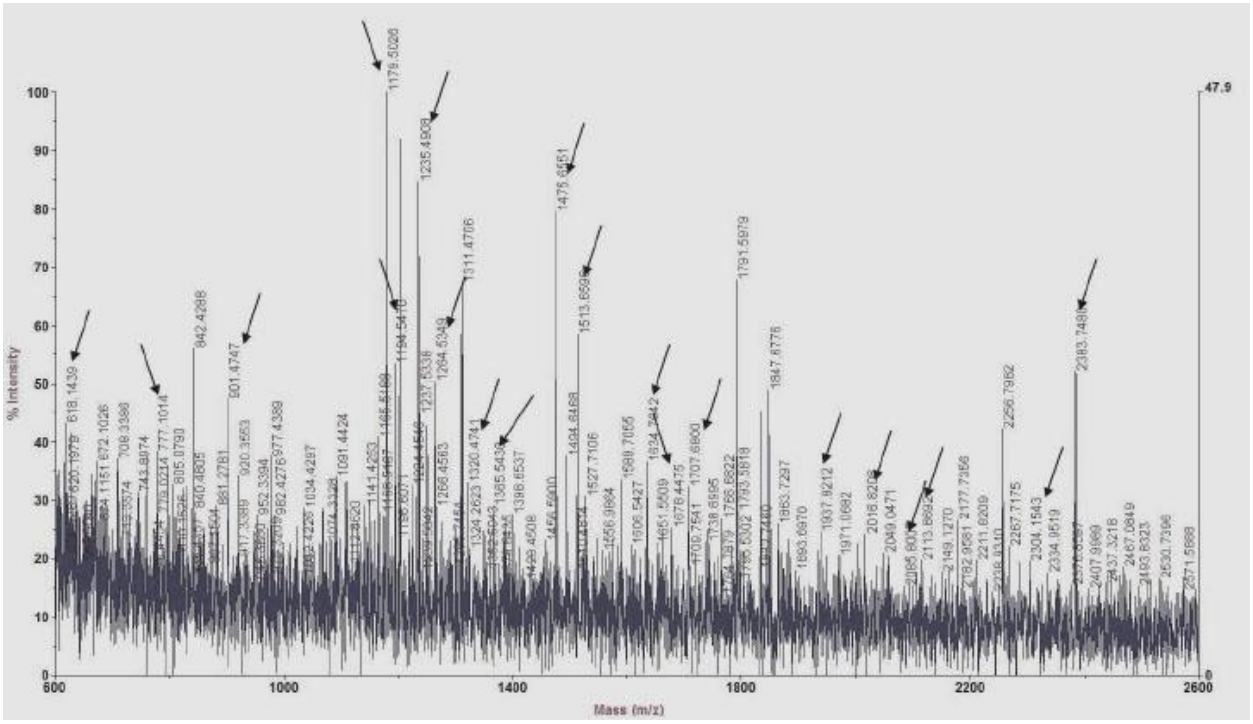

Figure 3.7: MALDI-mass spectrum (ranging from 600 to 2600 Dalton) of the digested peptides from the immunoprecipitated MARK4L protein band. Of the 29 signals assigned to MARK4L, only 20 (arrowed) are visible because of the compactness of the mass spectrum

3.2.2 MARK4S antibody validation

Anti-MARK4S antibody from GenScript was tested by peptide-competition assay (data not shown) and was checked for its ability to recognize MARK4S recombinant protein and to not cross react with MARK4L (figure 3.6).

Both anti-MARK4S antibodies, from Sigma and GenScript, give a near identical staining in Immunofluorescence and these data establish specificity for both of them. Indeed, the feature by which two antibodies raised against different and non-overlapping epitopes of the same protein show the same staining pattern is considered a strong indicator of specificity of the observed staining [Holmseth 2006; Bjorling 2008].

3.3 MARK4L AND MARK4S EXPRESSION ANALYSIS

Following mutation analysis, which did not reveal any genomic alteration (as did not the array-CHG analysis previously performed on most of the glioma cell lines [Roversi 2006]), we analyzed MARK4L and MARK4S relative gene and protein expression in the gliomas under study (21 cell lines, 35 tissue samples and 6 glioblastoma-derived cancer stem cells – GBM CSC).

To expand literature data [Beghini 2003; Moroni 2006], a wider panel of tissue samples and also GBM-derived CSC (which reproduce the genotypic and phenotypic features of GBM more faithfully than standard glioma cell lines [Lee 2006]) were examined. Moreover, a quantitative approach (Real-time PCR) was applied for mRNA analyses and protein expression was tested too, by Immunoblotting and by Immunohistochemistry (which allows to distinguish between tumor and normal cells).

3.3.1 MARK4 mRNA expression profile in glioma cell lines

Real-time PCR analyses on 9 non-GBM and 12 GBM cell lines (figure 3.8) indicate that MARK4L is the main isoform and is overexpressed in 16/21 samples as compared to Normal Human Neural Progenitor cells (t-test; $p<0.05$). In a previous study [Beghini 2003], a direct correlation between MARK4L levels and malignancy grade in glioma cell lines was found by using a semi-quantitative approach. Differently, quantitative PCR does not reveal significant differences in MARK4L levels between the two glioma subgroups.

Furthermore, the S isoform of MARK4 is expressed concomitantly to MARK4L, although it shows a significant decrease in expression levels when compared to NHNP (t-test: $p=0.002$ *versus* non-GBM, $p=0.00014$ *versus* GBM).

It can also be noted that both isoforms have a heterogeneous expression within and across the two subgroups.

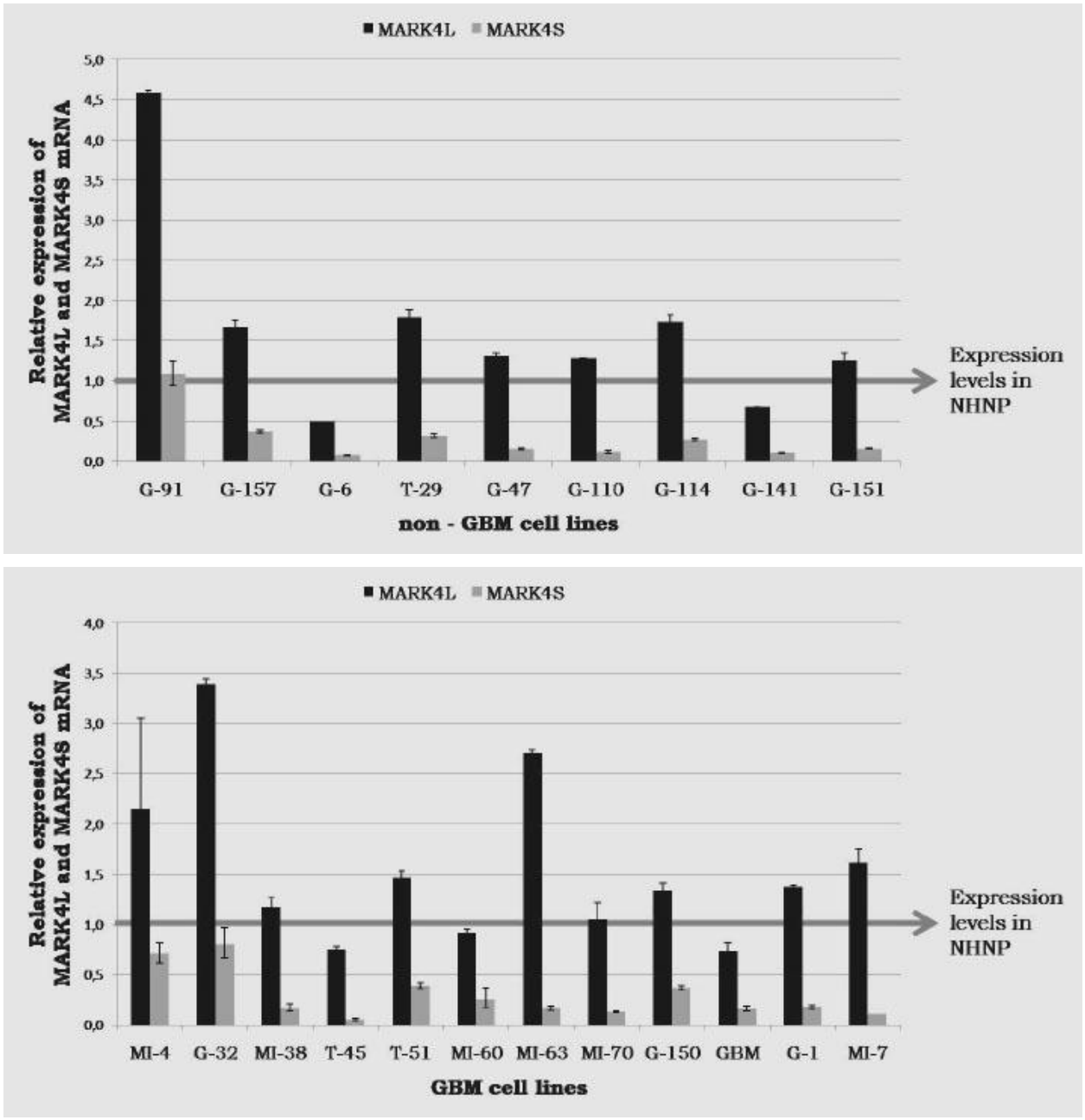

Figure 3.8: relative expression ($2^{-\Delta\Delta C_T}$) of MARK4L and MARK4S in non-GBM (top) and GBM (bottom) cell lines by Real-time quantitative PCR. Expression levels in glioma samples are referred to Normal Human Neural Progenitor cells (NHNP), chosen as reference and whose values were accordingly set as 1. Expression data are shown as mean ± standard error.

3.3.2 MARK4 mRNA expression profile in glioma tissue samples

Real-time PCR analyses (figure 3.9) on 16 Oligodendrogliomas (WHO II grade), 7 Astrocytomas (II/III grade) and 12 Glioblastomas (IV grade), confirm the MARK4L prevalence and the heterogeneous expression of both MARK4 isoforms also seen in cell lines.

As regards MARK4L, there are no statistically significant differences among the three subgroups, although a slight decrease is observed when considering the $2^{-\Delta\Delta CT}$ mean values (A=1.41; O=1.09; GBM=0.86; HNB set as 1).

In line with cell lines data, MARK4S is expressed concomitantly to MARK4L, and its expression levels are reduced in glioma samples as compared to Human Normal Brain (HNB; $2^{-\Delta\Delta CT}$ value set as 1): in detail II grade oligodendrogliomas show a $2^{-\Delta\Delta CT}$ mean value of 0.42, II/III grade astrocytomas a $2^{-\Delta\Delta CT}$ mean value of 0.16 and IV grade glioblastomas a $2^{-\Delta\Delta CT}$ mean value of 0.09. Interestingly, in astrocytic tumors (A and GBM) the decrease of MARK4S levels inversely correlates with tumor grade, as confirmed by the statistical analysis using the Kruskal-Wallis test (KW p=0.043 A *versus* GBM). Samples deriving from different cell types (oligodendrogliomas and astrocytomas) also show statistically different MARK4S expression levels (KW p=0.033 A *versus* O).

There are no correlations between MARK4 levels and the molecular diagnostic and prognostic markers (mMGMT, 1p and 19q deletions and closeness of the tumor to the Sub-Ventricular Zone) by using the KW test.

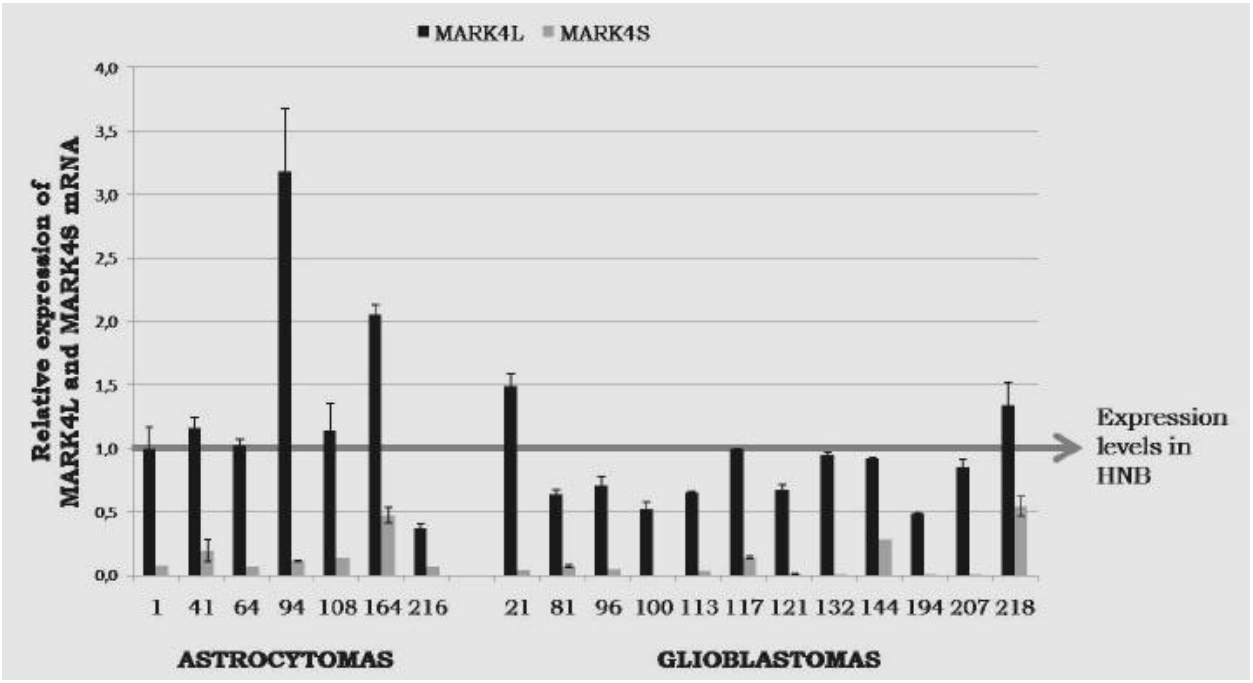

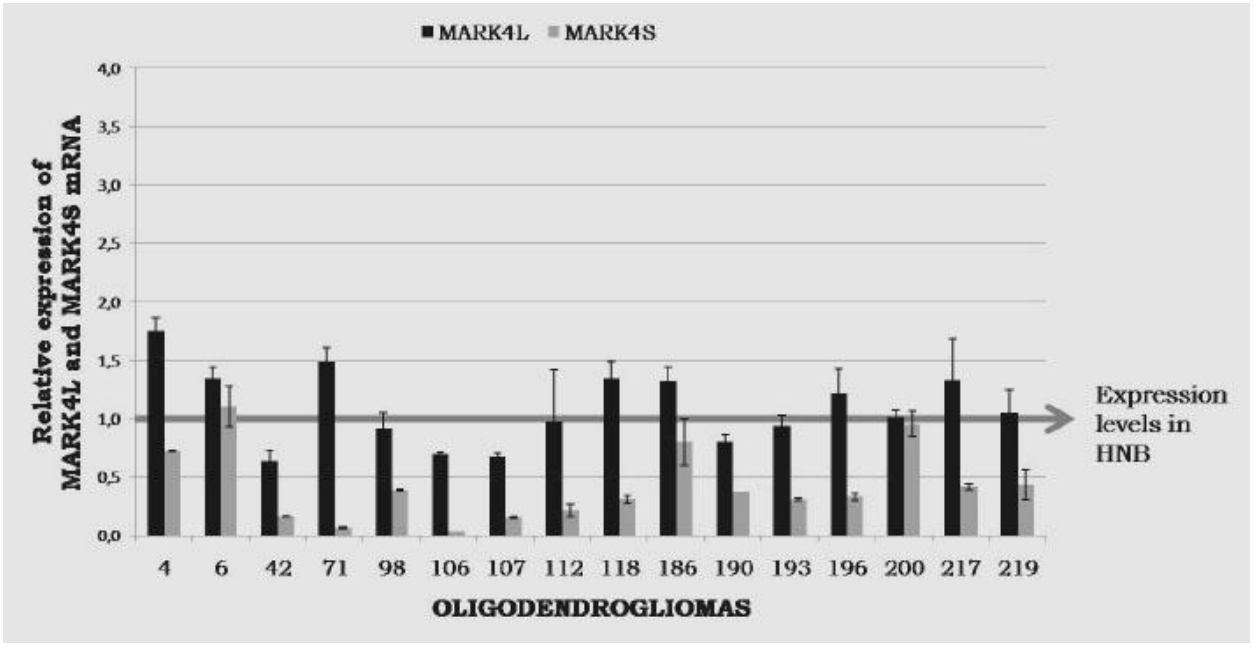

Figure 3.9: [top] relative expression ($2^{-\Delta\Delta C_T}$) of MARK4L and MARK4S in astrocytic tumors by Real-time quantitative PCR. MARK4S expression levels show a significant decrease that correlates with tumor grade (from II/III grade astrocytomas - left - to IV grade glioblastomas - right). **[Bottom]** relative expression ($2^{-\Delta\Delta C_T}$) of MARK4L and MARK4S in oligodendroglioma tissue samples by Real-time quantitative PCR.

Expression levels are referred to Human Normal Brain (HNB), which displays similar amounts of MARK4S (C_T=23.7) and MARK4L (C_T=24.5) mRNAs, and whose values were set as 1. Expression data are shown as mean ± standard error.

3.3.3 MARK4L/S imbalance tags the undifferentiated phenotype of GBM, GBM-derived cancer stem cells and neural stem cells

To further investigate the MARK4 imbalance found in the most malignant and undifferentiated tumoral subgroups, we analyzed MARK4 expression profile in 6 glioblastoma-derived Cancer Stem Cell lines (GBM CSC) and in a mouse sub-ventricular Neural Stem Cell line.

Quantitative PCR results indicate that MARK4L, though heterogeneous, is the predominant isoform in both GBM CSCs and neural stem cells, whereas MARK4S is hardly detectable (figure 3.10).

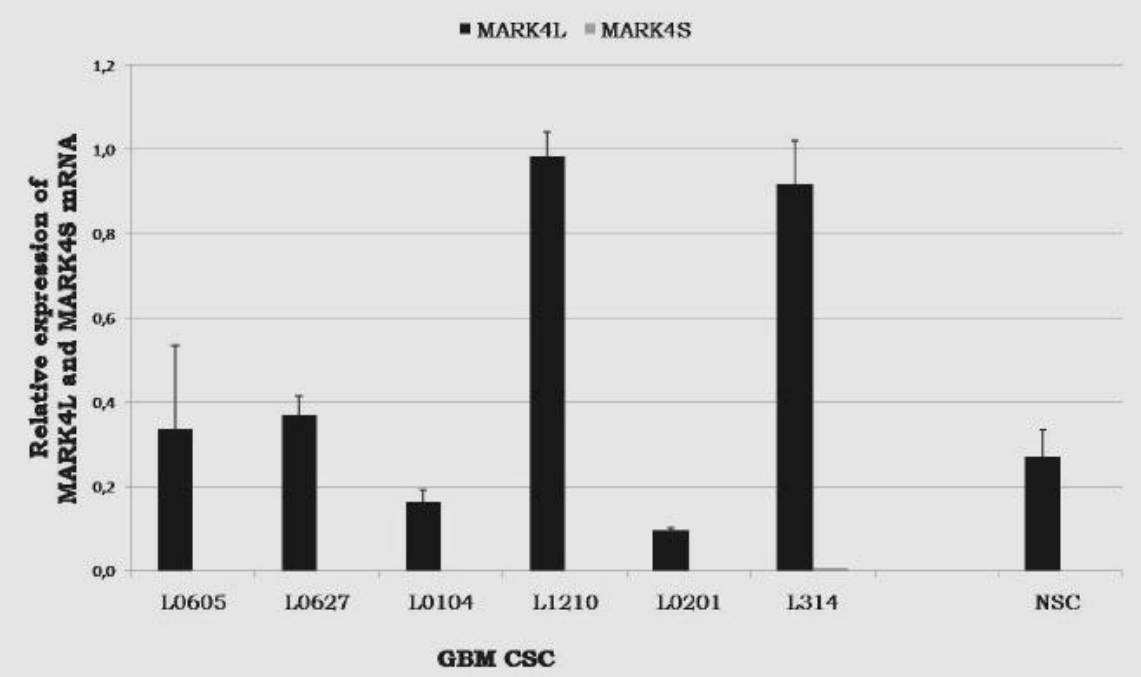

Figure 3.10: relative expression ($2^{-\Delta\Delta CT}$) of MARK4L and MARK4S in GBM CSC and NSC by Real-time quantitative PCR. Expression levels are referred to Human Normal Brain (HNB), chosen as reference and whose values were set as 1. Expression data are shown as mean ± standard error.

The relative expression pattern of MARK4 isoforms in GBM CSC resembles that of glioblastomas, showing a prevalent MARK4L expression and low MARK4S levels. By comparing the profile of astrocytic tumors (A and GBM) and GBM-derived cancer stem cells, it can be seen that, following the strong MARK4S reduction (figure 3.11), the ratio between MARK4L and MARK4S gets progressively higher in parallel to the increase of malignancy and of the un-differentiated state (figure 3.12).

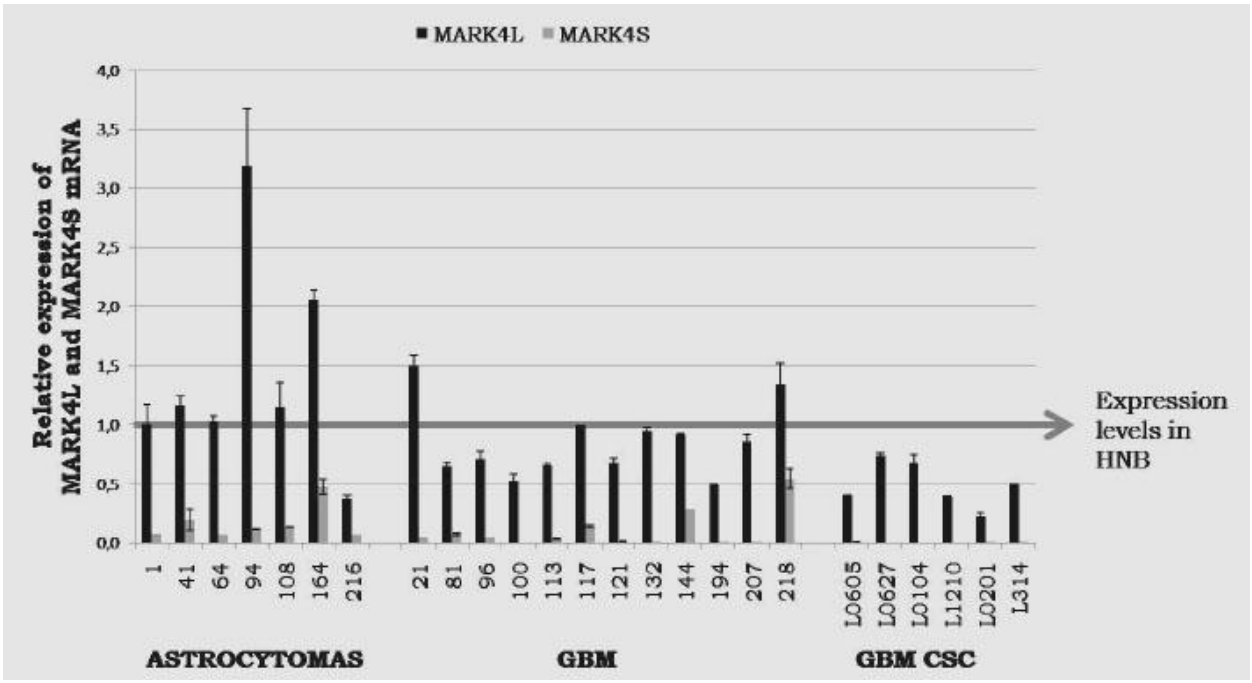

Figure 3.11: relative expression ($2^{-\Delta\Delta CT}$) of MARK4L and MARK4S in astrocytomas, glioblastomas (GBM) and GBM-derived cancer stem cells (GBM CSC) by Real-time quantitative PCR. Expression levels are referred to Human Normal Brain (HNB), chosen as reference and whose values were set as 1. Expression data are shown as mean ± standard error.

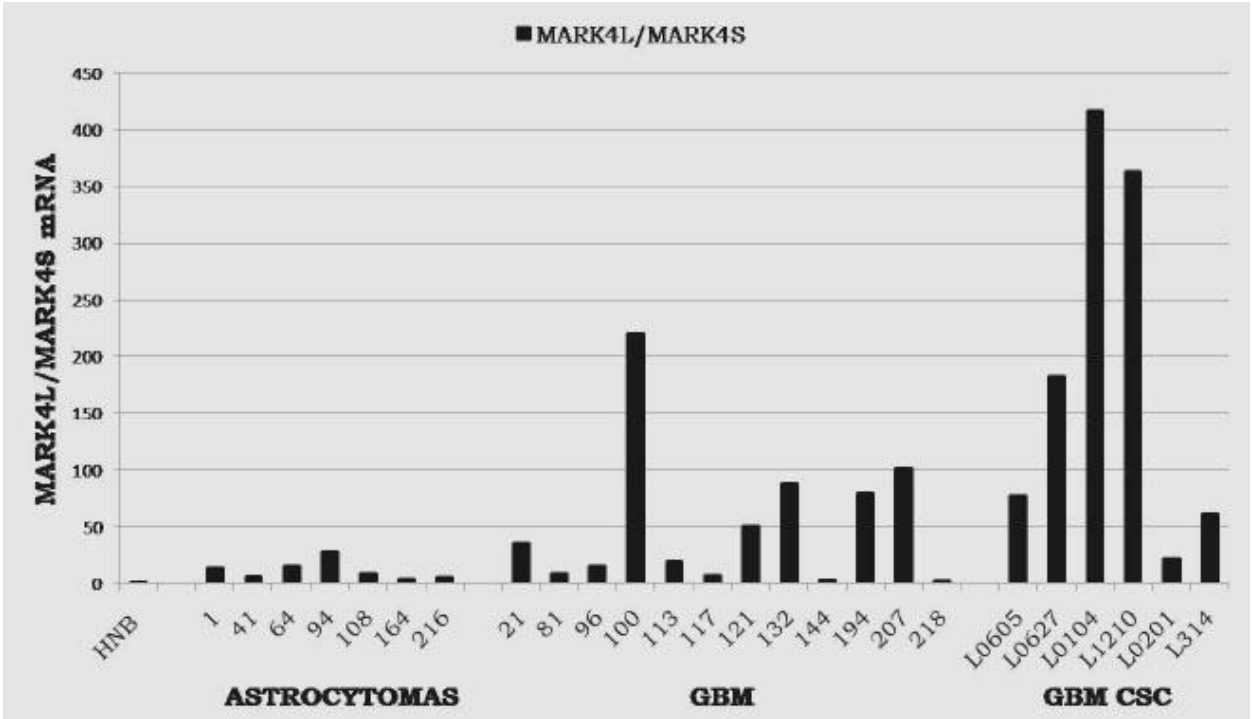

Figure 3.12: ratio between MARK4L and MARK4S mRNA in Human Normal Brain (HNB), astrocytomas, glioblastomas (GBM) and GBM CSC by Real-time quantitative PCR.

3.3.4 MARK4L protein expression profile in glioma cell lines

Immunoblotting experiments, achieved only for the L isoform (Immunoblotting for MARK4S is currently in progress), on the same glioma cell lines analyzed by Real-time PCR, show increased MARK4L expression in both non-GBM and GBM subgroups compared to NHNP, in agreement with mRNA data (figure 3.13):

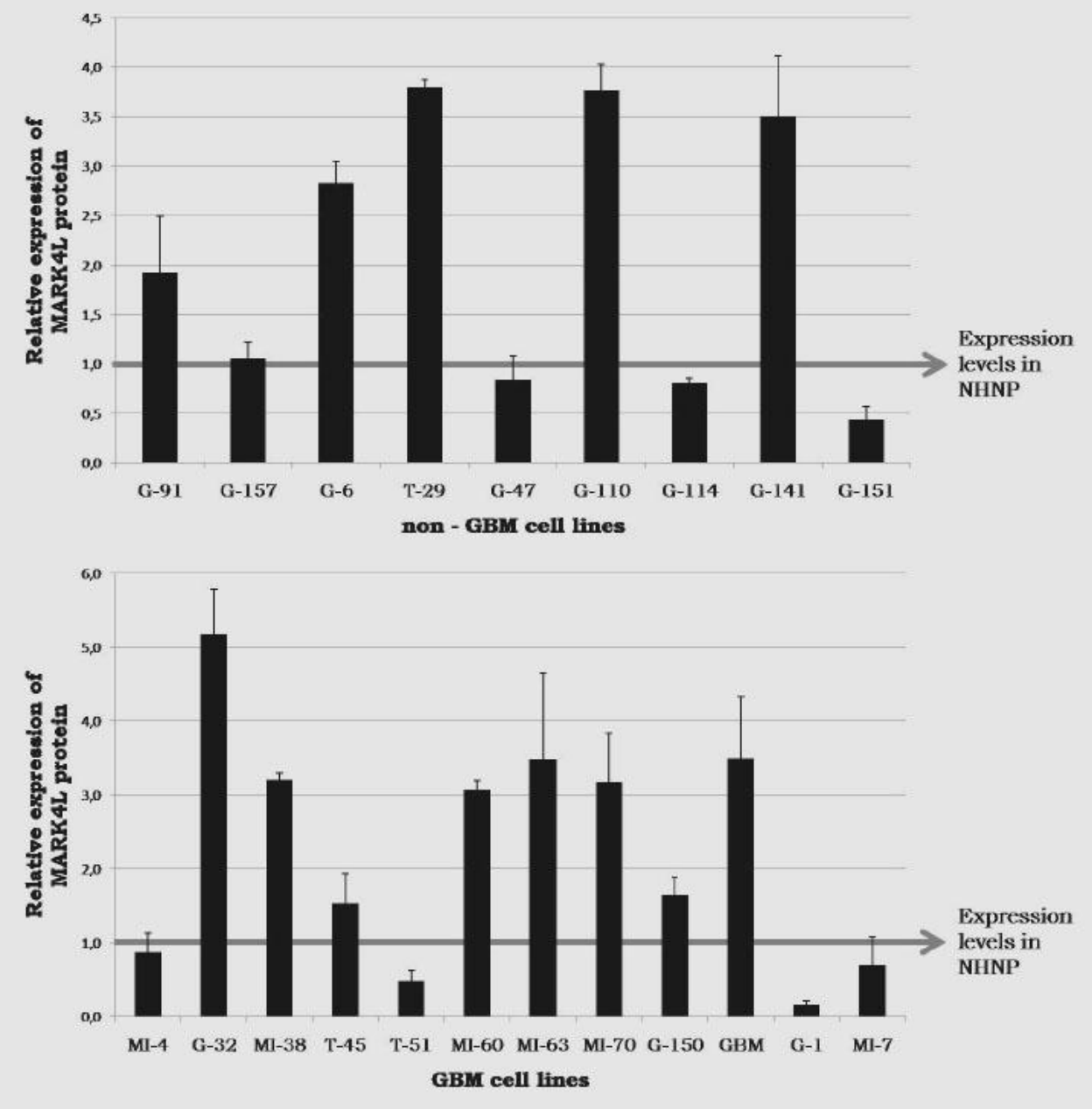

Figure 3.13: MARK4L protein relative expression in non-GBM (top) and GBM (bottom) cell lines by Immunoblotting experiments. Expression levels in glioma samples are referred to Normal Human Neural Progenitor cells (NHNP), chosen as reference and whose value was set as 1. Expression data are shown as mean ± standard deviation.

3.3.5 MARK4 protein expression profile in glioma tissue samples

MARK4L semi-quantitative Immunoblotting results (figure 3.14), matching the same tissue samples analyzed by Real-time PCR, confirm mRNA data showing a slight MARK4L decrease in GBM samples when compared to Astrocytomas (mean values: O=1.01; A=1.56; GBM=0.8), although the differences are not statistically significant.

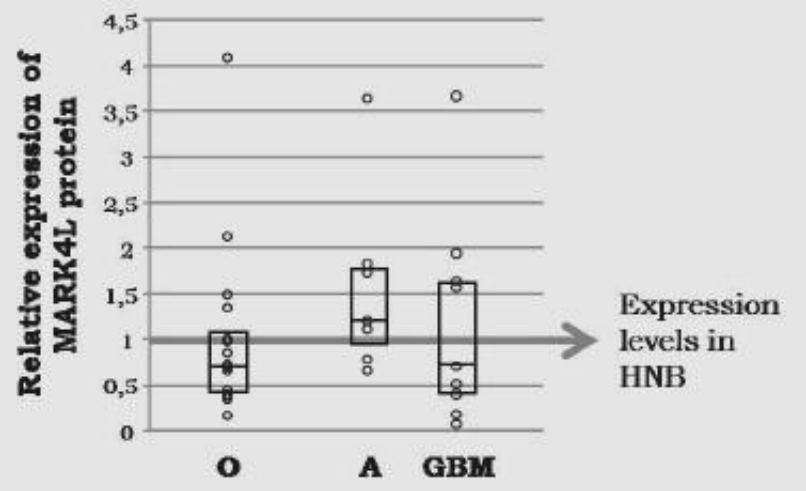

Figure 3.14: distribution of MARK4L protein relative expression values in oligodendroglioma (O), astrocytoma (A) and glioblastoma (GBM) tissue samples, by Immunoblotting experiments. Expression levels are referred to Human Normal Brain (HNB), chosen as reference and whose value was set as 1. Boxes indicate the median and the 25th and 75th percentiles.

By Immunohistochemistry we evaluated the localization and the expression levels (semi-quantitatively) of both MARK4 proteins in paraffin-embedded glioma sections matching the same tissue specimens. The resulting profiles are reported in table 3.1.

The assigned expression values, concordantly with Immunoblotting data, pinpoint the heterogeneous expression of both MARK4 isoforms among and within glioma subgroups.

In detail, it can be seen that anti-MARK4L antibody labels all the oligodendrogliomas and astrocytomas under study and among glioblastomas only one sample out of 12 is negative. The anti- MARK4S antibody is instead detectable in 12 samples out of 14 analyzed O, 6 samples out of 10 tested GBM and in all the evaluated astrocytomas.

TISSUE SAMPLE		MARK4L			MARK4S		
		STAINING INTENSITY	LABELLING EXTENT	COMPOSITE SCORE	STAINING INTENSITY	LABELLING EXTENT	COMPOSITE SCORE
OLIGODENDROGLIOMAS	4	2	2	4	1	2	2
	6	3	3	9	N.E	N.E.	N.E.
	42	3	3	9	1	1	1
	71	3	2	6	0	0	0
	98	2	3	6	1	2	2
	106	3	2	6	0	0	0
	107	2	2	4	3	2	6
	112	2	2	4	2	2	4
	118	2	1	2	1	1	1
	186	3	1	3	1	1	1
	190	2	2	4	1	2	2
	193	3	1	3	2	2	4
	196	3	2	6	N.E	N.E.	N.E.
	200	2	1	2	1	1	1
	217	1	2	2	1	2	2
	219	2	2	4	2	2	4
ASTROC	1	3	3	9	2	3	6
	41	N.E.	N.E.	N.E.	N.E.	N.E.	N.E.
	64	3	2	6	N.E.	N.E.	N.E.
	94	N.E.	N.E.	N.E.	N.E.	N.E.	N.E.
	108	3	1	3	1	1	1
	164	2	1	2	1	1	1
	216	3	2	6	2	2	4
GLIOBLASTOMAS	21	2	3	6	2	2	4
	81	2	2	4	1	2	2
	96	1	1	1	1	1	1
	100	3	3	9	0	0	0
	113	2	2	4	1	1	1
	117	2	1	2	0	0	0
	121	2	2	4	1	1	1
	132	3	1	3	0	0	0
	144	0	0	0	N.E.	N.E.	N.E.
	194	1	1	1	0	0	0
	207	1	2	2	N.E.	N.E.	N.E.
	218	1	2	2	2	2	4

Table 3.1: MARK4L (left) and MARK4S (right) protein expression values in Oligodendroglioma, Astrocytoma and Glioblastoma tissue sections by Immunohistochemistry.
For each protein, staining intensity was graded visually on a scale ranging from 0 to 3 (0= no staining; 1= weak, 2= moderate and 3= strong staining). The percentage of immunopositive cells (labelling extent) was scored in four categories (0≤ 5%; 1= 6–35%; 2= 36–66%; 3≥ 67%). Intensity and extent scores were multiplied to obtain the composite score. N.E.=not evaluated.

Figure 3.15 depicts few representative immunohistochemistry images; it also shows that both MARK4S and MARK4L antibodies label few differentiated neurons entrapped in the tumor mass (arrowed).

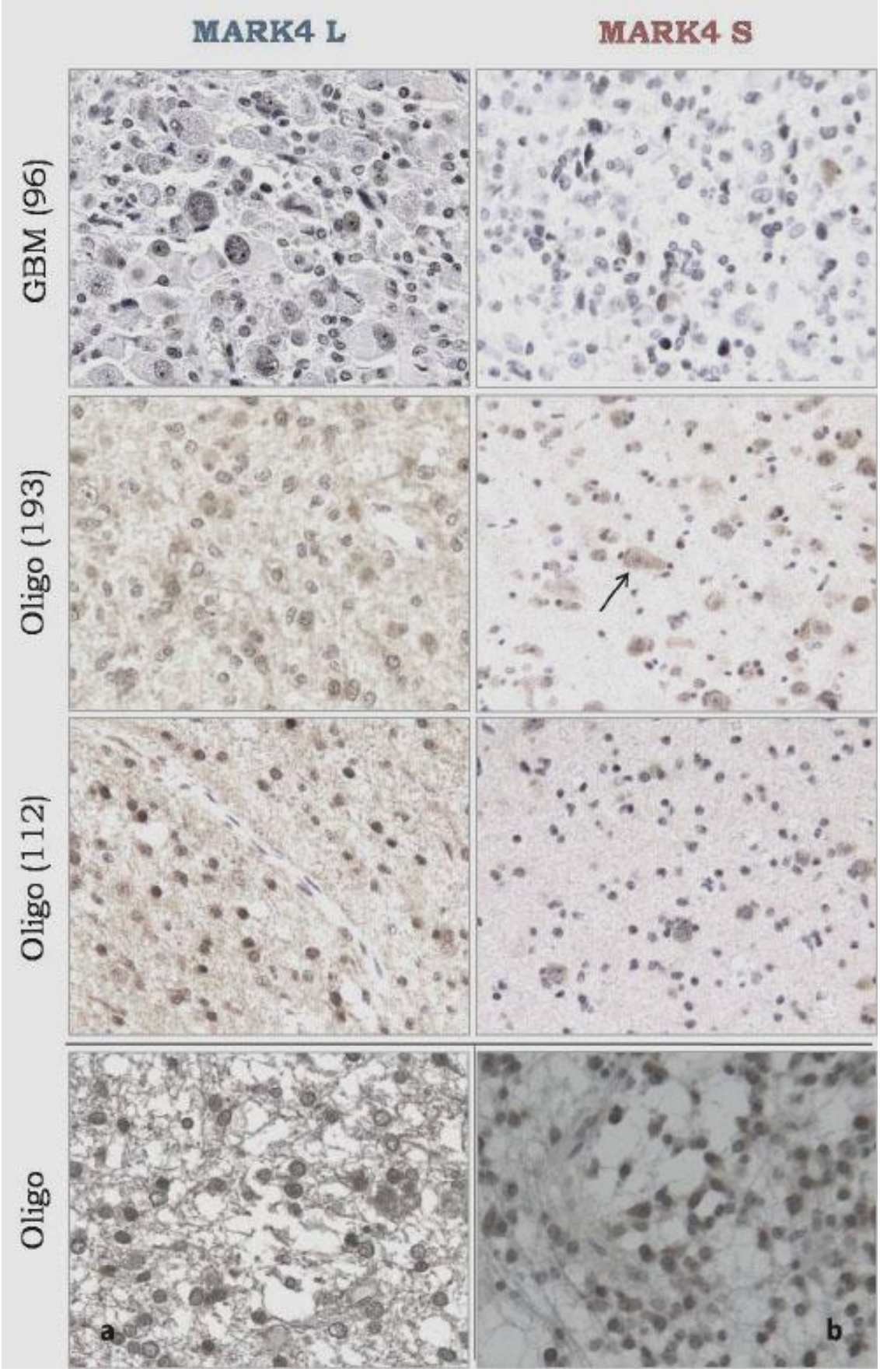

Figure 3.15: representative IHC images of MARK4L (left) and MARK4S (right) immunostaining. The arrow indicates one neuron. **a:** tissue sample 196 (Oligo), MARK4L; **b:** tissue sample 107 (Oligo), MARK4S.

3.4 DISTRIBUTION OF MARK4L AND MARK4S ISOFORMS IN BRAIN SECTIONS

We analyzed MARK4L and S protein localization on both human and rodent tissues from adult and embryonic brain. We found no significant differences between the two species.

The overall distribution of the two isoforms is similar in the cortical grey and white matter. In the cerebral cortex, both the new MARK4L and MARK4S antibodies detect, in agreement with previous data [Moroni 2006], most but not all of the neurons distributed throughout the cortical layers, and some glial cells, with different staining intensities (figure 3.16 a, b). Moreover, also in the white matter, some glial cells appear intensely immunolabelled for MARK4L and fewer cells are MARK4S-positive (figure 3.16 c, d).

On the contrary, the distribution of the two isoforms differs in the embryonic ventricular zone and in the adult subventricular zone, known germinal region in the adult brain. In embryos, MARK4L is expressed in some cells located in the ventricular zone (figure 3.17 a), likely neural stem cells, and in some postmitotic neurons in the intermediate zone and in the cortical plate (data not shown). MARK4S, though expressed in the embryonic postmitotic neurons, is not expressed in the ventricular zone (figure 3.17 b). Interestingly, in the adult rodents MARK4L is expressed in some cells of the subventricular zone, whereas MARK4S is not expressed (figure 3.17 c,d).

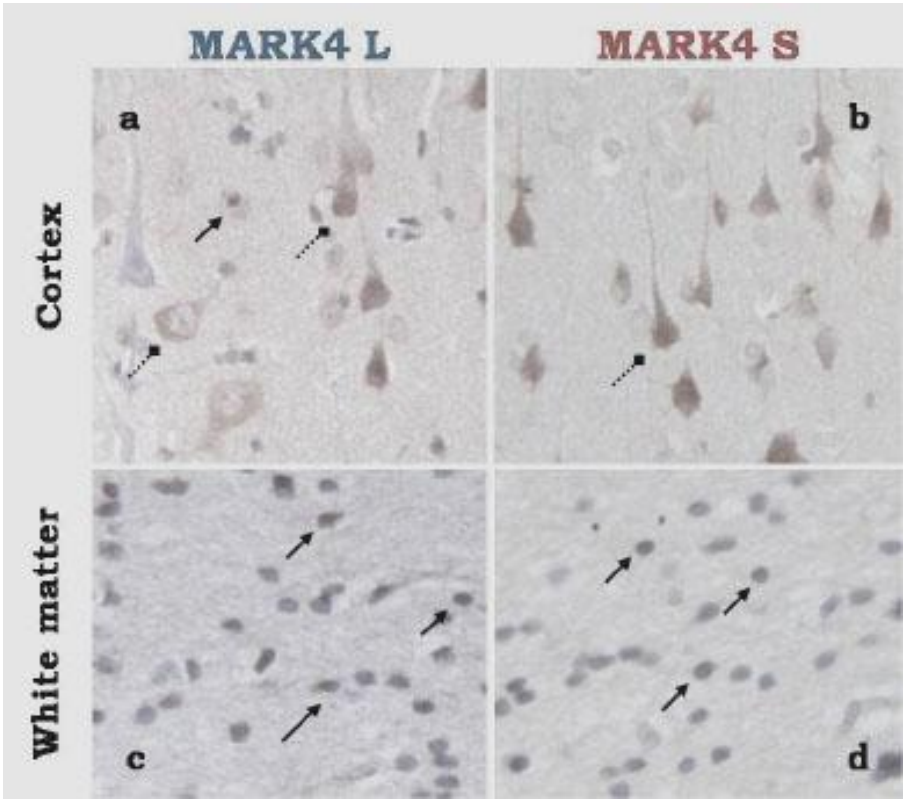

Figure 3.16: expression of MARK4L (a,c) and MARK4S (b,d) proteins in human adult brain. Both the isoforms are expressed in several neurons (dotted arrows) and in glial cells (arrows) in the cerebral cortex (a,b) and in some glial cells (arrowed) in the white matter (c,d).

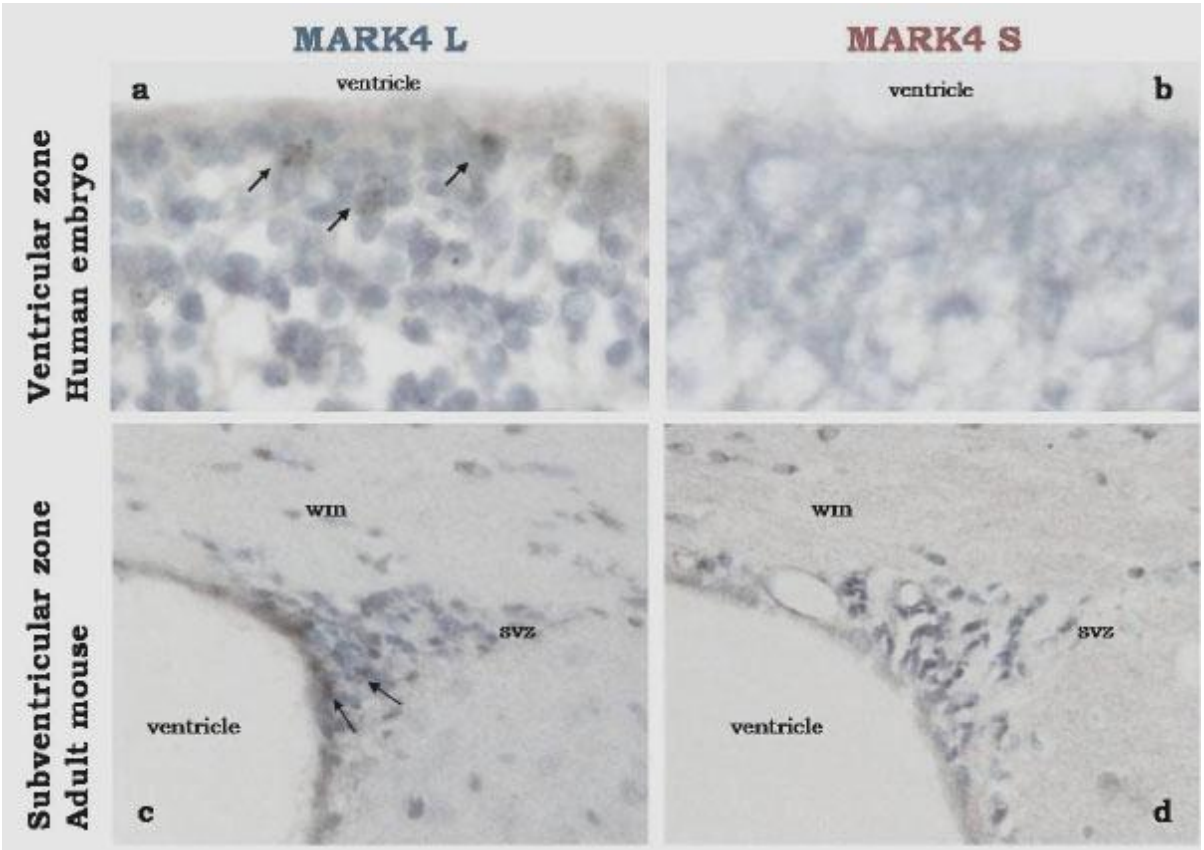

Figure 3.17: expression of MARK4L (a,c) and MARK4S (b,d) proteins in human embryo (a,b) and in adult mouse (c,d). wm=white matter; svz=subventricular zone.

3.5 MARK4L AND MARK4S ISOFORM SUB-CELLULAR LOCALIZATION

In early experiments we assessed MARK4L localization in glioma cell lines, by Immunofluorescence (IF) with an isoform-specific antibody by Primm [Magnani 2009]; these published results are here reported for a better comprehension of the present data.

We found MARK4L association with interphase centrosomes and also with the aberrant centrosomes frequently observed in gliomas (figure 3.18 A). Co-labelling with MARK4L and γ-tubulin antibodies revealed two kinds of abnormal perinuclear distribution in the investigated glioma cell lines: a clustered (top) and a random one (bottom).

We also demonstrated that MARK4L localizes in the nucleolus, by means of the silver colloid method (figure 3.18 B; left) and dual IF staining with anti-nucleolin antibody (figure 3.18 B; right).

MARK4L localization throughout cell division showed that the kinase was also associated to mitotic centrosomes, being concentrated at the spindle poles in prometaphase and metaphase; at anaphase it was detected in the midzone and at late anaphase it was repositioned outside the nucleus (figure 3.18 C). In addition, MARK4L protein gave a bright fluorescent signal in the centre of the midbody at the contact point between the two daughter cells during cytokinesis (figure 3.18 D).

In the present work, the above Immunofluorescence results were confirmed in glioma cell lines by using the new, not-commercial anti-MARK4L antibody (GenScript), which does not overlap that by Primm (figure 3.19; top).

We also extended the analyses to the subcellular localization of MARK4 S isoform in glioma cell lines: the results show that MARK4S, like the L isoform, localizes in centrosomes and midbodies but, in contrast, does not label the nucleolus (figure 3.19 bottom), thus delineating MARK4L protein as a specific isoform associated with the nucleolus.

We then investigated the localization of both MARK4 isoforms in different normal cells, including the neural progenitor cells *ReNcellCX,* fibroblasts and myoblasts. We found that MARK4L and S share the same centrosome and midbody staining pattern, as in glioma cell lines; conversely both of them are undetectable in the nucleolus (figure 3.20).

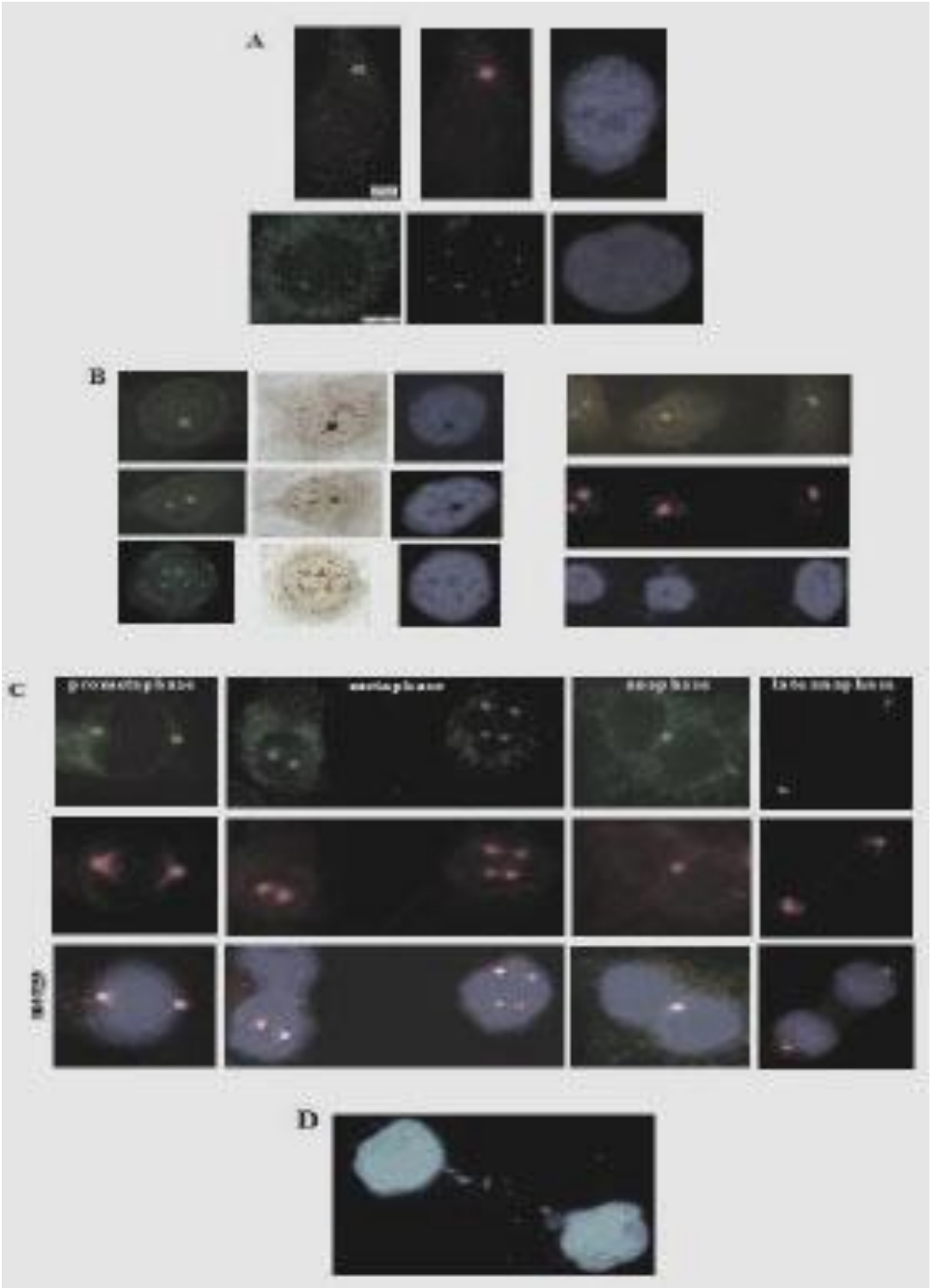

Figure 3.18 [Magnani 2009]: [A] dual IF staining with MARK4L (green; left) and γ-tubulin (red; middle) in MI-60 interphase cells. The nuclei are counterstained with DAPI (blue; right). The two main configurations of amplified centrosomes are shown: a large clustered signal (top) and multiple random signals (bottom). **[B; left]** anti-MARK4L antibody (green; left) and silver colloid method (middle) showing MARK4 nucleolar localization in G-91, MI-60 and MI-4 cells (top to bottom). **[B; right]** double immunostaining of MARK4L (green, top) and nucleolin (red, middle) showing co-localization in Mi-60 cells. **[C]** dual IF labelling with MARK4L (green; top) and γ-tubulin (red; middle) in all mitotic phases of MI-60 cells. Merge of the two signals is shown in the lower panels. **[D]** localization of MARK4L (green) to the midbody formed during cytokinesis in MI-60 cells.

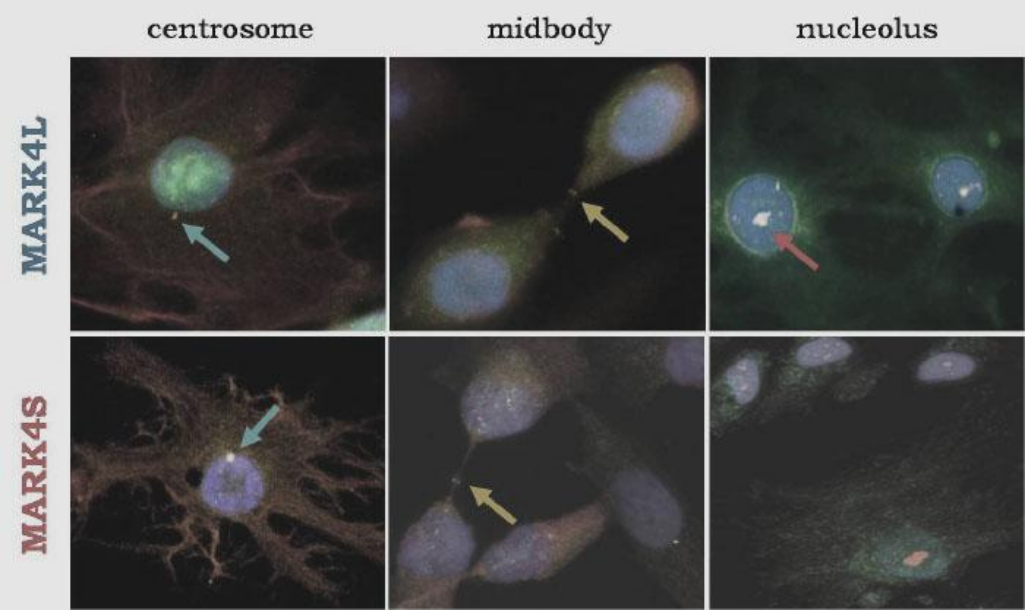

Figure 3.19: localization of MARK4L (top) and MARK4S (bottom) proteins in G91 **glioma cell line**. Both the isoforms associate with centrosomes (left; light blue arrow) and midbodies (middle; yellow arrow), but only MARK4L localizes in the nucleolus (right; red arrow). MARK4L and S antibodies were revealed by a FITC-secondary antibody (green signal), while γtubulin and nucleolin antibodies by a TRITC-secondary antiserum (red signal). Colocalization results in a yellow signal. Nuclei are counterstained with DAPI.

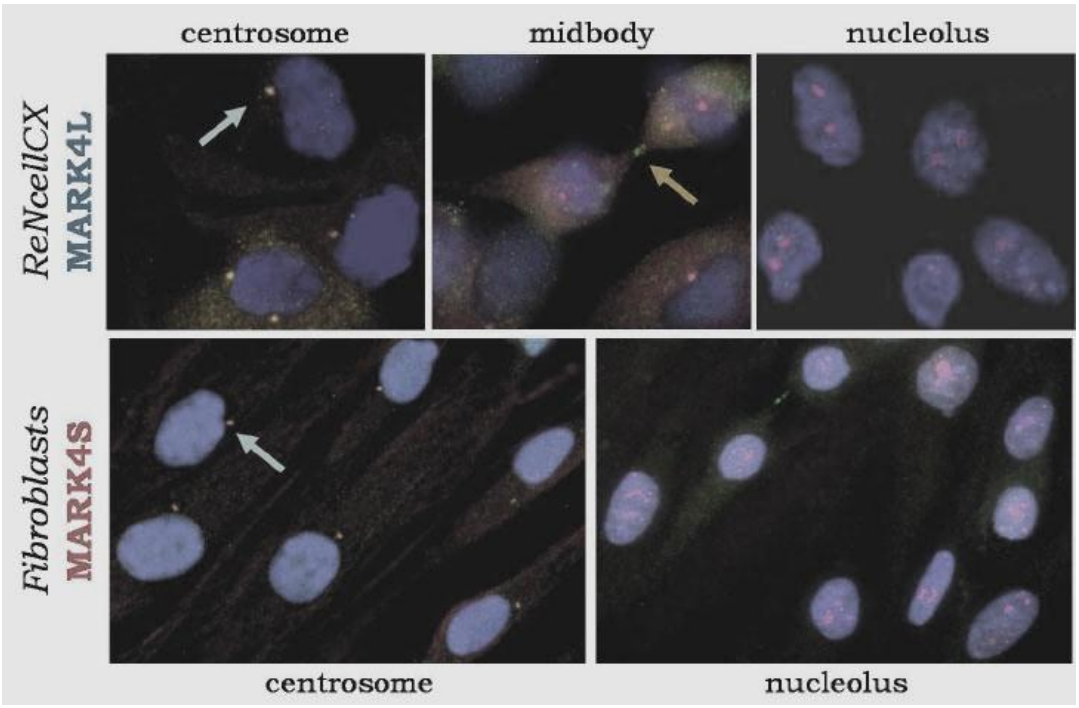

Figure 3.20: localization of MARK4L isoform in *ReNcellCX* cell line (top) and of MARK4S protein in fibroblasts (bottom). Both the isoforms associate with centrosomes (left; light blue arrow) and midbodies (middle; yellow arrow), but none of the two proteins localizes in the nucleolus (right; in the fibroblast image MARK4S localization in the midbody but not in the nucleolus is shown). MARK4L and S antibodies were revealed by a FITC-secondary antibody (green signal), while γ-tubulin and nucleolin antibodies by a TRITC-secondary antiserum (red signal). Colocalization results in a yellow signal. Nuclei are counterstained with DAPI.

We finally analyzed MARK4L protein in Neural Stem Cells (NSC) and glioblastoma-derived cancer stem cells (GBM CSC). By double-IF with anti-MARK4L and anti-nucleolin antibodies we found a specific nucleolar association of the kinase in two out of three GBM CSC samples (figure 3.21 a), which in their differentiated progenies exhibit even stronger MARK4L signals in the nucleoli (figure 3.21 b). Conversely, MARK4L was not detected in both undifferentiated and differentiated mouse sub-ventricular Neural Stem Cells (figure 3.21 c,d). Hence, the nucleolar association appears a specific feature of the sole L isoform of MARK4, exclusively visible in tumor cells.

[Specific signals as those described above were never found when using the pre-immune serum or the secondary antibody in the absence of primary antibodies (data not shown).]

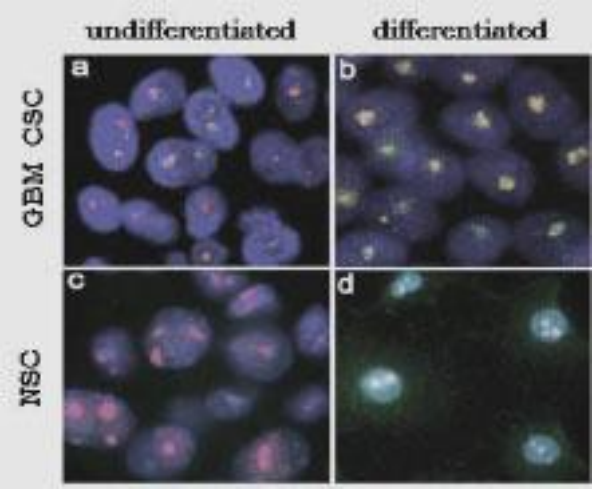

Figure 3.21: MARK4L IF in human GBM CSC (top) showing a faint labelling of the kinase in the nucleoli of undifferentiated GBM CSC (**a**) and increased signals in differentiated cells (**b**). Notably, MARK4L is not visible both in undifferentiated and differentiated mouse NSC nucleoli (bottom; **c**, **d**). MARK4L antibody signals were revealed by a FITC-secondary antibody (green), while nucleolin antibody by a TRITC-secondary antiserum (red signal). Colocalization results in a yellow signal. Nuclei are counterstained with DAPI.

We finally texted if RNase treatment, removing RNA from the nucleoli, affected the nucleolar retention of MARK4L. By IF on fixed MI-4 GBM cells, we found that both MARK4L and nucleophosmin (an abundant nucleolar protein) are absent in nucleoli of RNase-treated cells (figure 3.22 a), compared to the untreated cells (figure 3.22 b). This result suggests that MARK4L is physically associated with either ribosomal RNA or proteins bound to RNA in nucleoli.

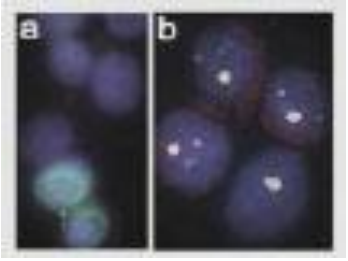

Figure 3.22: RNA depletion by RNase treatment affects MARK4L retention, as showed by the absence of MARK4L signal in nuclei and its presence in the midbody in MI4 cell line (**a**). The untreated cells show MARK4L co-localizing with the nucleolar protein nucleophosmin (**b**).
.

Discussion

The duplication of *MARK4* gene in a glioblastoma cell line and the up-regulation of the alternatively spliced MARK4L isoform in gliomas [Beghini 2003] and in hepatocarcinoma cells [Kato 2001] suggested that MARK4L could be implicated in proliferating cells. Differently, MARK4S predominance in normal brain has been related to a putative role in neuronal differentiation [Moroni 2006].

To further investigate MARK4 up-regulation in glial tumors, we analyzed a panel of 35 glioma tissue samples and 21 glioma cell lines in addition to 6 glioblastoma-derived cancer stem cell populations (GBM CSC). Human neural progenitors, total human normal brain and mouse neural stem cells (NSC, isolated from the sub-ventricular zone) were also included in the study. A quantitative approach (Real-time PCR) was applied for mRNA analyses, whereas MARK4 protein levels and localization were tested by Immunoblotting, Immunohistochemistry (IHC) and Immunofluorescence (IF).

The current mutational analysis of the main *MARK4* domains did not detect any alteration and the previously performed array-CGH analysis did not evidence any loss or gain of the *MARK4* containing region [Roversi 2006], thus ruling out two potential causes of kinase activation. However, CpG methylation and/or promoter amplification have not yet been investigated. Few *MARK4* alterations are reported in literature data, and among 91 analyzed GBM only a splice-site mutation in exon 13 affected *MARK4* gene [The Cancer Genome Atlas Research Network 2008].

Current Real-time PCR results highlight MARK4L as the prevalent isoform in all the glioma samples, strengthening previous published data achieved through semi-quantitative analysis [Beghini 2003], and a dysregulated L/S ratio in the most malignant and undifferentiated tumors/cell lines (Glioblastomas–GBM and GBM CSCs) as compared to normal brain and low grade gliomas. Thus MARK4L appears the most abundant isoform, whereas MARK4S mRNA levels show a significant decrease in parallel to the increase of malignancy and undifferentiated state. IHC results on matched glioma sections confirm Real-time PCR data, showing that 4 out of 10 GBM are negative for the S isoform. Concordantly with the cellular heterogeneity characterizing gliomas, MARK4L and MARK4S gene and protein expression appear very heterogeneous within and among different glioma subtypes.

All the above findings, namely the fact that either Neural Stem Cells of the SVZ, GBM CSC and GBM are characterized by MARK4L predominant expression and undetectable MARK4S levels (Real-time data), together with the observation that in normal brain only the L isoform localizes in the embryonic ventricular zone (VZ) and adult sub-ventricular zone (SVZ) where undifferentiated cells reside, associates exclusively the L isoform to stem cells and suggests that some Glioblastomas of our

panel may have a stem-cell origin, also supported by the evidence that many of the analyzed glioblastomas were contacting the SVZ. In contrast, the concomitant expression of both MARK4 isoforms in cells of the white matter, containing both differentiated glial cells and many cycling cells that belong to early glial lineages also thought to generate gliomas, could explain the origin of the Oligodendrogliomas, Astrocytomas and of some GBM here studied, which express both MARK4L and MARK4S.

In summary, Real-time PCR shows that a higher MARK4L prevalence in parallel to low levels of MARK4S characterizes highly undifferentiated cells, such as Neural Stem Cells, and highly malignant cells, such as GBM-derived Cancer Stem Cells and glioblastomas, favouring the hypothesis that the ratio between the two MARK4 isoforms is strictly regulated along neural differentiation and may be subverted in gliomagenesis. Furthermore, both MARK4 isoforms are concomitantly expressed in glial cells and in neurons (including those entrapped in oligodendrogliomas and neurons in normal brain) extending published data of MARK4S as a neuron-specific marker in mouse CNS [Moroni 2006]. Nevertheless, MARK4S role in differentiation is confirmed, but is not exclusive of neurons: the S isoform levels decrease along with dedifferentiation of glial cells and MARK4S protein is not found in the VZ and SVZ, where stem cells reside.

Different studies have been demonstrated that stem cells can undergo both symmetric and asymmetric division, the latter leading to a stem daughter cell and to a differentiation-committed daughter cell. Asymmetric division can be induced by an extrinsic signal (stem cell position relative to the niche and exposure to external factors) or by an intrinsic signal (asymmetric partitioning of cell components that determine cell fate, such as cell polarity factors) [Morrison 2006]. Genes regulating polarity, such as Par, Miranda and aPKC in *C. elegans* and *D. melanogaster*, may be responsible for the asymmetric division of stem cells [Clevers 2005]. Notably, MARK kinases have been implicated in both establishing cell polarity, by inducing asymmetric division in the *D. melanogaster* and *C. elegans* embryos [Tomankak 2000], and regulating polarization processes in epithelial and neuronal cells [Bohm 1997; Matenia 2009]. Many hypotheses have been raised suggesting that loss of asymmetry and switch to a prevalent symmetric division would lead to unrestrained growth of cells with stem features, and to expansion of cancer stem cells. It has been recently observed that the presence of extra centrosomes in flies' larval neural stem cells causes a non correct alignment of the spindles, leading to an increase in symmetric divisions and an expansion in the number of stem cells in larval brains. A correlation

between these defects in the asymmetric divisions and the ability of injected mutant brain tissue to form tumors has been also indicated [Basto 2008]. Supernumerary centrosomes are a common feature of different tumors, including gliomas, and may lead to the formation of a multipolar spindle which distributes chromosomes to more than two daughter cells, generating aneuploidies. Interestingly, we previously found MARK4 protein in association with the aberrant centrosomes observed in glioma, suggesting a possible role of the kinase in the abnormal mitotic processes of human glioma [Magnani 2009]. On the other hand, symmetric division, besides promoting the expansion of stem cell numbers, may also be permissive for secondary events leading to aneuploidies, since the machinery that controls asymmetric division also regulates the orientation of mitotic spindles and of centrosomes [Morrison 2006].

As already mentioned, the two MARK4 isoforms differ in their C-terminal region, suggesting different functions that could be directly mediated by the protein structure or depend on interactor proteins. In this study, at completion of MARK4 sub-cellular localization, we found by Immunofluorescence that both MARK4 S and L localize in centrosomes and midbody of normal and glioma cell lines, whereas the sole L isoform is associated with the nucleolus and exclusively in glioma cells, defining MARK4L as a tumor marker through its nucleolar association.

Several proteins are functionally involved in the nucleolus: some are requested for building and maintenance of this organelle, others may regulate cell growth, acting on ribosome biogenesis that affects protein synthesis needed for cell proliferation [Zhang 2010]. Besides the “traditional” ribosome biogenesis activity, the nucleolus is indeed involved in the response to cellular stress, in the regulation of cell cycle [Visintin 2000] and cell growth [Zhang 2010], and in post-translational modifications (phosphorylation and sumoylation) of proteins. It is worth noting that MARK4 activity is regulated by post-translational modifications, such as phosphorylation and ubiquitinylation at specific sites: its activation may hence account for the different functional states of the two isoforms in glioma, notwithstanding their different expression pattern. Many proteins are instead sequestered in the nucleolus and then released according to a temporally regulated activity, since they must exert their function in certain phases of the cell cycle [Visintin 2000]. The nucleolar localization of a protein may also influence its stability, protecting the protein from proteasomal degradation, since proteasomes are present throughout the nucleoplasm but not in nucleoli [Wojcik 2003]. We also hypothesize that MARK4L association to the nucleolus in glioma could be due or be a consequence of the dysregulation of MARK4 isoforms expression as we mentioned above.

It is important to recall that the L isoform of MARK4 results by an alternative splicing. Alternative splicing is a mechanism for increasing protein diversity and splicing choices are spatially and temporally regulated, for example by tissue-specific factors or by nuclear transcription factors. Specific splice variants (or splicing regulatory factors) are found differentially expressed in the Central Nervous System, both in subsequent steps of physiological processes and in pathologic or cancer tissues compared to normal tissue [Chen M. 2009].

As examples, PTB and nPTB are isoforms of a brain-specific factor: PTB is expressed in neural progenitors (and also found in glial cells and in the sub-ventricular zone) but is down-regulated in differentiated neurons, where nPTB is instead up-regulated (in addition to the brain, nPTB is also prevalent in testis). In neuronal cells, the PTB-to-nPTB switch provides a post-translational mechanism important for programming neuronal differentiation and is responsible for about 25% of nervous-system specific alternative splicing (in addition, it's likely that PTB and nPTB target genes affect cytoskeletal rearrangements and vesicular or protein transport) [Boutz 2007; Chen 2009]. Aberrations in Tau splicing regulation (physiologically producing spatially and temporally specific isoforms) directly cause several neurodegenerative diseases [Andreadis 2005], while myotonic dystrophy and spinal muscular atrophy are caused by an imbalance of the activities of splicing regulators [Hartmann 2009]. In addition, the "Survivin" protein, regulating apoptosis and microtubule dynamics, exists in two variants whose balance controls a pro-apoptotic *versus* anti-apoptotic signal in vascular smooth muscle cells [Small 2009]. As regards cancer, a role for the transcription factor C/EBP[44]β isoforms has been suggested in breast cancer: the ratio between these isoforms is crucial for the maintenance of normal growth and development (one variant is a transcriptional activator and is associated with differentiation, the other one is elevated in proliferative tissues and acts as an inhibitor of transcription) and increases in this ratio lead to aggressive form of breast cancer [Zahnow 2009]. The long (Q2L) and short (Q2S) splice variants of the *KCNQ2* gene, encoding a K^+ channel, differ in the C-terminal tail and in their expression profile: Q2L is preferentially expressed in differentiated neurons, whereas Q2S is prominent in fetal brain, undifferentiated neuroblastoma cells and brain tumors [Smith 2001].

In keeping with this body of literature, the differential expression of MARK4 isoforms in undifferentiated and glial malignant cells expands the concept of MARK4 splice variants dysregulation in mediating tumor initiation and progression.

[44] CCAAT/Enhancer-Binding Proteins.

Perspectives

Based on the achieved results, further advances will be focused to the following aims:

- investigate MARK4S and MARK4L functions by isoform-specific overexpression and siRNA-mediated depletion (this topic is already in progress in our laboratory);
- analyze MARK4 activation state (phosphorylation; ubiquitinylation) in glioma samples;
- unravel the mechanisms by which alternative splicing is "altered" in undifferentiated and malignant cells compared to normal differentiated cells (by analyzing the expression and phosphorylation profile of splicing factors, both enhancers and silencers);
- verify MARK4 localization in other cancers (already in progress);
- shed light on the functional relevance of MARK4L nucleolar association in cancer cells by:
    - further investigating MARK4L targeting to the nucleolus (probably mediated through association with ribosomal RNA or proteins bound to RNA in nucleoli, as suggested by RNA-depletion experiments),
    - establishing whether nucleolus-targeting occurs at a specific cell cycle phase,
    - assessing whether C-terminal sequence alterations and post-translational modifications or interactor expression might account for the different localization pattern in tumor and normal cells,
    - assessing MARK4L protein stability by inhibiting proteasomes (already in progress).

This study was supported by a grant from the *Associazione Italiana per la Ricerca sul Cancro* (AIRC).

The data here reported are part of a manuscript in preparation and have been also subject of oral communications and poster presentations at national and international conferences (corresponding abstracts are published).
MARK4L subcellular localization in glioma is described in a published paper:

- Magnani I, Novielli C, Bellini M, Roversi G, Bello L, Larizza L.
  "Multiple localization of endogenous MARK4L protein in human glioma".
  Cellular oncology 2009; 31: 357-70.

- Magnani I, Novielli C, Tabano S, Fontana L, Moroni RF, Colombo EA, Monti L, Bello L, Bauer D, Mazzoleni S, Galli R, Porta G, Frassoni C, Larizza L.
  "MARK4: a tricky balance of L and S isoforms rules glial differentiation and glioma progression".
  Presented at the International Society for Cellular Oncology (ISCO) Congress (Dresden; March 2010) and published in Cellular Oncology 2010; 32(3): 175.

- Magnani I, Novielli C, Tabano S, Fontana L, Moroni RF, Colombo EA, Monti L, Bello L, Bauer D, Mazzoleni S, Galli R, Porta G, Frassoni C, Larizza L.
  "Dysregulated ratio between MARK4L and S isoforms during glioma progression".
- Magnani I, Novielli C, Rovina D, Monti L, Larizza L.
  "The centrosomal protein MARK4 exhibits specificity of the L isoform through nucleolar association in tumor cell lines".
  Both abstracts have been presented at the XII European Workshop on Cytogenetics and Molecular Genetics of Solid Tumors (Nijmegen; June 2010) and are in the press in Cancer Genetics and Cytogenetics.

References

Al-Hakim AK, Zagorska A, Chapman L, *et al.*
Control of AMPK-related kinases by USP9X and atypical Lys^{29}/Lys^{33}-linked polyubiquitin chains.
The Biochemical journal 2008; 411: 249-60.

Angrand PO, Segura I, Völkel P, *et al.*
Transgenic mouse proteomics identifies new 14-3-3-associated proteins involved in cytoskeletal rearrangements and cell signaling
Molecular and cellular proteomics 2006; 5(12): 2211-27.

Andreadis A.
Tau gene alternative splicing: expression patterns, regulation and modulation of function in normal brain and neurodegenerative diseases.
Biochimica and biophysica acta 2005; 1739: 91-103.

Bachmann M, Hennemann H, Xing PX, *et al.*
The oncogenic serine/threonine kinase Pim-1 phosphorylates and inhibits the activity of Cdc25C-associated kinase 1 (C-TAK1): a novel role for Pim-1 at the G2/M cell cycle checkpoint.
Journal of biological chemistry 2004; 279: 48319-28.

Bachoo RM, Maher EA, Ligon KL, *et al.*
Epidermal growth factor receptor and Ink4a/Arf: convergent mechanisms governing terminal differentiation and transformation along the neuronal stem cell to astrocyte axis.
Cancer cell 2002; 1(3): 269-77.

Basto R, Brunk K, Vinadogrova T, *et al.*
Centrosome amplification can initiate tumorigenesis in flies.
Cell 2008; 133(6): 1032-42.

Beghini A, Magnani I, Roversi G, *et al.*
The neural progenitor-restricted isoform of the MARK4 gene in 19q13.2 is upregulated in human gliomas and overexpressed in a subset of glioblastoma cell lines.
Oncogene 2003; 22: 2581-91.

Benton R, Palacios IM and St Johnston D.
Drosophila 14-3-3/PAR-5 is an essential mediator of PAR-1 function in axis formation.
Developmental Cell 2002; 3: 659-71.

Bessone S, Vidal F, le Bouc Y, *et al.*
EMK protein kinase-null mice: dwarfism and hypofertility associated with alterations in the somatotrope and prolactin pathways.
Developmental biology 1999; 214: 87-101.

Bjorling E and Uhlen M.
Antibodypedia, a portal for sharing antibody and antigen validation data.
Molecular and cellular proteomics 2008; 7.10: 2028-37.

Bohm H, Brinkmann V, Drab M, *et al.*
Mammalian homologues of *C. Elegans* PAR-1 are asymmetrically localized in epithelial cells and may influence their polarity.
Current biology 1997; 7: R603-6.

Boutz PL, Stoilov P, Li Q, *et al.*
A post-transcriptional regulatory switch in polypyrimidine tract-binding proteins reprograms alternative splicing in developing neurons.
Genes and development 2007; 21(13): 1636-52.

Brajenovic M, Joberty G, Küster B, *et al.*
Comprehensive proteomic analysis of human Par protein complexes reveals an interconnected protein network.
The journal of biological chemistry 2004; 279(13): 12804-11.

Bright NJ, Carling D and Thornton C.
The regulation and function of mammalian AMPK-related kinases.
Acta Physiologica 2009; 196: 15-6.

Bringmann H
Cytokinesis and the spindle midzone.
Cell cycle 2005; 4(12): 1709-12.

Canoll P and Goldman JE.
The interface between glial progenitors and gliomas.
Acta neuropathologica 2008; 116: 465-77.

Carmo-Fonseca M, Mendes-Soares L and Campos I.
To be or not to be in the nucleolus.
Nature cell biology 2000; 2: E107-12.

Chatterjee S, Sang TK, Lawless GM, *et al.*
Dissociation of tau toxicity and phosphorylation: role of GSK-3β, MARK and Cdk5 in a *Drosophila* model.
Human molecular genetics 2009; 18(1): 164-77.

Chauhan SC, Vinayek N, Maher DM, *et al.*
Combined staining of TAG-72, MUC1 and CA125 improves labelling sensitivity in ovarian cancer: antigens for multi-targeted antibody-guided therapy.
Journal of histochemistry and cytochemistry 2007; 55(8): 867-75.

Chen YM, Wang QJ, Hu HS, *et al.*
Microtubule affinity-regulating kinase 2 functions downstream of the PAR-3/PAR-6/atypical PKC complex in regulating hippocampal neuronal polarity.
Proceedings of the National academy of science of the United States of America 2006; 103: 8534-9.

Chen L, Jiao ZH, Zheng LS, *et al.*
Structural insight into the autoinhibition mechanism of AMP-activated protein kinase.
Nature 2009; 459: 1146-50.

Chen M and Manley JL.
Mechanisms of alternative splicing regulation: insights from molecular and genomics approaches.
Nature reviews. Molecular cell biology 2009; 10: 741-54.

Chen R, Nishimura MC, Bumbaca SM, *et al.*
A hierarchy of self-renewing Tumor-Initiating Cell types in glioblastoma.
Cancer cell 2010; 17: 362-75.

Chi AS and Wen PY.
Inhibiting kinases in malignant gliomas.
Expert opinion on therapeutic targets 2007; 11(4): 473-96.

Chin J, Knowles RB, Schneider A, *et al.*
Microtubule-Affinity Regulating Kinase (MARK) is tightly associated with neurofibrillary tangles in Alzheimer brain: a fluorescence energy transfer study.
Journal of neuropathology and experimental neurology 2000; 59(11): 966-71.

Clevers H.
Stem cells, asymmetric division and cancer.
Nature genetics 2005; 37(10): 1027-8.

Cohen D, Brennwald PJ, Rodriguez-Boulan E, *et al.*
Mammalian PAR-1 determines epithelial lumen polarity by organizing the microtubule cytoskeleton.
Journal of cell biology 2004; 164: 717-27.

Collins VP.
Brain tumors: classification and genes.
Journal of neurology, neurosurgery and psychiatry 2004; 75(Suppl II): ii2-ii11.

de Leng WWJ, Jansen M, Carvalho R, *et al.*
Genetic defects underlying Peutz-Jeghers syndrome (PJS) and exclusion of the polarity-associated *MARK/Par1* gene family as potential PJS candidates.
Clinical genetics 2007; 72: 568-73.

Dequiedt F, Martin M, Von Blume J, *et al.*
New role for hPar-1 kinases EMK and C-TAK1 in regulating localization and activity of class IIa histone deacetylases.
Molecular cell biology 2006; 26(19): 7086-102.

Doxsey S.
Re-evaluating centrosome function.
Nature 2001; 2(9): 688-98.

Doxsey S, McCollum and Theurkauf W.
Centrosomes in cellular regulation.
Annual review of cell and developmental biology 2005; 21: 411-34.

Drewes G, Ebneth A, Preuss U, *et al.*
MARK, a novel family of protein kinases that phosphorylate microtubule-associated proteins and trigger microtubule disruption.
Cell 1997; 89: 297-308.

Drewes G and Nurse P.
The protein kinase kin1, the fission yeast hortologue of mammalian MARK/PAR-1, localizes to new cell ends after mitosis and is important for bipolar growth.
FEBS letters 2003; 554: 45-9.

Drewes G.
MARKing tau for tangles and toxicity.
TRENDS in biochemical science 2004; 29(10): 548-55.

Elbert M, Rossi G and Brennwald P.
The yeast Par-1 homologs Kin1 and Kin2 show genetic and physical interactions with components of the exocytic machinery.
Molecular biology of the cell 2005; 16: 532-49.

Espinosa L and Navarro E.
Human serine/threonine protein kinase EMK1: genomic structure and cDNA cloning of isoforms produced by alternative splicing.
Cytogenetics and cell genetics 1998; 81: 278-82.

Fischer JL, Schwartzbaum JA, Wrensch M, *et al.*
Epidemiology of brain tumors.
Neurologic clinics 2007; 25(4): 867-90.

Foroni C, Galli R, Cipelletti B, *et al.*
Resilience to transformation and inherent genetic and functional stability of adult neural stem cells *ex vivo*.
Cancer research 2007; 67(8): 3725-33.

Fukasawa K.
Introduction.
Oncogene 2002; 21: 6140-5.

Galli R, Gritti A, Bonfanti L, *et al.*
Neural stem cells. An overview.
Circulating research 2003; 92; 598-608.

Galli R, Binda E, Orfanelli U, *et al.*
Isolation and characterization of tumorigenic, stem-like neural precursors from human glioblastoma.
Cancer research 2004; 64: 7011-21.

Gamblin TC, Chen F, Zambrano A, *et al.*
Caspase cleavage of tau: linking amyloid and neurofibrillary tangles in Alzheimer's disease.
Proceedings of the National Academy of Sciences of the United States of America 2003; 100(17): 10032-7.

Germano I, Swiss V and Casaccia P.
Primary brain tumors, neural stem cell and brain tumor cancer cells: where is the link?
Neuropharmacology 2010; 58: 903-10.

Gladson CL, Prayson RA and Liu WM.
The pathobiology of glioma tumors.
Annual review of pathology 2010; 5: 33-50.

Greenman C, Stephens P, Smith R, *et al.*
Patterns of somatic mutation in human cancer genomes.
Nature 2007; 446: 153-8.

Gritti A and Bonfanti L.
Neuronal-glial interactions in central nervous system neurogenesis: the neural stem cell perspective.
Neuron glia biology 2007; 3(4): 309-23.

Günther HS, Schmidt NO, Phillips HS, *et al.*
Glioblastoma-derived stem cell-enriched cultures form distinct subgroups according to molecular and phenotypic criteria.
Oncogene 2008; 27(20): 2897-909.

Hartmann C, Johnk L, Litange G, *et al.*
Transcript map of the 3.7 Mb D19S112-D19S246 candidate tumor suppressor region on the long arm of chromosome 19.
Cancer Research 2002; 62: 4100-8.

Hartmann B and Valcárcel J.
Decrypting the genome's alternative messages.
Current opinion in cell biology 2009; 21: 377-86.

Holmseth S, Lehre KP and Danbolt NC.
Specificity controls for immunocytochemistry.
Anatomy and Embryology 2006; 211: 257-66.

Hurov JB, Stappenbeck TS, Zmasek CM, *et al.*
Immune system dysfunction and autoimmune disease in mice lacking Emk (Par-1) protein kinase.
Molecular cell biology 2001; 21: 3206-19.

Hurov JB, Watkins JL and Piwnica-Worms H.
Atypical PKC phosporylates PAR-1 kinases to regulate localization and activity.
Current Biology 2004; 14: 736-41.

Hurov J and Piwnica-Worms H.
The Par-1/MARK family of protein kinases: from polarity to metabolism.
Cell cycle 2007; 6: 1966-9.

Huse JT and Holland EC.
Targeting brain cancer: advances in the molecular pathology of malignant glioma and medulloblastoma.
Nature reviews 2010; 10: 319-30.

Ignatova TN, Kukekov VG, Laywell ED, *et al.*
Human cortical glial tumors contain neural stem-like cells expressing astroglial and neuronal markers in vitro.
Glia 2002; 39(3): 193-206.

Jain RK, di Tomaso E, Duda DG, *et al.*
Angiogenesis in brain tumours.
Nature reviews. Neuroscience 2007; 8(8): 610-22.

Jeon S, Kim YS, Park J, *et al.*
Microtubule Affinity-Regulating Kinase 1 (MARK1) is activated by electroconvulsive shock in the rat hippocampus.
Journal of neurochemistry 2005; 95: 1608-18.

Kato T, Satoh S, Okabe H, *et al.*
Isolation of a novel human gene, MARKL1, homologous to MARK3 and its involvement in hepatocellular carcinogenesis.
Neoplasia 2001; 3(1): 4-9.

Katsetos CD, Reddy G, Dráberová E, *et al.*
Altered cellular distribution and subcellular sorting of γ-tubulin in diffuse astrocytic gliomas and human glioblastoma cell lines.
Journal of neuropathology and experimental neurology 2006; 65(5): 465-77.

Kondo T and Raff M.
Oligodendrocyte precursor cells reprogrammed to become multipotential CNS stem cells.
Science 2000; 289(5485): 1754-7.

Kramer A, Neben K and Ho AD.
Centrosome replication, genomic instability and cancer.
Leukemia 2002; 16: 767-75.

Lee J, Kotliarova S, Kotliarov Y, et al.
Tumor stem cells derived from glioblastomas cultured in bFGF and EGF more closely mirror the phenotype and genotype of primary tumors than do serum-cultured cell lines.
Cancer cell 2006; 9: 391-403.

Lim DA, Cha S, Mayo MC, *et al.*
Relationship of glioblastoma multiforme to neural stem cell regions predicts invasive and multifocal tumor phenotype.
Neuro-oncology 2007; 9(4): 424-9.

Linos E, Raine T, Alonso A, *et al.*
Atopy and risk of brain tumors: a meta-analysis.
Journal of the National Cancer Institute 2007; 99(20): 1544-50.

Livak KJ and Schmittgen TD.
Analysis of relative gene expression data using real-time quantitative PCR and the $2^{-\Delta\Delta C_T}$ method.
Methods 2001; 25:402-8.

Lizcano JM, Göransson O, Toth R, *et al.*
LKB1 is a master kinase that activates 13 kinases of the AMPK subfamily, including MARK/par-1.
The EMBO Journal 2004; 23(4): 833-43.

Lottaz C, Beier D, Meyer K, *et al.*
Transcriptional profiles of CD133+ and CD133- glioblastoma-derived cancer stem cell lines suggest different cells of origin.
Cancer research 2010; 70(5): 2030-40.

Magnani I, Guerneri S, Pollo B, *et al.*
Increasing complexity of the karyotype in 50 human gliomas.
Cancer genetics and cytogenetics 1994; 75: 77-89.

Magnani I, Novielli C, Bellini M, *et al.*
Multiple localization of endogenous MARK4L protein in human glioma.
Cellular oncology 2009; 31: 357-70.

Mandelkow EM, Thies E, Trinczek B, *et al.*
MARK/PAR1 kinase is a regulator of microtubule-dependent transport in axons.
The journal of cell biology 2004; 167(1): 99-110.

Martinez-Garay I, Rustom A, Gerdes HH, *et al.*
The novel centrosomal associated protein CEP55 is present in the spindle midzone and the midbody.
Genomics 2006; 87: 243–53.

Marx A, Nugoor C, Panneerselvam S, *et al.*
Structure and function of polarity-inducing kinase family MARK/Par-1 within the branch of AMPK/Snf1-related kinases.
The FASEB journal 2010; 24: 1637-48.

Matenia D, Griesshaber B, Li XY, *et al.*
PAK5 kinase is an inhibitor of MARK/Par-1, which leads to stable microtubules and dynamic actin.
Molecular biology of the cell 2005; 16: 4410-22.

Matenia D and Mandelkow EM.
The tau of MARK: a polarized view of the cytoskeleton.
Trends in biochemical sciences 2009; 34(7): 332-42.

Maussion G, Carayol J, Lepagno-bestel AM, *et al.*
Convergent evidence indentifying MAP/Microtubule Affinity-Regulating Kinase 1 (MARK1) as a susceptibility gene for autism.
Human molecular genetics 2008; 17(16): 2541-51.

Mazzoleni S, Politi LS, Pala M, *et al.*
Epidermal Growth Factor Receptor expression identifies functionally and molecularly distinct Tumor-Initiating Cells in human Glioblastoma Multiforme and is required for gliomagenesis.
Cancer research 2010; 70(19): 7500-13.

Mitchell DA, Xie W, Schmittling R, *et al.*
Sensitive detection of human cytomegalovirus in tumors and peripheral blood of patients diagnosed with glioblastoma.
Neuro-oncology 2008; 10(1): 10-8.

Moroni RF, De Biasi S, Colapietro P, *et al.*
Distinct expression pattern of microtubule-associated protein/microtubule affinity-regulating kinase 4 in differentiated neurons.
Neuroscience 2006; 143: 83-94.

Morrison SJ and Kimble J.
Asymmetric and symmetric stem-cell divisions in development and cancer.
Nature 2006; 44:1068-74.

Müller J, Ory S, Copeland T, *et al.*
C-TAK1 regulates Ras signalling by phophorylating the MAPK scaffolds, KSR1.
Molecular cell 2001; 8: 983-93.

Müller J, Ritt DA, Copeland T, *et al.*
Functional analysis of C-TAK1 substrate binding and identification of PKP2 as a new C-TAK1 substrate.
EMBO journal 2003; 22: 4431-42.

Mullins JM and Biesele JJ.
Terminal phase of cytokinesis in D-98S cells.
The journal of cell biology 1977; 73: 672-684.

Mullins JM and McIntosh JR.
Isolation and initial characterization of the mammalian midbody.
The journal of cell biology 1982; 94: 654-61.

Murphy JM, Korzhnev DM, Ceccarelli DF, *et al.*
Conformational instability of the MARK3 UBA domain compromises ubiquitin recognition and promotes interaction with the adjacent kinase domain.
Proceedings of the National academy of science of the United States of America 2007; 104: 14336-41.

Nesic D, Miller MC, Quinkert ZT, *et al.*
Helicobacter pylori CagA inhibits PAR1-MARK family kinases by mimicking host substrates.
Nature structural & molecular biology 2010; 17(1): 130-2.

Ney DE and Lassman AB.
Molecular profiling of oligodendrogliomas: impact on prognosis, treatment, and future directions.
Current oncology reports 2009; 11(1): 62-7.

Ohgaki H.
Epidemiology of brain tumors.
Methods in molecular biology 2009; 472: 323-42.

Panneerselvam S, Marx A, Mandelkow EM, *et al.*
Structure of the catalytic and ubiquitin-associated domains of the protein kinase MARK/Par-1.
Structure 2006; 14: 173-83.

Park DM and Rich JN.
Biology of glioma cancer stem cells.
Molecules and cells 2009; 28: 7-12.

Pelliccia F, Curatolo A, Limongi ZM, *et al.*
Transcriptional profiling of genes at the human common fragile site FRA1H in tumor-derived cell lines.
Cancer genetics and cytogenetics 2007; 178(2): 144-50.

Peng CY, Graves PR, Ogg S, *et al.*
C-TAK1 protein kinase phosphorylates human Cdc25C on serine 216 and promotes 14-3-3 protein binding.
Cell growth and differentiation 1998; 9:197-208.

Perego P, Boiardi A, Carenini N, *et al.*
Characterization o fan established human, malignant, glioblastoma cell line (GBM) and its response to conventional drugs.
Journal of cancer research and clinical oncology 1994; 120(10): 585-92.

Podusio SE and Yin X
A new locus on chromosome 19 linked with late-onset Alzheimer Disease.
Neuroreport 2001; 12(17): 3759-61.

Purow BW, Haque RM, Noel MW, *et al.*
Expression of Notch-1 and its ligands, Delta-like-1 and Jagged-1, is critical for glioma cell survival and proliferation.
Cancer research 2005; 65(6): 2353-63.

Quingley MR, Post C and Ehrlich G.
Some speculation on the origin of glioblastoma.
Neurosurgery reviews 2007; 30: 16-21.

Raemaekers T, Ribbeck K, Beaudouin J, *et al.*
Nusap, a novel microtubule-associated protein involved in mitotic spindle organization.
The journal of cell biology 2003; 162(6): 1017-29.

Reifenberger J, Ring GU, Gies U, *et al.*
Analysis of p53 mutation and epidermal growth factor receptor amplification in recurrent gliomas with malignant progression.
Journal of neuropathology and experimental neurology 1996; 55(7): 822-31.

Reya T, Morrison SJ, Clarke MF, *et al.*
Stem cells, cancer, and cancer stem cells.
Nature 2001; 414(6859): 105-11.

Reynolds BA and Rietze RL.
Neural stem cells and neurospheres--re-evaluating the relationship.
Nature Methods 2005; 2(5):333-6.

Roversi G, Pfundt R, Moroni RF, *et al.*
Identification of novel genomic markers related to progression to glioblastoma through genomic profiling of 25 primary glioma cell lines.
Oncogene 2006; 25: 1571-83.

Rousseau A, Mokhtari K and Duyckaerts C.
The 2007 WHO classification of tumors of the central nervous system – what has changed?
Current opinions in neurology 2008; 21(6): 720-7.

Saadat I, Higashi H, Obuse C, *et al.*
Helicobacter pylori CagA targets PAR1/MARK kinase to disrupt epithelial cell polarity.
Nature 2007; 447: 330-3.

Sapir T, Sapoznik S, Levy T, *et al.*
Accurate balance of the polarity kinase MARK2/Par-1 is required for proper cortical neuronal migration.
Journal of neuroscience 2008; 28: 5710-20.

Sathornsumetee S, Reardon DA, Desjardins A, *et al.*
Molecularly targeted therapy for malignant glioma.
Cancer 2007; 110(1): 13-24.

Schaar BT, Kinoshita K, McConnell SK.
Doublecortin microtubule affinity is regulated by a balance of kinase and phosphatase activity at the leading edge of migrating neurons.
Neuron 2004; 41: 203-13.

Schmitt-Ulms G, Matenia D, Drewes G, *et al.*
Interactions of MAP/Microtubule Affinity Regulating Kinases with the Adaptor Complex AP-2 of clathrin-coated vesicles.
Cell motility and the cytoskeleton 2009; 66: 661-72.

Schneider A, Laage R, von Ahsen O, *et al.*
Identification of regulated genes during permanent focal cerebral ischemia: characterization of the protein kinase 9b5/MARKL1/MARK4.
Journal of Neurochemistry 2004; 88: 1114-26.

Schwarzacher HG and Wachtler F.
Nucleolus organizer regions and nucleoli.
Human genetics 1983; 63: 89-99.

Segu L, Pascaud A, Costet P, *et al.*
Impairment of spatial learning and memory in ELKL Motif Kinase 1 (EMK1/MARK2) knockout mice.
Neurobiology of aging 2008; 29: 231-40.

Seshadri S, Fitzpatrick AL, Ikram MA, *et al.*
Genome-wide analysis of genetic loci associated with Alzheimer Disease.
Journal of the American medical association (JAMA) 2010; 303(18): 1832-40.

Shapiro JR.
Genetic alterations associated with adult diffuse astrocytic tumors.
American journal of medical genetics 2002; 115: 194-201.

Shete S, Hosking FJ, Robertson LB, *et al.*
Genome-wide association study identifies five susceptibility loci for glioma.
Nature genetics 2009; 41: 899-904.

Singh SK, Clarke ID, Hide T, *et al.*
Cancer stem cells in nervous system tumours.
Oncogene 2004; 23(43): 7267-73.

Sirchia SM, Ramoscelli L, Grati FR, *et al.*
Loss of the inactive X chromosome and replication of the active X in BRCA1-defective and wild-type breast cancer cells.
Cancer research 2005; 65(6): 2139-46.

Small TW and Pickering JG.
Nuclear degradation of Wilms Tumor 1-associating protein and Survivin splice variants switching underlie IGF-1-mediated survival.
Journal of biological chemistry 2009; 284(37): 24684-95.

Smith JS, Tachibana I, Lee HK, *et al.*
Mapping of the chromosome 19 q-arm glioma tumor suppressor gene using fluorescence in situ hybridization and novel microsatellite markers.
Genes, chromosomes and cancer 2000; 29(1): 16-25.

Smith JS, Iannotti CA, Dargis P, *et al.*
Differential expression of KCNQ2 splice variants: implications to M current function during neuronal development.
The journal of neuroscience 2001; 21(4): 1096-1103.

Spradling A, Drummond-Barbosa D and Kai T.
Stem cells find their niche.
Nature 2001; 414: 98-104.

Stiles CD and Rowitch DH.
Glioma Stem Cells: a midterm exam.
Neuron 2008; 58: 832-46.

Sun W, Zhang K, Zhang X, *et al.*
Identification of differentially expressed genes in human lung squamous cell carcinoma using suppression subtractive hybridization.
Cancer letters 2004; 212(1): 83-93.

Terabayashim T, Itoh TJ, Yamaguchi H, *et al.*
Polarity-regulating kinase partitioning-defective 1/microtubule affinity-regulating kinase 2 negatively regulates development of dendrites on hippocampal neurons.
Journal of neuroscience 2007; 27: 2896-907.

The Cancer Genome Atlas (TGCA) Research Network
Comprehensive genomic characterization defines human glioblastoma genes and core pathways.
Nature 2008; 455(7216): 1061-8.

Thies E and Mandelkow EM.
Missorting of tau in neurons causes degeneration of synapses that can be rescued by the kinase MARK2/Par-1.
The journal of neuroscience 2007; 27(11): 2896-907.

Timm T, Marx A, Panneerselvam S, *et al.*
Structure and regulation of MARK, a kinase involved in abnormal phosphorylation of Tau protein.
BMC Neuroscience 2008; 9(Suppl 2): S9.

Tochio N, Koshiba S, Kobayashi N, *et al.*
Solution structure of the kinase-associated domain 1 of mouse microtubule-associated protein/microtubule affinity-regulating kinase 3.
Protein science 2006; 15: 2534-43.

Tomankak P, Piano F, Riechmann V, *et al.*
A *Drosophila melanogaster* homologue of *Caenorhabditis elegans* par-1 acts at an early step in embryonic-axis formation.
Nature Cell biology 2000; 2: 458-60.

Trinczek B, Brajenovic M, Ebneth A, *et al.*
MARK4 is a novel Microtubule-associated Proteins/Microtubule Affinity-regulating Kinase that binds to the cellular microtubule network and to centrosomes.
The journal of biological chemistry 2004; 279(7): 5915-23.

Umeda M, Murata-Kamiya N, Saito Y, *et al.*
Helicobacter pylori CagA causes mitotic impairment and induces chromosomal instability.
Journal of biological chemistry 2009; 284(33): 22166-72.

Vandesompele J, De Preter K, Pattyn P, *et al.*
Accurate normalization of real-time quantitative RT-PCR data by geometric averaging of multiple internal control genes.
Genome biology 2002; 3(7):research0034.1-11.

Vescovi AL, Galli R, Reynolds BA.
Brain tumour stem cells.
Nature reviews. Cancer 2006; 6(6): 425-36.

Visintin R. and Amon A.
The nucleolus: the magician's hat for cell cycle tricks.
Current opinion in cell biology 2000; 12(3): 372-7.

Wojcik C and DeMartino GN.
Intracellular localization of proteasomes.
The international journal of biochemistry & cell biology 2003; 35(5): 579-89.

Wrensch M, Wiencke JK, Wiemels J, *et al.*
Serum IgE, tumor epidermal growth factor receptor expression, and inherited polymorphisms associated with glioma survival.
Cancer Research 2006; 66(8): 4531-41.

Wrensch M, Jenkins RB, Chang JS, *et al.*
Variants in the CDKN2B and RTEL1 regions are associated with high-grade glioma susceptibility.
Nature genetics 2009; 41: 905-8.

Yamamoto Y, Matsuyama H, Furuya T, *et al.*
Centrosome hyperamplification predicts progression and tumor recurrence in bladder cancer.
Clinical Cancer Research 2004; 10: 6449-55.

Yamashita S, Tsujino Y, Moriguchi K, *et al.*
Chemical genomic screening for methylation-silenced genes in gastric cancer cell lines using 5-aza-2'deoxycytidine treatment and oligonucleotide microarray.
Cancer science 2006; 97(1): 64-71.

Zahnow CA.
CCAAT/enhancer-binding protein beta: its role in breast cancer and associations with receptor tyrosine kinases.
Expert reviews in molecular medicine 2009; 11: e12.

Zempel H, Thies E, Mandelkow E, *et al.*
Aβ oligomers cause localized Ca^{2+} elevation, missorting of endogenous tau into dendrites, tau phosphorylation and destruction of microtubules and spines.
The journal of neuroscience 2010; 30(36): 11938-50.

Zhang H, Ma X, Shi T, *et al.*
NSA2, a novel nucleolus protein regulates cell proliferation and cell cycle.
Biochemical and biophysical research communications 2010; 391(1): 651-8.

Zhu Y and Parada LF.
The molecular and genetic basis of neurological tumours.
Nature reviews. Cancer 2002; 2(8): 616-26.